

AN INVESTIGATION OF CORROSION
BEHAVIOR OF ALLOY 800

BY

ZAHEER BABAR KHAN

Bachelor of Engineering

N.E.D. University of Engineering and Technology

Karachi, Pakistan

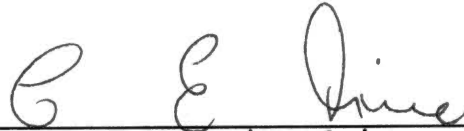
1987

Submitted to the Faculty of the Graduate College
of the Oklahoma State University
in partial fulfillment of the requirement
for the degree of
MASTER OF SCIENCE
May 1991

Thesis
1991
K451


AN INVESTIGATION OF CORROSION
BEHAVIOR OF ALLOY 800

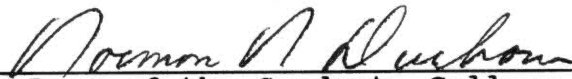
Thesis Approved :



Thesis Advisor







Dean of the Graduate College

To my parents, who were and would always remain,
a source of inspiration and encouragement.

ACKNOWLEDGEMENTS

It is a pleasure to express my gratitude to all those who helped me during this study. Sincerest thanks to Dr. C.E. Price, my major advisor, for his scholarly and thought provoking lectures throughout the coursework. His keen interest, timely professional advices, and continuous encouragement is highly appreciated. Thanks to Dr. Y.C. Shiau and Dr. J. K. Good for graciously serving on my committee.

Raja Baharuddin deserves thanks for the care he took in typing the manuscript.

My profound gratitude to my parents and other family members for their encouragement and support.

Finally, I would like to thank my wife, Amera, and daughter, Hurmah, for their sacrifices, patience, and understanding during my absence for the accomplishment of this goal.

TABLE OF CONTENTS

Chapter	Page
I. INTRODUCTION	1
II. CORROSION BEHAVIOR OF ALLOY 800.	4
2.1 Alloy 800	4
2.2 Corrosion Behavior.	10
2.3 Literature Review	11
III. PITTING AND STRESS CORROSION CRACKING.	25
3.1 Theory of Pitting	25
3.2 Environment-Assisted Cracking	28
IV. EXPERIMENTAL PROCEDURE	31
4.1 Test Program.	31
4.2 Immersion Tests	32
4.3 Stress Corrosion Cracking Tests	37
4.4 Fatigue Tests	43
V. RESULTS AND DISCUSSION	45
5.1 Crevice Corrosion	45
5.2 Pitting Tests	58
5.3 Stress Corrosion Cracking	109
5.4 Liquid Metal Embrittlement (Fatigue Tests)	111
5.5 Corrosion Fatigue	134
VI. SUMMARY.	142
VII. RECOMMENDATIONS FOR FUTURE STUDIES	145
BIBLIOGRAPHY	147

LIST OF TABLES

Table	Page
I. Limiting Chemical Composition, %, of Incoloy Alloy 800.	5
II. Layout of Pitting Tests	35
III. Effect of Crevice Corrosion on Pitting.	52
IV. Results of Pitting Tests in Various Concentrations of Ferric Chloride Conducted on Unsensitized Specimen at Ambient Temperature for 24h	61
V. Results of the Sensitized Specimen Tested for Different Time Intervals in 0.4M Ferric Chloride at Ambient temperature	61
VI. Hardness Data with Respect to Sensitization	83
VII. Pitting Results of Unsensitized, Completely Sensitized, and Partly Sensitized Specimens Tested in 20% Ferric Chloride	86
VIII. Results of the Slow Strain Rate Tests Conducted in 0.4M Ferric Chloride at Different Heat Treatments.	110
IX. Results of Fatigue Tests Conducted in Mercury and Ferric Chloride at Room Temperature	112
X. Variations in Hardness.	116

LIST OF FIGURES

Figure	Page
1. Microstructure of Sensitized Specimen (200 x) . .	9
2. Microstructure of an Unsensitized Specimen (200 x)	9
3. Schematic Sketch of Three Possible Initiation Processes for Pitting : (a) Through Incorporation of Anions into Passive Oxide, (b) Through Island Adsorption of Anions on the Passive Oxide, and (c) Through Tearing of the Passive Oxide [21]	27
4. Geometry of the Waisted Specimen Used for the Slow Strain Rate Tests	40
5. Mounting Arrangement of the Slow Strain Rate Testing Samples.	42
6. The Top Oxide Film Hanging Inwards of a Pit (200 x)	47
7. Crevice Corrosion on a Polished Bottom Face (200 x)	47
8. Severe Crevice Corrosion on the Unpolished Bottom Face of the Specimen in 1.11M FeCl ₃ . Note the Ring Pattern and Undercutting Along the Periphery.	49
9. Severity of Crevice Corrosion Has Increased with an Increase in Concentration to 1.85M of FeCl ₃ . The Ring Has Become More Deep and Wide	49
10. Magnified View of figure 9 (200 x)	51
11. Crevice Corrosion at the Plastic-metal Interface (200 x)	51
12. Pit Formed near the Metal/Coating Interface and Penetrated Under the Coating with Increasing Depth and Undercutting thus Causing Crevice Corrosion Beneath the Coating. (200 x)	55

Figure	Page
13. A Pit, Partly Under the Coating, is Initiating Crevice Corrosion (200 x)	55
14. Pit Formation Within a Crevice Corrosion Site (200 x)	57
15. The Scratches Carried 0.6M Cupric Chloride Underneath the Coating Thus Causing Crevice Corrosion	57
16. Pits Formed on the Sides of the Specimens are Following the Pre-working Marks	60
17. Longitudinal Side Pit Following the Rubbing marks.	60
18. General View of Pits. Note Their Irregularity in Size and Distribution. This is typical (10 x).	64
19. The Top Pit of a Vertical Line of Three at the Center of Figure 18. It is Faceted and Has an Irregular Shape (1000 x)	64
20. The Middle of the Three Pits Mentioned in Figure 19. Faceted Structure and Shiny Titanium Nitride is Visible. Seen are Precipitate Particles and Corrosion Debris on the Surfaces of the Facets (1000 x)	66
21. Closer View of a Medium Size Pit of Figure 18. Preferred Crystal Planes are Outlined (1000 x)	66
22. Structure of the Pit: Facets are Finer near the Edge and the Root While Coarser in between	68
23. Internal Detail of a Fully Developed Pit. Faceted, Shiny, Crystalline Structure. Features of Figure 22 Can Be Seen (200 x)	68
24. The Pit Shape is a Combination of Elliptical and Horizontal Pits	70
25. Deep, Broad, and Undercut Pits Formed During a 24h Test in 1.85 (50%) Ferric Chloride	72
26. The Black Shiny Particle at the Center is Titanium Nitride which is Serving as a Pit Initiation Site. the Solution Used is 0.4M Ferric Chloride (200 x)	75
27. The Pit Has Started Developing and is Polygonal (200 x)	75

Figure	Page
28. The Size of the Pit Has Increased as Compared to That in Figure 27 But is Irregular in Shape (200 x)	77
29. One-half of the Pit Has Become Round While the Other Half is Irregular in Shape (200 x) . . .	77
30. Fully Developed Round Pit (200 x)	79
31. Coalescing Process of Pits Observed in 1.85M Ferric Chloride in 9 min of Immersion Test (200 x)	81
32. General View of the Pitted Unsensitized Specimen Tested in 20 % Ferric Chloride for 24 h. Scattered Polygonal Pits Can Be Seen where Shiny Particles are Titanium Nitride (300 x).	88
33. Center-right Particle of Figure 32 (5000 x) Which is Titanium Nitride. Note that the Surrounding Material is Corroding by Pit Formation	88
34. General View of the Partly Sensitized (As-received) Sample Tested in 20 % Ferric Chloride for 24 h. The Pits are Well Formed, and Round in Shape (30 x).	90
35. Bigger Pit, Adjacent to the Center Twin Pits of Figure 34 (1000 x). The Structure is Faceted and Crystalline With Pits Within the Pit . . .	90
36. General View of a Portion of the Completely Sensitized Specimen tested in 20 % Ferric Chloride	93
37. Severe Pitting Along the Grain Boundries and Within the Matrix on a Completely Sensitized Specimen (200 x). It was Tested in 20 % Ferric Chloride for 24 h.	93
38. An Exploded View of the Center of Figure 37 (1000 x). Grain Boundaries are Severly Attacked	95
39. Closer View of the Pitted Upper-Right Matrix of Figure 37 (500 x).	95
40. A High Magnification (1500 x) View of Figure 39 Showing intensive Pitting. The Pits are Pyramidical in Shape and Faceted	97

Figure	Page
41. A Large Irregular Pit Formed on the Completely Sensitized Specimen Discussed in the Above Figures. Compare the Size of This Pit (30 x) With Those Shown in Figure 40 at 1500 x. . . .	97
42. Detail of the Central Flat Surface of the Pit Shown in Figure 41, Which is Under Severe Attack (200 x)	99
43. The Pattern of Pitting Attack when the As-received Specimen was Tested for 45 minutes in 1.85M Ferric Chloride. It Looks Like a General Attack but Actually Consists of a Number of Pits Joined Together	101
44. Magnified View of Figure 43. It Shows the Preferential Attack along the Grain Boundaries. This Attack Consist of Many Pits which Have Been Coalesced (200 x). The Attack is Mainly Intergranular With Pits Within the Matrix (200 x)	101
45. Detail of the Intergranular Attack Showing Crystallographic, Shiny, Faceted Structure Which is Similar to That Found at the Bottom of the Pit (200 x)	103
46. Photograph Taken After 24h Immersion Test in 1.85M Ferric Chloride. Although it Shows a General Corrosion but is Actually the Result of Pit Formation and Coalescence. It Has a Shiny, Crystalline Structure with Undercutting at the Edges (200 x).	103
47. Graph of Concentration vs. Number of Pits . . .	106
48. Graph of Time vs. Number of Pits	108
49. Fatigue Life Depends on Relative Extent of Initiation and Propagation Stages [38]	114
50. Wohler's S-N Curves for Krupp Axle Steel [38]. .	118
51. General View. From Right to Left Are Fatigue Zone (50 %) and Overload Zone (50 %) With Secondary Cracking (20 x)	120
52. The Center of the Right Hand Side is the Point of Fatigue Zone Initiation. Lines are Radiating Away From That Point. Faceted Transgranular Separation is Visible (240 x)	120

Figure	Page
53. Detail of the Fatigue Initiation Zone Shown in Figure 44. Tear Ridges and Striations Can be Seen (1000 x)	122
54. General View Showing Fatigue (Bottom Right) and Overload Zones (Fatigue Zone is Approximately 25 %). Microvoids Can Be Seen in the Overload Zone (20 x)	124
55. Initiation of Fatigue Zone (Bottom Left). At Origin Can Be Seen Rubbing, a Very Localized IG Zone, Then a Faceted IG Zone that Quickly Becomes More Irregular, Less Planar (240 x). .	124
56. Detail of the Center of Figure 55. Secondary Cracks Can Now Be Seen. They Develop as Major Cracks Grow (1000 x)	127
57. Lower Right Hand Side of Figure 55. Secondary Cracks and Their Internal Details can Be Easily Seen, as Can Striations That are Somewhat Disturbed by Rubbing (1000 x)	127
58. A Portion of a Transverse Side Crack. The Irregular Pattern Shows That it is Not Due to Any Peripheral Grinding Mark. Observe That the Crack is Open and Contain Debris (1000 x) . .	129
59. General View of the Fractured Surface. Center of the Right Hand Side is the Fatigue Initiation Zone (20 x)	131
60. Fatigue Initiation Point. Observe in This Instance Zones of IG Fracture (240 x)	131
61. The Upper-right View of Figure 60. Detail of the IG Fracture Zone (1000 x)	133
62. An IG Zone in More Detail Showing Corrosion (3000 x)	133
63. General View. 3 Distinct Fatigue Zones. Fracture was Brittle. A Big Pit, Which Served as a Crack Initiation Site, is Located on the Top-left Side. The Specimen is Sensitized Hence Undercutting is Significant. Side Cracking can Also be Seen (20 x)	136
64. Higher Magnification View of the Pit (240 x). Faceted Structure, Intergranular Attack, and Cracks are Visible	136

Figure	Page
65. Extreme Right End of Figure 64 Showing the Root/Edge of the Pit. IG Cracking is Apparent	138
66. Lower-left View of Figure 65. IG Cracking Can be Seen. There are Some Cavities as if the Particles Have Floated Out. Observe That the Rectangular Particle of Titanium Nitride is Not Corroding Rather it is Acting as a Cathode and the Matrix Around it Corrodes. The faceted structure is Typical of a Pit and Resembles that seen in Figure 22 (1000 x)	138
67. Center of the Extreme Right-end of Figure 65. Corrosion and Intergranular Attack Can Be Seen. Again Observe the Titanium Nitride Particle and the Corroding Matrix (1000 x).	141

CHAPTER I

INTRODUCTION

Ni-base alloys are gaining popularity and widespread application as the awareness to the corrosion problems such as localized corrosion, stress corrosion cracking, oxidation, carburization, and other related phenomena is increasing. The technological advancements in chemical plants, petrochemical industry and power generation units have enhanced the need for materials which can provide dependable service in highly corrosive environments at high temperature, under high stresses, and their combinations [1,2,3,4]. The nickel-base alloys possess a face-centered cubic crystal structure which results in superior mechanical properties to other structures. Unique intermetallic phases can form between nickel and some of its alloying elements producing very high strength alloys for both low and high temperature applications.

The broad range of available forms, strength and corrosion resistance, and the ease with which it is fabricated have made Alloy 800 (UNS N08800) an economical choice for equipment designed to operate in a wider spectrum of aggressive environments. By virtue of its high nickel content, Alloy 800 , is stably austenitic and is

not embrittled by the precipitation of the intermetallic compound sigma phase [4]. It has relative freedom from stress-corrosion cracking in solutions containing chlorides and has good resistance against pitting; even greater than Alloy 600 and Alloy 400 [6].

Pitting corrosion is a form of localized corrosion that is exceedingly destructive, since a perforation resulting from a single pit can cause complete sudden failure of the system. Furthermore, pits can produce premature service failure, since they usually provide sites for crack initiation [5,7]. It is often difficult to predict the pit initiation sites. This is the reason that there are various techniques to evaluate pitting including electrochemical, immersion, and statistical approaches. Similarly, the stress-corrosion cracking (SCC) phenomenon is also of great practical importance and is not fully understood, thus requires intensive research. The most reliable and useful information is obtained from empirical experiments [5].

Evaluation of new or old alloys or metals to determine the environments in which they are suitable, is one of the objectives of corrosion testing. Aggression of the environment can be changed by using different concentrations of the solutions, altering the temperature or varying the time depending upon the investigator's objective. The information obtained aids in the selection of material for the specific application.

The sequence of this study is firstly to observe the trend of pitting in Alloy 800, by immersion tests using ferric chloride, ammonium persulfate and cupric chloride solutions. These are the aggressive solutions that commonly cause pitting in a wide range of alloys. HCl solutions are used for obtaining general corrosion for comparison. The test procedure is similar to the ASTM designation G48 [15]. Some guidance regarding examination and evaluation of pitting has been taken from ASTM designation G46 [16]. The parameters varied during testing are concentration, time and temperature. The study is then extended to SCC testing by the slow strain rate test method (SST) as well as studying fatigue behavior in mercury.

The intent of this investigation is to seek correlations between the pitting susceptibility and stress corrosion cracking and, indeed to determine whether stress corrosion cracking can be obtained in Alloy 800 at ambient temperatures. This is the case in other nickel-base alloys such as 400 and 600 and austenitic stainless steels [43]. Stress corrosion cracking is known at elevated temperatures, while hydrogen embrittlement by liquid mercury, during fatigue, has been reported at room temperature [35]. Literature on Alloy 800, related specifically to this theme, is very limited therefore articles regarding nickel-base alloys have also been consulted wherever found relevant.

CHAPTER II

CORROSION BEHAVIOR OF ALLOY 800

2.1 Alloy 800

Alloy 800 was developed in 1949 by the International Nickel Company, Incorporated. It was designed to provide good mechanical properties along with resistance to corrosion in a wide variety of aggressive industrial environments, even at elevated temperatures. The composition is shown in Table I [4,25]. Note that the nickel content is relatively low at 30-35 percent.

Like austenitic stainless steel, Alloy 800 is also susceptible to pitting in chloride containing solutions but to a lesser degree. The high nickel, high chromium balance imparts excellent resistance to oxidation and carburization at high temperatures. Weight-loss determinations under conditions of severe cyclic oxidation indicate the ability of the alloy to retain a protective oxide at 982 C (1800 F), where scaling resistance becomes a significant factor in service. Indeed, the modified version, 800 HT is one of very few alloys usable at 900 C (1650 F) requiring strength, oxidation resistance, easy weldability and ductility. In some environments which are oxidizing to chromium but reducing to nickel, Ni-Cr alloys become

TABLE I
LIMITING CHEMICAL COMPOSITION, %,
OF INCOLOY ALLOY 800

Nickel.....	30.0-35.0
Chromium	19.0-23.0
Iron	39.5 min
Carbon	0.10 max
Manganese	1.50 max
Sulfur.....	0.015 max
Silicon.....	1.0 max
Copper.....	0.75 max
Aluminium	0.15-0.60
Titanium.....	0.15-0.60

susceptible to internal oxidation which can cause severe embrittlement. The iron content of Alloy 800 reduces its susceptibility to this type of corrosion and provides resistance to sulfur attack. It has relative freedom from SCC in solutions containing chlorides. This property has also been studied in this research.

The ability of Alloy 800 to satisfy a multitude of stringent operating requirements in the home appliances, food processing, industrial heating, chemical and petrochemical fields has paved the way to its uses in other applications, notably in the power field. As an approved material of construction under the rules of the ASME Boiler and Pressure Vessel Code, Section I, III, and VIII, the alloy has already accumulated favorable service experience as boiler tube material in nuclear power systems. The alloy is also approved as heat exchanger tube material for sodium-cooled fast breeders and it is being evaluated for coal gasification reactor vessel internals [4]. Alloy 800 is also used in the Siemens' steam generator U-tubes operating in the relatively low temperature range up to 320 C. A fine grain, low carbon, fully stabilized grade was selected for optimal performance [1,4].

2.1.1 Metallography

Alloy 800 is an austenitic, solid-solution alloy. Titanium nitrides, titanium carbides, and chromium carbides normally appear in the alloy's microstructure and are

readily visible in the unetched state as small angular inclusions. The phases vary in color from the orange-yellow of the nitride to the grey-lavender tint of the carbide. The nitrides are stable at all temperatures below the melting point and are therefore unaffected by heat treatment. Figures 1 and 2 show the microstructure of alloy 800 in sensitized and unsensitized conditions respectively.

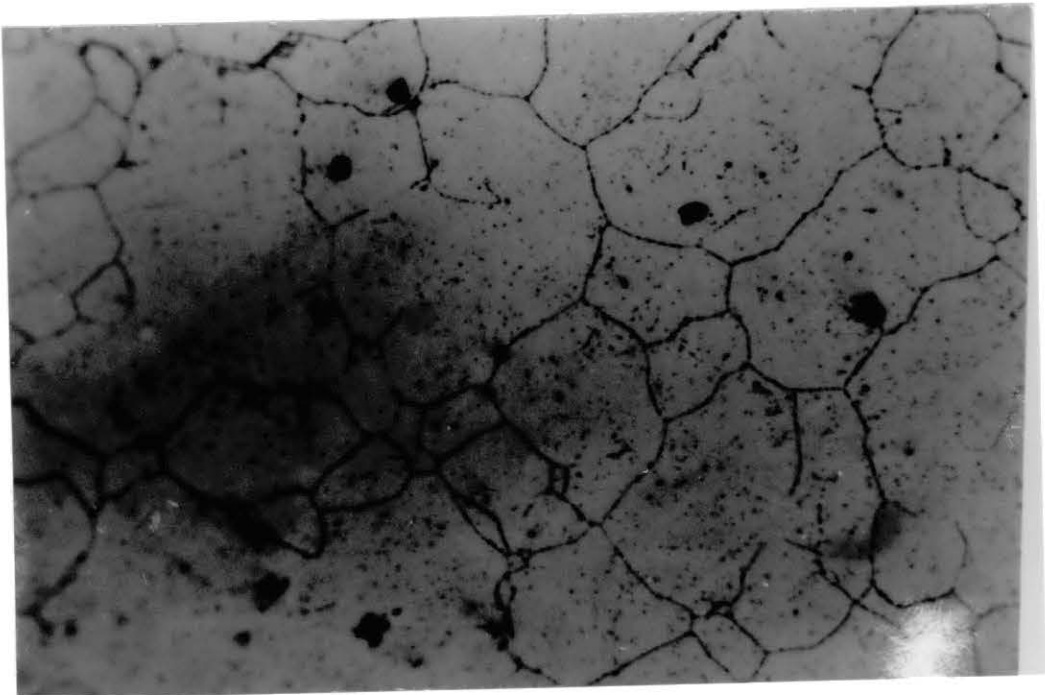
A gamma-prime phase (face-centered-cubic structure rich in nickel, aluminium, and titanium) may precipitate in the alloy during long time (over 100 h) exposure to temperatures in the range of about 1000 to 1300 F (540 - 705 C). Yield and tensile strengths are increased and elongation is decreased by the phase. Values of 20 % or higher are obtained with the phase present.

Chromium carbides precipitate in the alloy at temperatures between 1000 and 2000 F (540 - 1095 C). Consequently, Alloy 800 is similar to other austenitic alloys in that it can be rendered susceptible to intergranular corrosion (sensitized) in certain aggressive environments by exposure to temperatures of 1000 to 1400 F (540 - 760 C) [25].

In solution treated Alloy 800, it is generally assumed that during service at about 600 C, $M_{23}C_6$ will be precipitated within the grains and at grain boundaries. The literature shows that there will also be a significant rate of diffusion of chromium into the regions depleted in chromium. The extent to which "sensitization" is likely to

Figure 1. Microstructure of Sensitized Specimen (200 x)

Figure 2. Microstructure of an Unsensitized Specimen



arise therefore depends on the rate at which the carbide is precipitated, relative to the rate of chromium diffusion in the matrix. Important variables are the degree of cold work, the concentration of carbon in solution and the concentration of other elements, such as titanium, which decrease the rate of nucleation and growth of carbides by decreasing the carbon activity of the solid solution. It follows that the existence of carbides at grain boundaries, even chromium carbide, is not a sufficient indication of sensitization since chromium diffusion into the depleted region may have occurred. The recognition of the sensitized condition is therefore not simple and some of the chemical tests do not necessarily relate to performance in service. For example, the Huey test uses nitric acid which is known to dissolve TiC and could therefore wrongly indicate susceptibility to local attack in a non-sensitized material [1].

2.2 Corrosion Behavior

The alloy has good resistance to corrosion in a variety of aqueous media and its resistance to high temperature environments is outstanding. However, there is evidence of sulfidation attack on Alloy 800 test coupons exposed to a coal gasifier environment at 870 C (1600 F) for 100 h [25,27].

An important property of Alloy 800 is its relative freedom from SCC. In caustic solutions, over a wide range

of concentrations and at temperatures above 290 C (550 F), the alloy is susceptible to SCC. Cracking is predominantly intergranular (IG) [25,28]. In view of sensitization, care should be taken during welding. Huey test rates for sensitization can be obtained from the time-temperature diagram shown in reference 25. Note that stress corrosion cracking at room temperature has not been reported.

2.3 Literature Review

2.3.1 Oxidation of Incoloy 800

Elliot and Marsh [29] studied the oxidation behavior of Incoloy 800 in a slowly flowing environment of air containing 500 vpm ($\text{cm}^3 \text{min}^{-1}$) $\text{HCl}(\text{g})$ and 13,000 vpm $\text{H}_2\text{O}(\text{g})$ at a working temperature of 800 C for 250 h.

Pre-oxidation of Alloy 800 in clean air improves its performance in corrosive environments. Samples of Incoloy 800 were pre-oxidized in moist air for 100 h at 800 C and allowed to furnace-cool to produce a uniform adherent oxide scale. Metallographic examination indicated a small amount of internal oxidation. Electron microprobe analysis revealed a thick mainly Cr_2O_3 scale, with some iron and nickel-oxide incorporated in the outermost region.

Scanning Electron Microscope (SEM) examination of the samples, oxidized for 100 h at 800 C in air saturated with water vapor at 20 C, showed the oxide to be wrinkled and convoluted. The quickly-cooled samples had microspalled areas, whereas no spalling was observed within oxides on

furnace-cooled samples. Localized small areas of iron-rich oxide on a mainly chromic oxide scale were apparent and several small whiskers of iron oxide were observed on the iron-rich region.

SEM examination of small particles of oxide scale left on the alloy, after 100h exposure to the isothermal oxidation in moist air + 500 vpm HCl (g), showed a duplex nature with an outer nodular oxide. This oxide contained mainly iron, nickel and some titanium, upon a continuous, mainly Cr₂O₃ layer. Cohesive and adhesive strengths of the oxides were adversely affected by the presence of HCl(g) in the oxidizing environment. The 250 h exposure at 800 C revealed an additional localized phenomenon of titanium oxide present as colonies of crystallites. Chromium oxide-rich outcrops had a distinctive wart-like appearance. Iron oxide was mainly present at the surface in the form of platelets. Enrichment of titanium at the surface of oxides formed on the commercial alloys has also been observed in high temperature oxidation studies. This is because the presence of chloride at the alloy-oxide interface and within the lattice permits an increased rate of transport of metal ions.

2.3.2 Pitting of Alloy 800 in Chloride

Sulphate Media

This study was done by Palumbo, King, and Aust [9]. The specimens of 15.5 diameter tubing with wall thickness of

1mm were mechanically polished, ultrasonically cleaned and degreased, rinsed with water and dried. The pH was adjusted to 7.00 and the temperature to 30 C. Immunity to pitting was observed at chloride levels below 0.01 M. Chloride concentration plays a vital role. Decreasing the chloride concentration resulted in noble shifts of the critical nucleation potential while an increase in chloride concentration resulted in an increase in pit density. It had only minor effect on the general corrosion behavior.

Dilute chloride solutions containing low sulphate concentration had detrimental effects. At Chloride levels below 0.1M, the addition of sulfate to produce a $\text{SO}_4^{-2}/\text{Cl}^{-1} = 0.1$ resulted in an extension of pitting susceptibility to chloride levels as low as 0.001M; the reason being inefficient inhibition and film contamination by the sulphate. The addition of sulfate at a low concentration level also resulted in stable pit initiation in the transpassive region. Further increase in sulfate concentration restored the systems immunity to pitting, hence reducing the pit density. The diameter of the pits was larger in chloride-sulfate solutions than in only chloride solutions.

2.3.3 Pitting Corrosion of Nuclear

Steam Generator Materials

Experiments were conducted by King and Dautovich [6] to study the pitting of tubing alloys of Monel 400, Inconel

600, and Incoloy 800 at 288 C. The tubes were internally heated to provide heat transfer through the tube wall. In the crevice regions and under deposits, pitting was apparent. A crystallographic pitting morphology was usually found on Alloy 600 and Incoloy 800 and was likely caused by acid chloride attack. The attack on Monel 400 was mainly intergranular in nature. The pits formed on Incoloy 800 in lakewater, were usually faceted. The deposit covering the pits was found by Energy Dispersive X-ray Analysis (EDXA) to contain significant amounts of iron and silicon, and relatively little nickel or chromium. This specimen was tested in Lake Huron water. Some pits were observed to have bright, shiny metallic facets while others were covered with a thin dull oxide. This oxide is thin enough to allow the facets and other features of the pits to be visible. After the test, water sample analysis showed that the insoluble fraction contained various iron and copper oxides as well as nickel, calcium, and others as minor components.

In Lake Ontario's water, with tests of Incoloy 800 at 288 C, attack was noted only when copper chloride was added. Again, the pits showed crystallographic features, but were more irregular in shape and many had step structures at the edges.

Both Inconel 600 and Incoloy 800 underwent pitting in crevices and under sludges and deposits in steam-blanketed regions. The same pitting morphology was noted in acid chloride tests. Chloride was implicated as being a major

factor in pitting in concentrated lakewater. The authors referred to Pathania and McVey's [44] autoclave tests on Inconel 600 and Incoloy 800 in concentrated seawater where pitting reached a maximum depth of 50 μm . Pits on Inconel 600 reached this maximum within 56 days while those on Incoloy 800 took 28 days. No further increase in depth was observed for 140 days. Absence of attack was observed in alkaline chloride solutions.

2.3.4 Thermal Convection Loop study of Incoloy 800 in Molten $\text{NaNO}_3\text{-KNO}_3$

The thermal convection loop, initially charged with a commercial salt mixture of Partherm 430 60 $\text{NaNO}_3\text{-40 KNO}_3$ (weight percent), operated under steady-state conditions between 600 C and 300 C with a local variation of 5 C. Bradshaw [10] observed that the corrosion products primarily consisted of Fe_3O_4 and $\text{Fe}(\text{Fe},\text{Cr})_2\text{O}_4$ over most of the temperature range. At temperatures near 600 C, complex multilayer scales were observed. The corrosion morphology resulting from immersion in molten nitrate salt at 595 C shows the corrosion products consisted primarily of a series of iron and iron-chromium oxides. The corrosion scale consisted of three layers : magnetite (Fe_3O_4) with a minor amount of haematite (Fe_2O_3) at the outer, salt-contacting interface, followed by a chromium-rich rhombohedral oxide. The alloy adjacent to the scale was depleted in iron and chromium, but enriched in nickel. It also contained a small

amount of internally precipitated chromium nitride.

Extensive internal nitride formation has been reported at temperatures above 600 C.

A tendency for subsurface oxidation to occur intergranularly was evident. It may be due to relatively low chromium activity at grain boundaries rather than within grains, as a result of either chromium carbide precipitation or depletion into the salt.

At temperatures below 400 C, anomalous weight changes were noted that appeared to be caused by pitting. Coupons immersed at 333 C for 4991 h in molten nitrate showed a typical pit which tended to have planar surfaces as boundaries. Cross-sectional views of the pitted coupons did not reveal intergranular corrosion extending beyond the pit. Pitting could occur by dissolution of all the alloying elements (Fe, Ni, and Cr) as a result of a higher oxide ion activity in the pit relative to the bulk melt which would result from the nitrate reduction.

The number of pits observed in a typical cross-section corresponded roughly to the number of titanium carbonitride inclusions at the surface of unexposed coupons. It was speculated that pitting initiates primarily at these sites since they constitute flaws in the relatively thin tarnish film formed on the alloy at temperatures below 400 C.

2.3.5 Electrochemical Behavior in Occluded Corrosion Cells (OCC)

Batista, Louvise, Mattos and Sathler studied this behavior[12]. Occluded corrosion cell solutions were synthesized by a mixture of iron, nickel, and chromium chloride salts, the concentration of which was proportionally the same as that of the alloy matrix. A temperature of 25 - 0.5 C was maintained. Incoloy 800 was used as an electrode.

Variations of open circuit and of the potential-dynamic anodic polarization curves with increasing overall chloride concentration indicated that the corrosion behavior of Incoloy 800 changed from passive to the active dissolution corrosion mechanism. The pH decreased with increasing concentration of the solution; the reason being the hydrolysis reactions of the metallic ions formed due to the dissolutions of salts. The most concentrated solution had a pH of -0.6 inside the pit. The dissolution rate of alloy 800 in a given chloride concentration medium was lower than that of AISI 304 which attributed to higher Ni content.

2.3.6 The Role of Titanium in the Pitting Corrosion of Stainless Steel

This study of Srivastava and Ives [18] determined the manner in which titanium containing inclusions contributed to the localized attack of stainless steels. The observations of this research were in sequence with some

other studies done on Alloy 800 but with a different approach.

Beneficial as well as detrimental effects of titanium have been reported. Titanium may exist as an alloying element added to prevent intergranular corrosion since it combines with carbon and nitrogen, thus reducing the incidence of chromium and molybdenum carbides and nitrides, which would produce depleted zones of these elements in the alloy.

Titanium inclusions in 301 stainless steel appeared in two distinct forms: (i) mixed inclusions, comprising a central Ti-rich particle surrounded by sulfides, (ii) isolated Ti-rich inclusions. Under corrosive situations, the titanium inclusions invariably behaved cathodically, with either the adjacent sulfides preferentially dissolving or the nearby matrix alloy being attacked. The experiments showed that the sulfide (Mn,Fe)S portion of the inclusion dissolved preferentially in 0.3 M ferric chloride solution leaving the centrally located bright area of the undissolved titanium-rich oxide inclusions.

The heterogeneous microstructural features observed at the grain boundaries could be sites for anodic dissolution. It is not clear if the heterogeneity was caused by local variations in chemical concentration or merely the local region of enhanced strain concentration during cold work or both.

Lizlovs and Bond [45] have reported that titanium

increases the critical pitting potential but decreases if the titanium content increases from 0.91 to 1.758 in 18Cr-2Ni-2Mo steels. Ijzermans [46] found that in titanium-stabilized alloys the susceptibility to intergranular attacks decreases but leads to an increase in the rate of pitting corrosion [18,32].

2.3.7 The Influence of Silicon on 18Cr -8Ni

Stainless Steel

Silicon additions were made to 18 Cr - 8 Ni stainless steels to produce alloys with duplex microstructures (austenite and ferrite) [30]. The resistance of these silicon - stabilized duplex alloys to general acid corrosion, chloride SCC, and IG corrosion in the sensitized heat treated condition was markedly superior to that of any then available commercial austenitic stainless steels. Wilde[30] tested silicon duplex 18Cr - 8Ni alloys for pitting resistance in sodium chloride and acidified ferric chloride solutions.

A wide range of the potential independent passive current density (CD) was observed on each alloy , with a critical breakdown potential (E_c), marking the onset of pit initiation; the more noble or positive the E_c value, the more resistant the material was to pit initiation. Electrochemical polarization measurements conducted in aerated 3.5 wt. % NaCl at 25 C indicated a progressive increase in the critical breakdown potential for 18Cr - 8Ni alloys over the range 1.01 to 4.45 wt % silicon , thereby

predicting increasing resistance to pit initiation. Corrosion rates decreasing from 1016 to 50 milligrams weight loss per square decimeter per day (mdd) were observed over the above silicon range. This showed that increasing the silicon content in a duplex matrix, despite increasing the resistance to pit initiation, decreased the resistance of the alloy to crevice corrosion or pit propagation. The mechanistic reasons for this beneficial effect of silicon were still being investigated [30].

2.3.8 Effect of Nickel Content on Pitting

Roberge[31] selected AISI 304 SS, Alloy 800, and alloy 600, because of their practical importance as heat exchanger tubing materials and the fundamental interest due to the range of nickel content they offer. Adverse effects of nickel were seen at both low and high thiosulphate concentrations.

The larger amount of nickel in Alloy 800 and Alloy 600 stabilizes pit propagation. On a macroscopic basis, once pits are initiated they always propagate. It was observed that pitting potential (E_p) increases with an increase in current density that usually characterizes the onset of pitting no longer occurred. Although at high concentrations thiosulphate inhibited pitting, inhibition was less efficient for alloys containing about 75 % or more nickel.

2.3.9 Electrochemical Investigations of Pitting Behavior

Hickling and Wieling [8] tested Inconel 600, Incoloy 800, and type 347 stainless steel in the solutions of deionized water plus 5 or 20 ppm of PO_4^{3-} (added as Na_2HPO_4), 20 ppm of Cl^- (added as NaCl) and 6 ppm N_2H_4 at temperatures of 150, 200, and 250 C.

A comparison of material behavior indicated superior pitting resistance of Incoloy 800 versus Inconel 600. This tendency prevailed even in more concentrated chloride solutions at lower temperatures and is probably attributable to the higher chromium content of its 800 material. Metallographic examination of the specimens indicated an important difference in pit morphology; corrosion attack was relatively shallow (maximum pit depth typically $\leq 30 \mu\text{m}$) for both Inconel 600 and Incoloy 800 as compared to the deep, occluded pits observed on the stainless steel specimens. These latter pits sometimes acted as initiation sites for stress corrosion cracks, whose depth was nearly 350 μm . No cracking was observed on specimens from either Incoloy 800 or Inconel 600 steam generator tubing [8].

2.3.10 Other Relevant Developments

There are some other worthy researches directly or indirectly related to the present research but at this stage a short overview of a few of them should be sufficient. These articles will be referred to wherever necessary.

Tomashov, Chernova, and Marcova [19] studied the effect of supplementary alloying elements on pitting corrosion susceptibility of 18 Cr - 14 Ni stainless steel. The alloying elements, chosen for their stability in solutions containing chloride ions and their solubility in austenite, were Mo, Si, V, W, Ti, Ce, Nb, Ta, Zr, and Re.

Growth and repassivation of single corrosion pits in stainless steel were studied by Newman and Franz [20]. They found that even the smallest pit, although highly equiaxed, grew by coalescence from at least three nucleation points. Furthermore, there was a potential-dependent solution resistivity in the pit - the more rapidly the pit grows, the more concentrated (and therefore conductive) was the solution in the pit. Commenting on the shape of the pits, they were of the view that probably the higher currents for larger pits indicated that the small pits maintained a roughly hemispherical shape, whereas the larger ones tended to be slightly saucer-shaped due to secondary edge nucleation.

Lippold [11] investigated the cracking of superheated steam tubing operating in the temperature range of 550 to 650 C. The metallographic sections revealed a continuous carbide network along the grain boundaries. Since the starting microstructure was nearly free of grain boundary carbides, it appears that considerable carbide precipitation has occurred during service. Despite the presence of grain boundary carbides, the crack path was almost entirely

transgranular. Only sporadic instances of intergranular branching from the main crack were observed although SCC of Alloy 800 is generally intergranular in a steam environment. The tubing used in the central receiver contained high carbon and thus a $Ti/C = 5$. Cold work and sensitization further reduced the resistance of Alloy 800 to SCC in oxygen/chloride environments.

The effect of thermal treatments on SCC of Alloy 800 in a caustic environment was tested by Pathania and Cleland [33]. Generally the thermal treatments (500 to 850 C) inhibited the SCC of Alloy 800. No cracking was observed after a 700 C heat treatment for 300s.

2.3.11 Summary

The conclusions drawn from the foregoing review suggest that Alloy 800 should be used carefully in the chloride environment as it is one of the most corrosive solutions for this particular alloy. As compared to austenitic stainless steels, it is more resistant to pitting due to the higher chromium content. Increasing the sulphate concentration improves the chloride pitting resistance, while low-level sulfate addition to dilute chloride media is detrimental. Most of the pits were found to have a shiny, crystallographic, faceted structure. Oxide films, which mainly consisted of Cr_2O_3 alongwith iron and nickel oxide, were found to be more adherent on furnace cooled specimens, as compared to the quickly cooled ones. The literature also

shows some resemblance in the behavior of Alloy 800 and a few austenitic steels. Like AISI 304, larger amount of Ni gives stability to pit propagation. Increasing the Si content has the same effect on 18Cr - 8Ni steel and Alloy 800. It increases resistance to pit initiation but decreases resistance to crevice corrosion or pit propagation. Furthermore, the role of Ti in 301 stainless steel and Alloy 800 are identical. In both the materials it behaves cathodically, thus preferentially dissolves the nearby matrix. In caustic environments, thermal treatment can inhibit stress corrosion cracking. Most of the experiments on Alloy 800 have been performed at high temperatures.

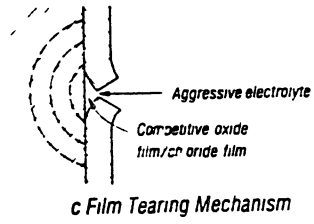
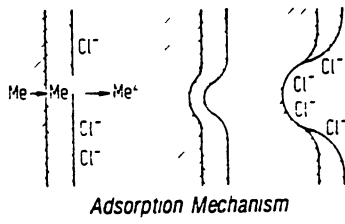
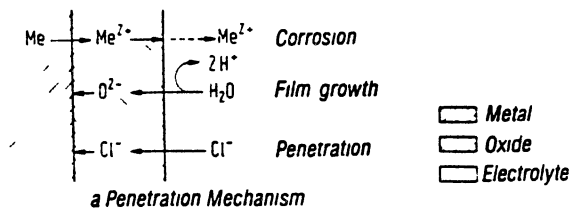
CHAPTER III

PITTING AND STRESS CORROSION CRACKING

3.1 Theory of Pitting

A number of theories have been presented on this topic. According to Evans [22], consider a piece of metal devoid of holes and pits immersed in an aerated sodium chloride solution. If, for any reason the rate of metal dissolution is momentarily high at one particular point, chloride ions will migrate to this point. Since chloride stimulates metal dissolution, this change tends to produce conditions that are favorable to further rapid dissolution at this point. Locally, dissolution may be momentarily high because of a surface scratch, an emerging dislocation, or other defect, or random variations in solution composition. Stagnant conditions and severe cold working increases the chances of pitting. Kaesche [21], is of the opinion that heterogeneous inclusions such as sulfide inclusions in Cr - Ni steels or chromium oxide inclusions in Cr steels, are preferred initiation sites for pitting. Figure 3 shows the possible variations for the pit initiation process, i.e., the formation of the first smallest site for active metal dissolution in the middle of the passive surface, namely the "penetration", the "adsorption", and the "film tearing"

Figure 3. Schematic Sketch of Three Possible Initiation Processes for Pitting : (a) Through Incorporation of Anions into Passive Oxide, (b) Through Island Adsorption of Anions on the Passive Oxide, and (c) Through Tearing of the Passive Oxide [21]



mechanisms.

Nishimura [40] studied the pitting behavior of nickel in phosphate solutions while Nishimura, along with Kudo,[41], studied pitting corrosion of AISI304 and 316. Both researchers are in conformity that passive film breakdown takes place in three stages viz. pit incubation time, pit nucleation, and pit growth. This explanation is close to the penetration and adsorption model of Kaesche [21].

Asphahani [2] points out that the breakdown of the passive film is followed by the formation of an electrolytic cell. The anode of this cell is a minute area of active metal , and the cathode is a considerable area of passive metal. The large potential difference, characteristic of this passive-active cell, accounts for the rapid corrosion at the small anode.

Fontana [5] and most of the researchers agree that once the pits are formed the mechanism is dictated by an autocatalytic process where the corrosion processes within a pit produce conditions which are both stimulating and necessary for the continuous activity of the pit. It can be said that the process is self-stimulating and self-propagating.

3.2 Environment-Assisted Cracking

The field of environment-assisted cracking(EAC) includes SCC, hydrogen embrittlement(HE), and liquid metal

embrittlement (LME). Various theories have been proposed and it is accepted that several mechanisms apply in different circumstances. This discussion, though not in the scope of the present study, is just to recall some pertinent features.

SCC has been explained by Bussle and Pugh [38] through the film rupture model which involves anodic dissolution at the crack tip. The basic idea of this model is that the protective surface film in the vicinity of the crack is ruptured by localized plastic flow. This creates an electrolytic cell, with the base metal at the crack tip serving as the anode and the broken protective surface film serving as the cathode. Rapid anodic dissolution takes place at the base metal which advances the crack. The rate of anodic dissolution and associated crack extension will depend partly on the repassivation rate. Intermediate passive rates maximize the SCC process. Craig [42] has also discussed this phenomenon with some additional remarks regarding crack propagation mechanism. The study suggested that breaking of the interactive bonds of the crack tip can be due to chemical solvation and dissolution, or mechanical failure. Kaesche [21] has also discussed this phenomenon in detail. Fontana [5] has discussed a number of variables involved and points out that high-nickel alloys and iron-chromium alloys often exhibit IG and TG cracking in the same alloy, depending on the environment or the metal structure.

LME can result due to liquid-metal chemisorption -

induced reduction in the cohesive strength of atomic bonds in the region of a stress concentration. The liquid-metal atom is believed to reduce the interactive bond strength between solid atom thereby causing bond rupture to occur at reduced stress levels [38]. According to Lynch [47] premature fracture results from a reduction in shear strength rather than the cohesive strength of atomic bonds at the crack tip. Lynch [47] also discussed the similarities between LME and HE.

CHAPTER IV

EXPERIMENTAL PROCEDURE

4.1 Test Program

A few preliminary tests involved immersion in 2, 5 and 10 % HCl acid solution to give general corrosion and a basis for comparison subsequently.

In order to achieve the intended goal of the research, the experiments were designed in the following sequence :

- (a) Immersion tests for pitting
- (b) SCC tests on pre-stressed samples
- (c) SCC tests using the SST technique.
- (d) Fatigue tests.

Immersion tests were considered the first step, since the results could give an idea regarding the solution and its effective concentration, the time required for pitting to occur at room temperature, the effect of surface conditions and the effect of different heat treatments. These results were then used to select the variables in the SCC tests, for example what concentration of ferric chloride would be sufficient to cause SCC in pre-stressed samples or how much time would be required to conduct a successful SST test in which the pit could transform into a crack. Fatigue test parameters were adjusted in the light of the above

experiments.

4.2 Immersion Tests

These tests were carried out on 0.5" discs cut from a 0.5" diameter rod of Alloy 800. The specimen proportion and testing procedure were principally in accordance with ASTM G48-80 [15] and ASTM G1-81, [17]. Initially, a few specimens were ground to 600 grit and mechanically polished by 0.05 micron gamma micropolish powder. This was followed by water and methanol rinsing, ultrasonic cleaning, and air drying. These specimens did not show any grain boundaries therefore a step of electrolytic polishing was added after mechanical polishing. It was applied for 45s at 20V using No.70 - 1730 Electromet III Polisher/Etcher equipment of Buehler Ltd. The solution used for electrolytic polishing consisted of H_3PO_4 (37ml), glycergia (56ml), and H_2O (7ml), based on the recommendation of the manufacturers' manual [25]; the rest of the procedure remained the same. When these specimens were tested in ferric chloride, crevice corrosion was observed on the bottom face. Lee [13] in his study on AISI 316L and cast duplex CF-8 stainless steels, observed that crevice corrosion occurred at a much lower potential than the pitting corrosion. Thus, many reports of pitting potentials were found to be the actual potentials of crevice corrosion at the interface between the specimen and the mounting material. In the light of these facts the procedure was further modified to 600 grit grinding,

mechanical polishing by 0.05 micron gamma powder, and then plastic mounting using a blend of 5 parts of resin (Expo - Kwick Resin No. 20 - 8136 - 128 of Buehler) and 1 part of resin (Expo - Kwick Hardner No. 20 - 8138 -032 of Buehler). After mounting, the plastic casting was drilled at the bottom to expose the specimen for the electrical contact necessary for electropolishing. The hole was sealed before the immersion test. Two coats of a commercial transparent nail polish, with a base of acrylates copolymers and cellulose acetate butyrate, were applied at top plastic - metal interface to avoid crevice corrosion. This technique proved effective unless a pit formed at the edge of the coating.

The specimens were tested for pitting using petri dishes and 50 ml beakers. A few specimens were also tested in the upside-down position with only the top face dipped into the solution, but they suffered slight crevice corrosion at the metal-clamp interface which later on corroded the steel clamp due to the galvanic corrosion. The role of the electrolyte was played by the vapors of the corrodant.

The solutions selected for pitting tests were (i) Ferric Chloride with concentrations of 0.04M, 0.2M, 0.4M, 0.75M, 1.11M, and 1.85M (ii) Ammonium peroxydisulfate with concentrations of 0.45M and 0.9M (iii) Cupric chloride of 0.6M concentration.

The alloy was tested in chloride solutions due to its

tendency towards pitting in neutral and acid chlorides. The table of corrosion rates in reference 25 shows that pitting occurred mostly in the environment of chlorides, for example, sodium chloride, ammonium chloride, acetic acid plus sodium chloride, zinc chloride, and barium chloride. The results of the table are based on tests conducted at 80 C while the present research consists of tests conducted at 22 C. Cupric chloride tests were conducted to fill-in the gaps of the table. Various concentrations were used to study the extent of pitting attack. Pitting tests have been conducted in chloride-sulphate media [9] but not in ammonium peroxydisulfate at room temperature. This was chosen because it caused pitting and SCC in Alloy 400 [43].

All the specimens were water rinsed, methanol flooded and ultrasonically cleaned after immersion. The mounted specimens were only rinsed with water because methanol acts as a solvent for the plastic casting and nail polish. Table II shows the layout of the above tests.

Examination of the specimens consisted of visual inspection and microscopic examination under (a) Bausch & Lomb Zoom Microscope at 70 X (b) Olympus Optical Microscope at 200 X and 800X. Some photographs were also taken through these microscopes. The significant samples were examined and photographed under a JEOL JSM-35 Scanning Electron

TABLE II
LAYOUT OF PITTING TESTS

SAMPLE	SENSITIZED	SURFACE TREATMENT	CONC	DURATION
SOLUTION : FERRIC CHLORIDE				
0A	Y ⁽¹⁾	MP	0.04	24 h
1A	Y	EP	0.04	24 h
2A	N ⁽²⁾	EP	0.04	96 h
0B	Y	MP	0.2	24 h
21B	N	EP	0.2	24 h
2B	N	EP	0.2	96 h
0C	Y	MP	0.4	24 h
1C	N	EP	0.4	24 h
2C	N	EP	0.4	96 h
3C	N	EP + MTD ⁽⁵⁾	0.4	24 h
4C/9	N	EP + MTD + NPC ⁽⁶⁾	0.4	9 min
4C/27	N	EP + MTD + NPC	0.4	27 min
4C/45	Y	EP + MTD + NPC	0.4	45 min
4C/90	N	EP + MTD + NPC	0.4	90 min
4C/12	Y	EP + MTD + NPC	0.4	12 h
US	N	EP	0.4	24 h
IS	Y	EP	0.4	24 h
AR	Y	EP	0.4	24 h
T1	Y	MP + ULT ⁽⁸⁾	0.4	24 h
T2	Y	EP	0.4	24 h
T3	Y	MP	0.4	24 h
T4	Y	EP + ULT	0.4	24 h
0D	Y	MP	0.4	24 h
1D	N	EP	0.75	24 h
2D	N	EP	0.75	72 h
2E	N	EP	0.92	36 h
2F	N	EP	1.11	36 h
2.1	N	EP	1.85	24 h
4H/9	Y	EP + MTD + NPC	1.85	9 min
4H/27	N	EP + MTD + NPC	1.85	27 min
4H/45	Y	EP + MTD + NPC	1.85	45 min
4H/90	N	EP + MTD + NPC	1.85	90 min
4H/24	Y	EP + MTD + NPC	1.85	24 h
SOLUTION : AMMONIUM PEROXYDISULFATE				
5AC/45	N	EP + MTD + NPC	0.45	45 min
5AC/24	Y	EP	0.94	24 h

TABLE II (Continued)

SAMPLE	SENSITIZED	SURFACE TREATMENT	CONC	DURATION
SOLUTION : CUPRIC CHLORIDE				
6cc/g	N	600 grit + NPC	0.6	24 h
6cc/p	N	EP + NPC	0.6	24 h
SOLUTION : HCl ACID				
2 H 1/24	Y	EP	2 %	24 h
5 H 1/24	Y	EP	5 %	24 h
10 H2/24	Y	EP	10 %	24 h

- (1) Yes
- (2) No
- (3) Mechanically polished
- (4) Electropolished
- (5) Mounted
- (6) Nail polish coating
- (7) Ultrasonic cleaning

Microscope (SEM).

During the experimentation the issue of heat treatment arose since the as-received bar was found to be sensitized to a higher degree. Desensitization was achieved by soaking the specimen for 2 h at 1090 C and then immediately quenching in water. In order to achieve ideal sensitization the specimen was soaked for 1 h at 1095 C water quenched and then resoaked for 2 h at 715 C followed by furnace cooling. These heat treatments were carried out without vacuum. The test results were confirmed by using the Streicher Test in accordance with ASTM-A-262.[24] The ditch structure (dark grain boundaries) occurred when the material was sensitized and the chromium carbides dissolved faster than the matrix. On the other hand the unsensitized specimen showed a step structure which was due to the normal difference in diffusion rates at different crystal orientations [39]. The samples were examined under the Olympus Optical Microscope at 200X.

4.3 Stress Corrosion Cracking Tests

Stress corrosion cracking tests were first performed on prestressed samples before switching over to SST.

The specimen were prepared in the same way as for pitting tests. After mechanical and (or) electropolishing, the top face was indented by a 3/16 inches diameter ball under a load of 8000 pound. The test samples were also subjected to various heat treatments. Long duration

immersion tests were then conducted on these specimens, ranging from 10 days in 0.4 M ferric chloride to 30 days in 2M magnesium chloride ($MgCl_2$), to get intergranular cracking. Tests in magnesium chloride were conducted at 82 C. Visual and microscopic examinations were then carried out. This technique has been used successfully by Markey [46].

For the SST study the specimens were machined to a waisted geometry from a hot rolled bar. The minimum diameter was 0.25 inches (6.35 millimeters) Figure 4 shows the geometry of the specimen. The samples were then heat treated, finished to 600 grit, and polished by 0.5 μm alumina powder to get an adequate surface, free from circumferential and longitudinal scratches and grinding marks. The heat treatments are given in Table VIII. It must be noted that vacuum was not maintained.

The tests were conducted at room temperature on an MTS machine with 0.4M ferric chloride contained in the solution cell. The arrangement is shown in Figure 5. The experiments were carried out under stroke control which was selected as 20 % of actual 6" stroke. The time of completion of this stroke (ramp rate) varied from 1×10^5 to 5×10^5 s (Table VIII). After failure, the samples were ultrasonically cleaned and dried in air. Later, visual examination, microscopic examination under the zoom microscope (70x), and SEM examination were performed.

Figure 4. Geometry of the Waisted Specimen Used for the Slow Strain Rate Tests

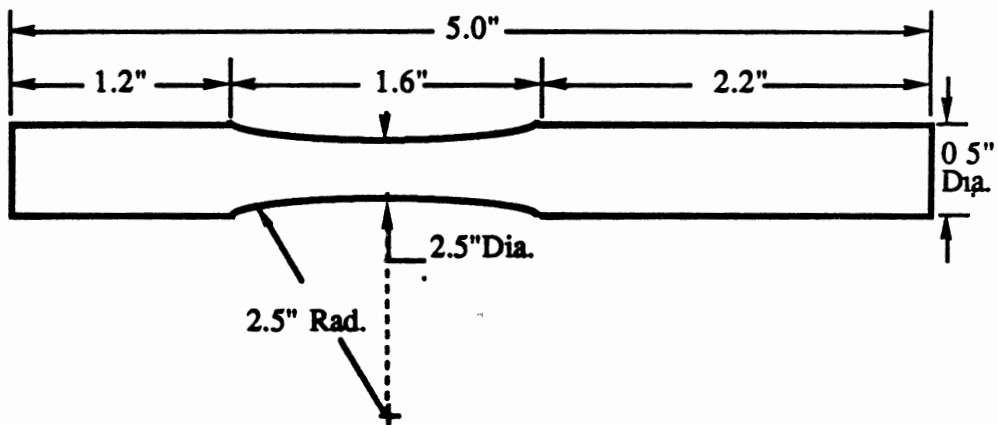
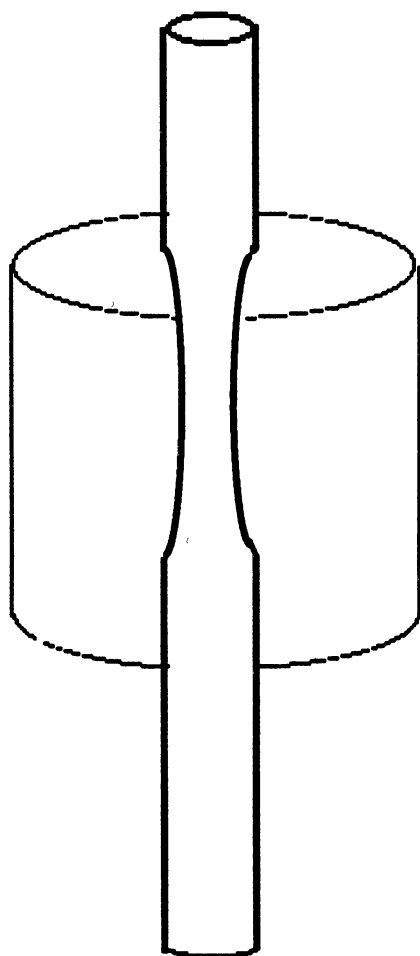


Figure 5. Mounting Arrangement of the Slow Strain Rate Testing Samples



4.4 Fatigue Tests

Fatigue tests were carried out to study LME in the mercury (Hg) environment and corrosion fatigue (CF) in 0.4M ferric chloride. These were done to clarify the sensitization issue.

The specimens were prepared in a similar way as for the slow strain rate tests except that a few of them were cleaned by a swab of 10 % HCl to get rid of the oxide film. All the tests were conducted at room temperature.

The MTS machine was set at 100 % stroke control while the fatigue tests were performed under load control at 50 % of the actual capacity. For 100 % stroke, the time selected was 5×10^3 s. Before the mounting of specimen, its hardness was tested at the constant diameter grip ends in order to get the tensile strength value from the graph of material strength vs. hardness [25]. Peak load was calculated on the basis of 70 % of the tensile strength while minimum load was fixed at 0.5 kips. Cyclic loading was applied using a sinusoidal wave form, mostly at 15Hz frequency. These experimental features are illustrated in Table IX. The fractured specimen were then flooded with trichoro ethylene, and ultrasonically cleaned and dried. After visual and microscopic (zoom microscope) examination, the edge (approximately 0.5") of the fractured specimen was cut for examination under JEOL JSM-35 Scanning Electron Microscope. The specimens of interest were photographed. The fractured waisted section were also tested for hardness. The

Streicher test was also applied on the specimens prepared from the grip-ends of the fractured sample so as to check the results of heat treatment.

CHAPTER V

RESULTS AND DISCUSSION

5.1 Crevice Corrosion

The immersion test results in ferric chloride show slight crevice corrosion and pitting with the top oxide film hanging inwards after undercutting, Figure 6. Due to the polished bottom surface, the crevice attack is less as compared to other samples, Figure 7, and thus less crystalline. Crevice corrosion of the unpolished surface is shown in Figures 8 and 9. The severity of the attack is due to the rough surface and the higher concentrations. A closer view of Figure 9 is shown in Figure 10 which is highly crystalline and shiny. Undercutting should also be noted at the edges of the circular rings in Figures 8 and 9. It can be observed in Table III that when crevice corrosion increases the number of pits and/or size of pits on the top face decreases. This fact points out that the top face acts as a cathode as compared to the bottom face which becomes an anode. Thus the bottom face is corroded more due to crevice attack.

When the specimens were mounted, the plastic-metal interface became the crevice site, Figure 11. The plastic-metal interface was later coated by a commercial nail polish

**Figure 6. The Top Oxide Film Hanging Inwards of a Pit
(200 x)**

**Figure 7. Crevice Corrosion on a Polished Bottom Face
(200 x)**

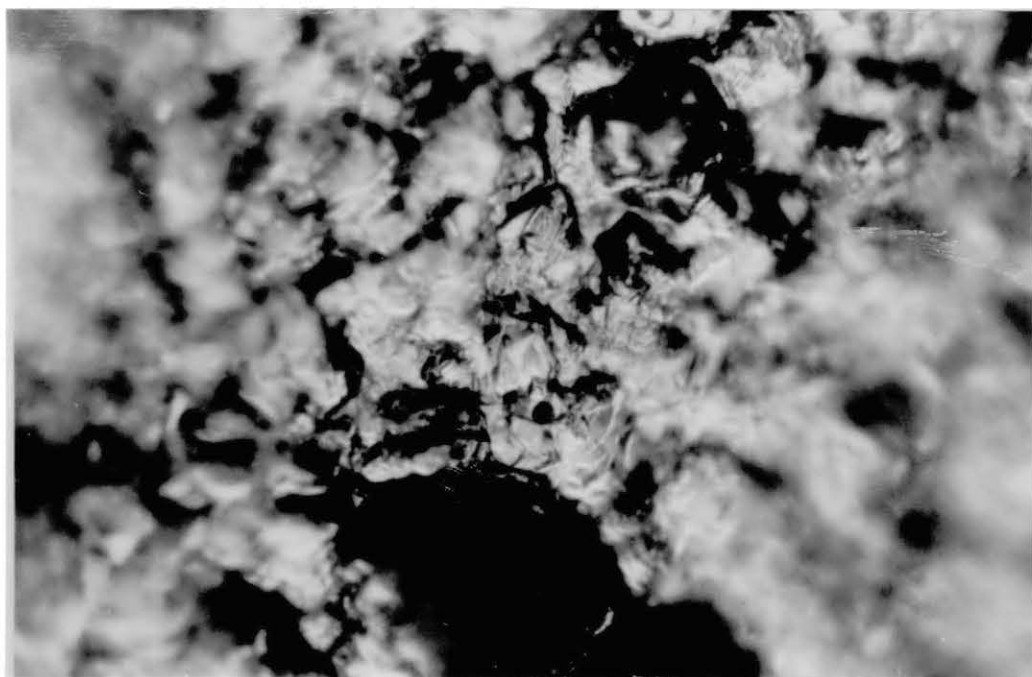


Figure 8. Severe Crevice Corrosion on the Unpolished Bottom Face of the Specimen in 1.11M FeCl_3 . Note the Ring Pattern and Undercutting Along the Periphery

Figure 9. Severity of Crevice Corrosion Has Increased with an Increase in Concentration to 1.85M of FeCl_3 . The Ring Has Become More Deep and Wide

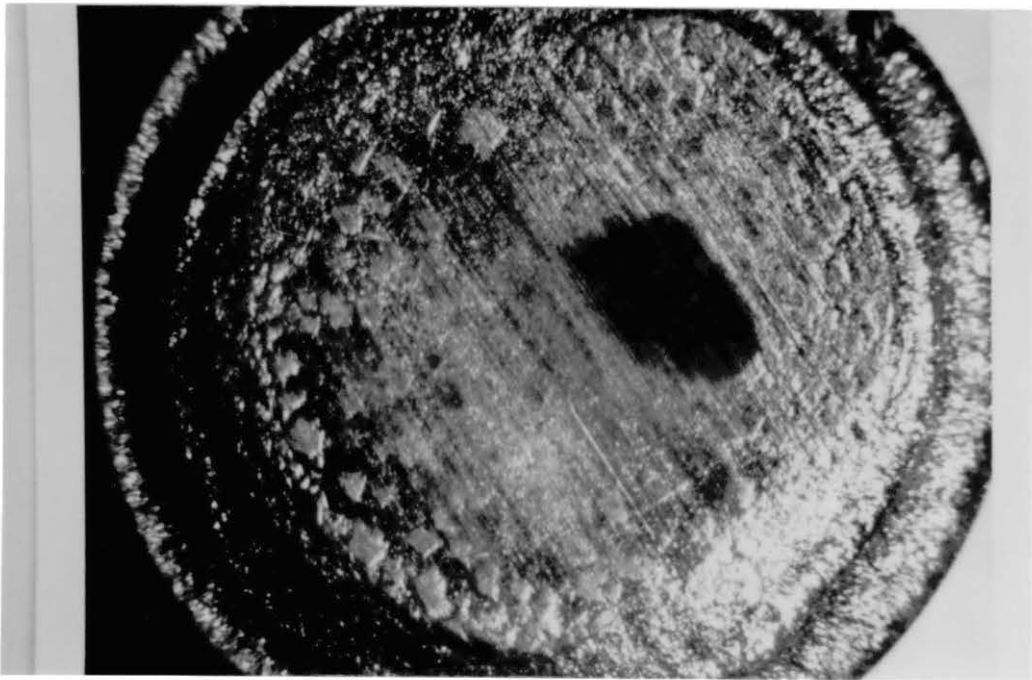
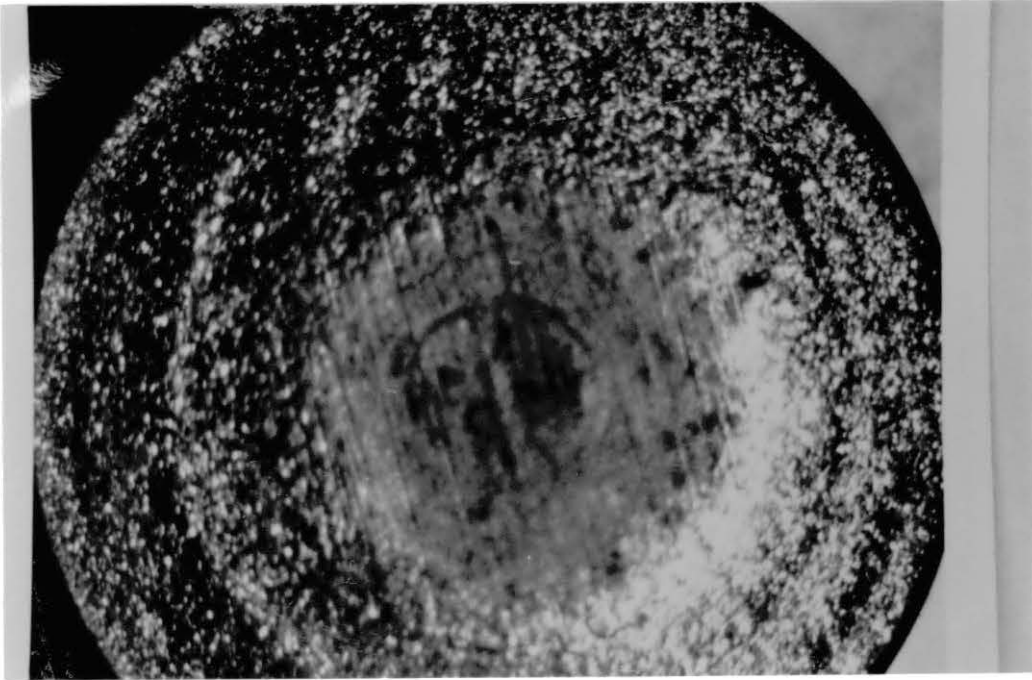


Figure 10. Magnified View of Figure 9 (200 x)

Figure 11. Crevice Corrosion at the Plastic-metal
Interface (200 x)

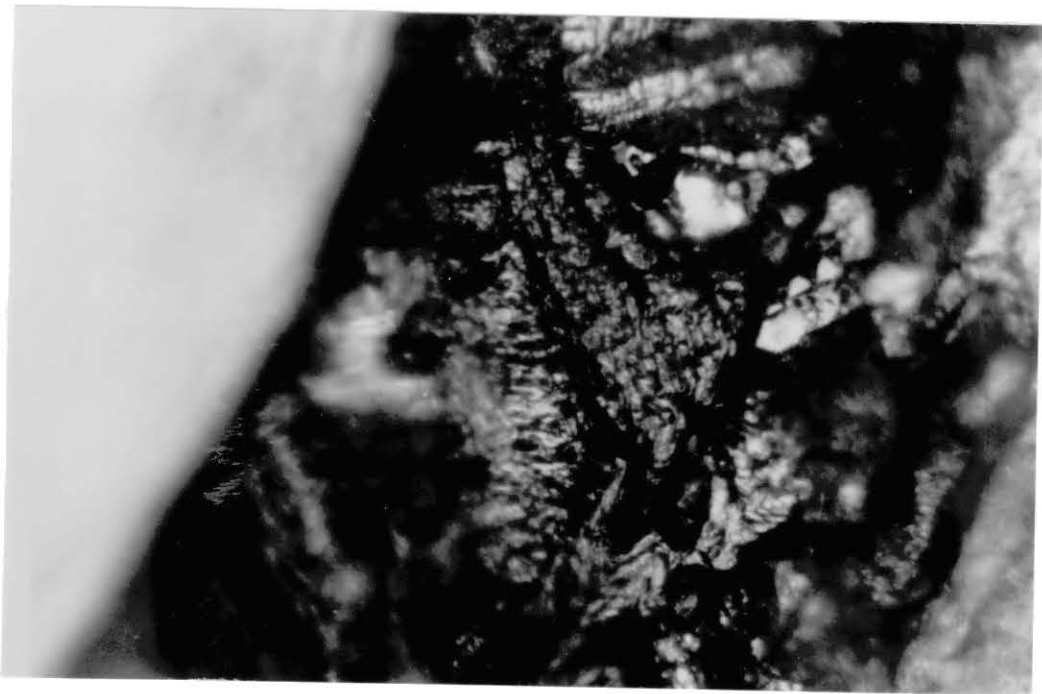
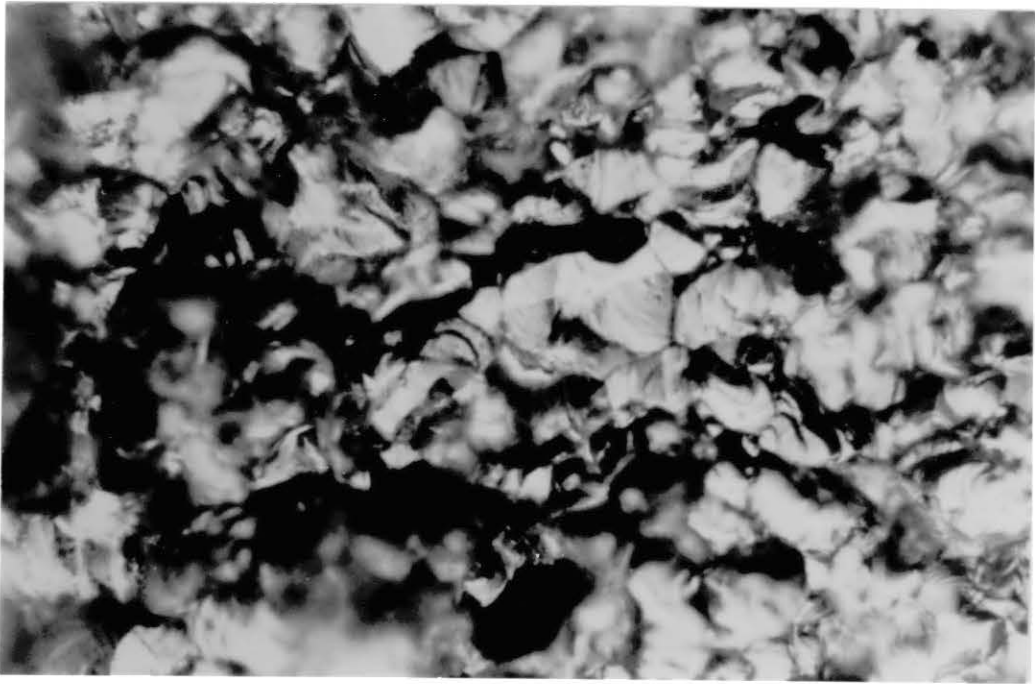


TABLE III
EFFECT OF CREVICE CORROSION ON PITTING

SAMPLE	CONC. (M)	# OF PITS	CREVICE CORR.
0A	0.04	3	-
1A	0.04	1	slight
2A	0.04	7	slight
0B	0.2	1	medium
1B	0.2	4	severe
2B	0.2	3	severe
0C	0.4	3	slight
1C	0.4	2	medium
T ₁	0.4	3	severe
T ₂	0.4	23	medium
T ₃	0.4	2	medium
T ₄	0.4	22	medium
0D	0.75	8	medium
1D	0.75	4	severe
2D	0.75	3	highly severe

which proved effective, Figure 2. Crevice corrosion under the nail polish was observed when a pit formed near the metal nail polish interface and went under the coating thus causing crevice corrosion, Figures 12 and 13. Alloy 800 is so prone to crevice corrosion in ferric chloride that even vapors and slight crevices are enough to initiate the attack. This was observed when a few samples were tested in 0.4M of ferric chloride by clamping them upside down so that only the top face was immersed. The interface of steel clamp and the specimen served as a crevice for the evaporating solution and it started corroding the sample. On the other hand, galvanic corrosion started between Alloy 800 and the steel clamp which destroyed the ends of the clamp. Even during the slow strain rate tests and fatigue test in 0.4M FeCl_3 the specimens experienced crevice corrosion at the metal-cup interface. Figure 14 shows pitting within the crevice corrosion site.

The tendency towards crevice corrosion is higher in Alloy 800 as compared to Alloy 400 and Alloy 600. This trend can be attributed to the higher silicon content of Alloy 800 which no doubt increases the resistance to pit initiation but decreases its resistance to crevice corrosion [30].

During the immersion tests in ferric chloride, it was found that in the case of corrosion, a color change took place from dark yellow to yellowish-green which later changed to a dark patina color. Evans [22] related the

Figure 12. Pit Formed near the Metal/Coating Interface and Penetrated Under the Coating with Increasing Depth and Undercutting thus Causing Crevice Corrosion Beneath the Coating (200 x)

Figure 13. A Pit, Partly Under the Coating, is Initiating Crevice Corrosion (200 x)

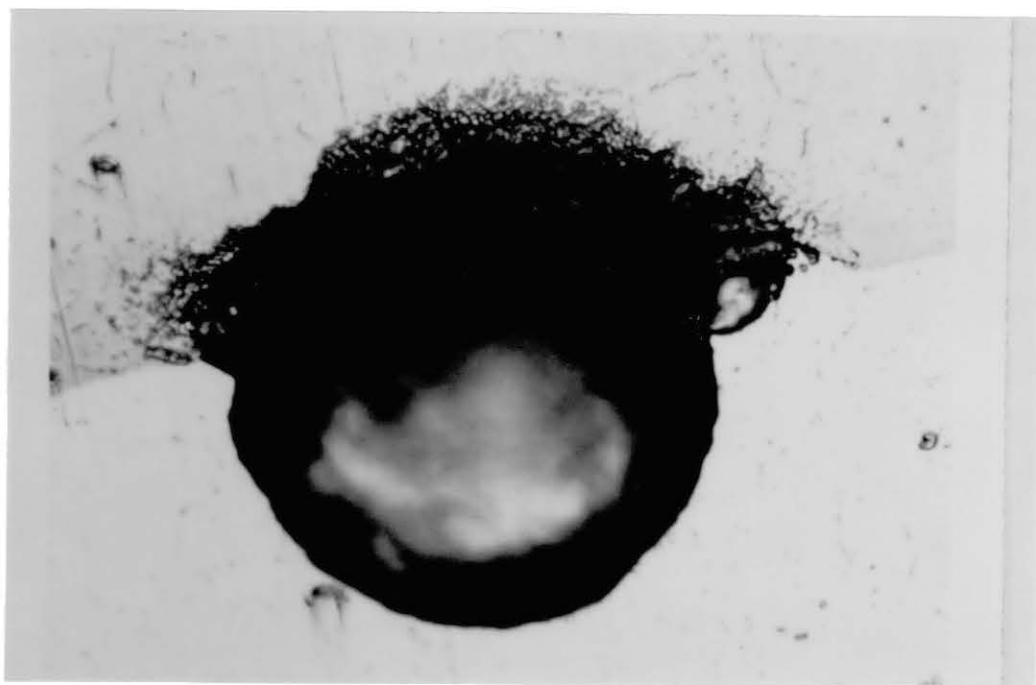
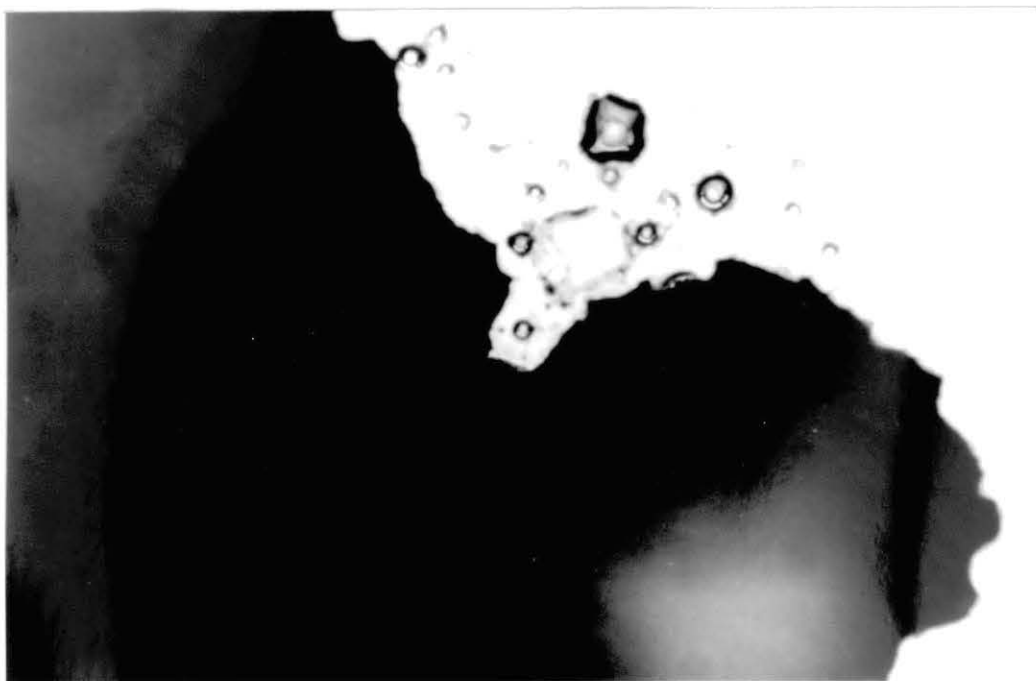
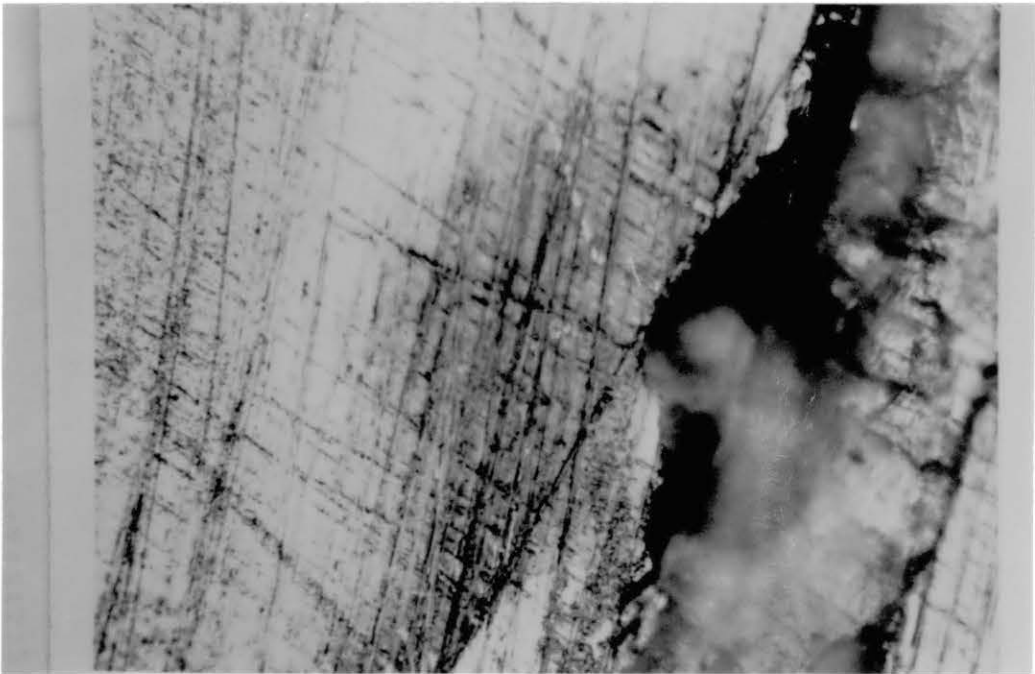
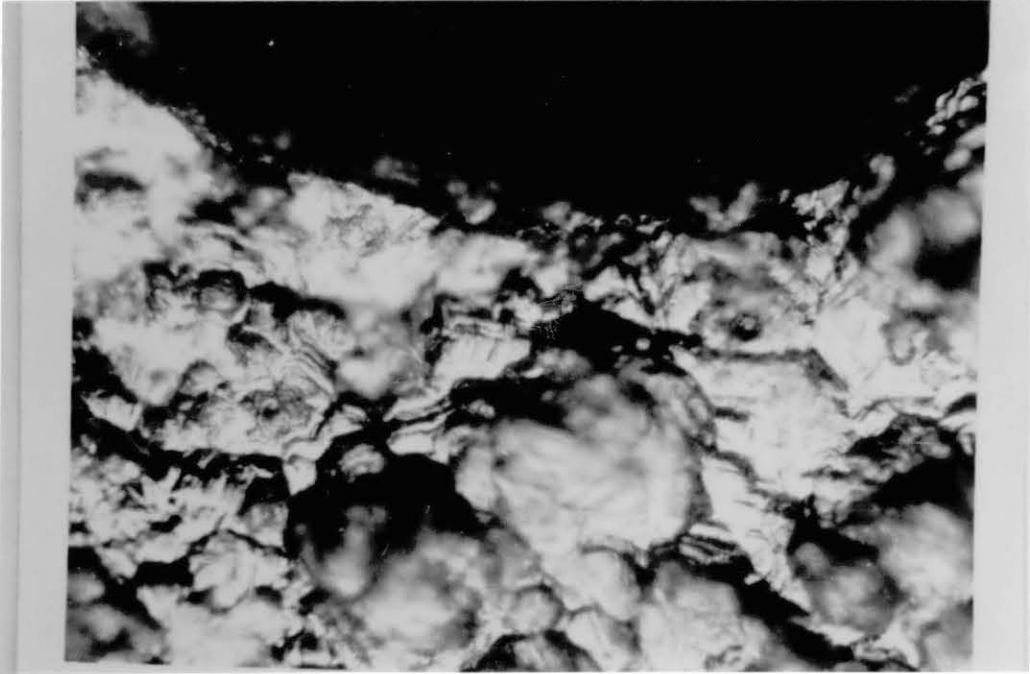


Figure 14. Pit Formation Within a Crevice Corrosion Site
(200 x)

Figure 15. The Scratches Carried 0.6M Cupric Chloride
Underneath the Coating Thus Causing Crevice
Corrosion



green color to cupric chloride which forms by the action of oxygen on the small amount of cuprous chloride present in the solution.

Scratches on the surface had to be avoided because when they occurred they served as capillaries to carry the corrodant underneath the coating and hence caused crevice corrosion, Figure 15.

5.2 Pitting Tests

The results of pitting test indicate that basically pit initiation is dependent upon surface finish, alloying elements and their composition, and heat treatment including the degree of sensitization and oxide film formation. The scratches on the surface can only be deleterious if there is any residual stress associated with it. Figure 16 and 17 show side pitting, which was caused due to scratch marks formed during hot rolling. These scratches along with residual stresses become a preferential pit site, Figure 16 shows the scratches and a few round pits while Figure 17 shows a longitudinal pit following the scratch. Some pitting results are tabulated in Tables IV and V.

Alloying elements and their composition also play a vital role in pit initiation, for example Ni, Cr, Si, Mo, Ti or Ti-C ratio etc [10,18,30,31,32,19]. The critical alloying element in Alloy 800 is titanium. Although it is added to prevent intergranular corrosion but it becomes a pitting site as pointed out in references 10 and 18.

Figure 16. Pits Formed on the Sides of the Specimens are
Following the Pre-working Marks

Figure 17. Longitudinal Side Pit Following the Rubbing
marks

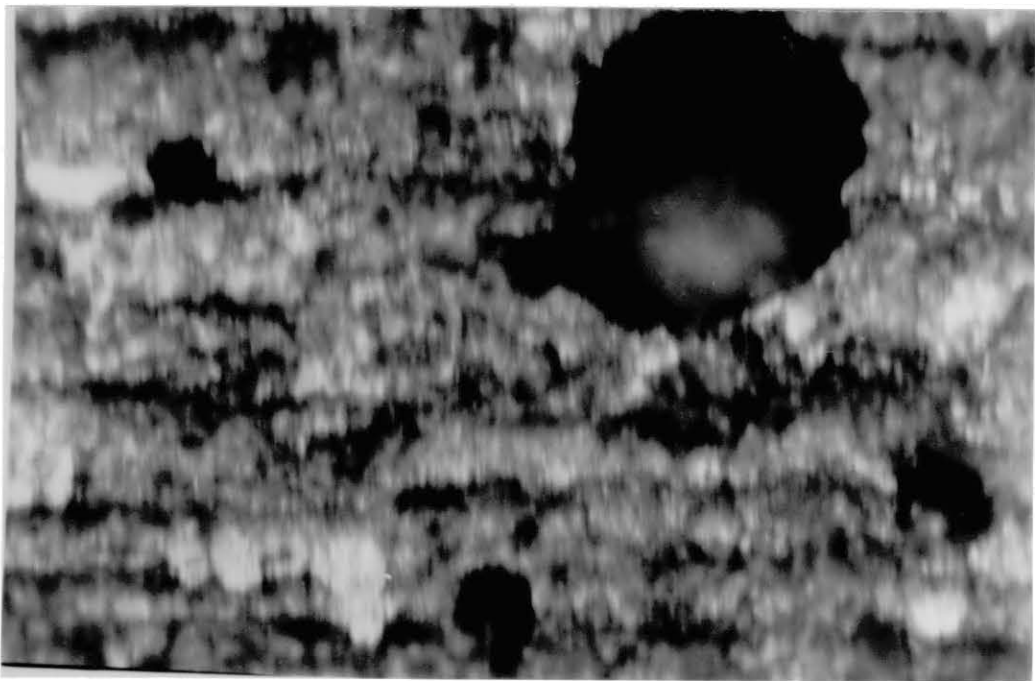
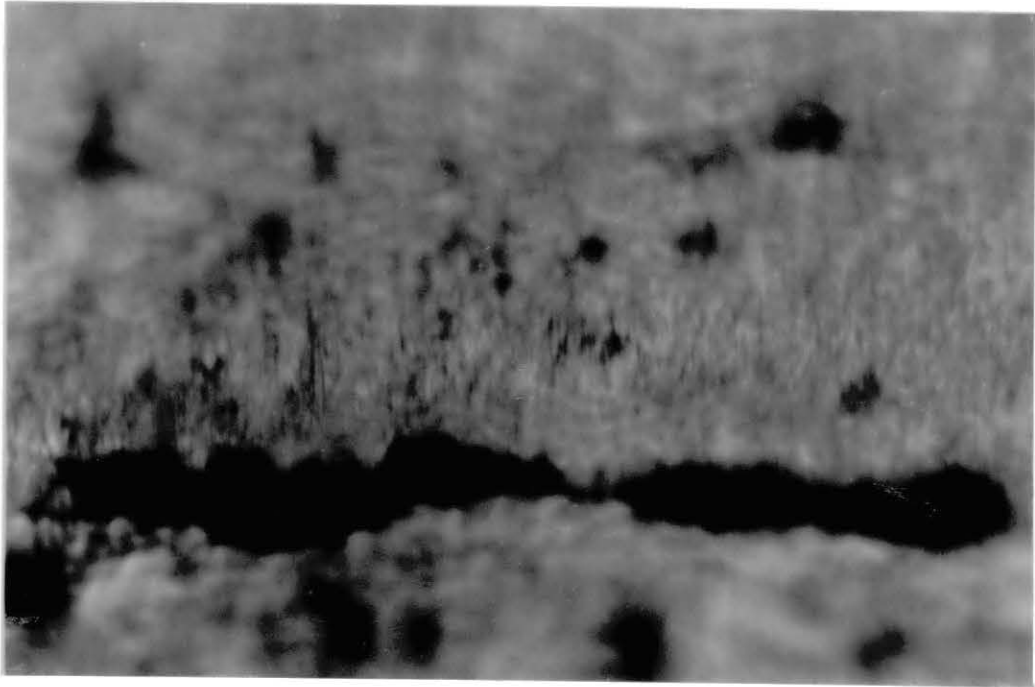


TABLE IV

RESULTS OF PITTING TESTS IN VARIOUS CONCENTRATIONS
OF FERRIC CHLORIDE CONDUCTED ON UNSENSITIZED SPECIMEN
AT AMBIENT TEMPERATURES FOR 24 H.

Sample	Concentration (M)	No. Of Pits
1A	0.04	1
1B	0.2	4
1C	0.4	3
1D	0.75	7
2E	0.92	5
2F	1.11	11
2.1	1.85	36

TABLE V

RESULTS OF THE SENSITIZED SPECIMENS TESTED FOR
DIFFERENT TIME INTERVALS IN 0.4M. FERRIC CHLORIDE
AT AMBIENT TEMPERATURE

Sample	Time	No. Of Pits
4C/45	45 min	12
4C/12	12 h	34
4C/24	24 h	100

Figure 18 shows a general view of the pitted surface tested in 0.4M FeCl₃. Figure 19 (is the smallest pit that can be seen in Figure 18. Figure 20 is slightly larger. Notice the shiny particles of titanium nitride. These titanium nitride particles do not corrode themselves rather they behave cathodically thus causing preferential attack on the nearby matrix alloy. Bradshaw [18] in his high temperature study (below 400 C) found out that roughly the number of pits were equal to the number of titanium carbonitride inclusions. The present study does not show one-to-one correspondence.

From the morphology point of view, the interior of the pit is composed of shiny, crystalline facets (Figures 18, 19, 20, 21). The size of the facets change through the depth of the pit in a set pattern. As shown in Figure 22, the facets are finer near the surface but increase in size and become regular in shape when one goes further deep down. Again, at the root the facets gets finer. This pattern looks like a partially open bud, Figure 23. The shape of the pit is a combination of elliptical and horizontal pits [16] as shown in Figure 24 with a common feature of undercutting. Undercutting was severe when the specimen was sensitized. Severe pitting can be seen in Figure 25 where an unsensitized specimen was tested in 1.85M solution of ferric chloride for 24 hours.

Figure 26, 27, 28, 29, 30 shows the gradual pit growth in Alloy 800. At the center of Figure 26 the shiny black

Figure 18. General View of Pits. Note Their Irregularity
in Size and Distribution. This is typical
(10 x)

Figure 19. The Top Pit of a Vertical Line of Three at the
Center of Figure 18. It is Faceted and Has an
Irregular Shape (1000 x)

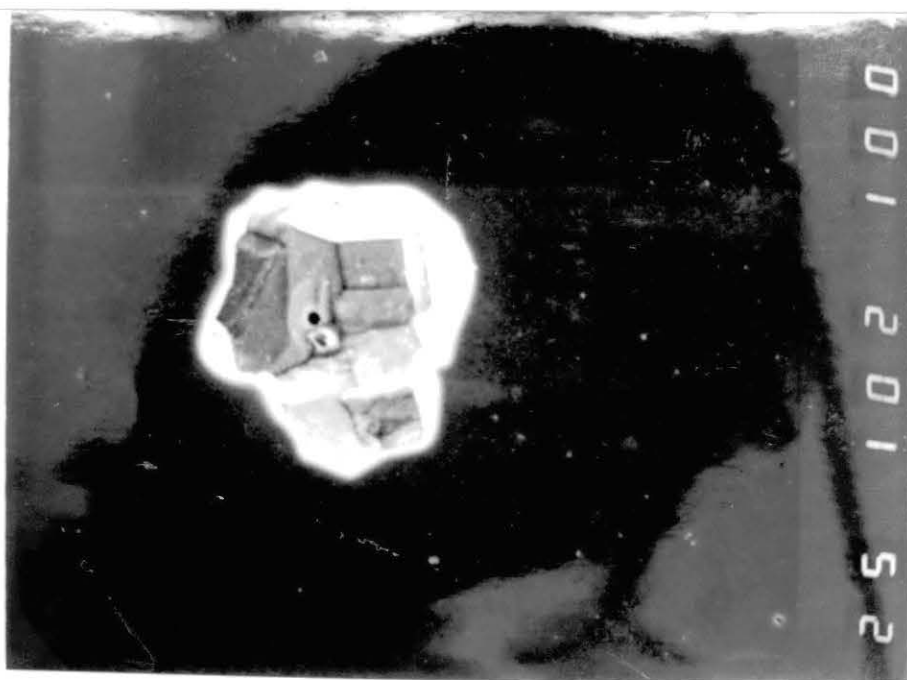
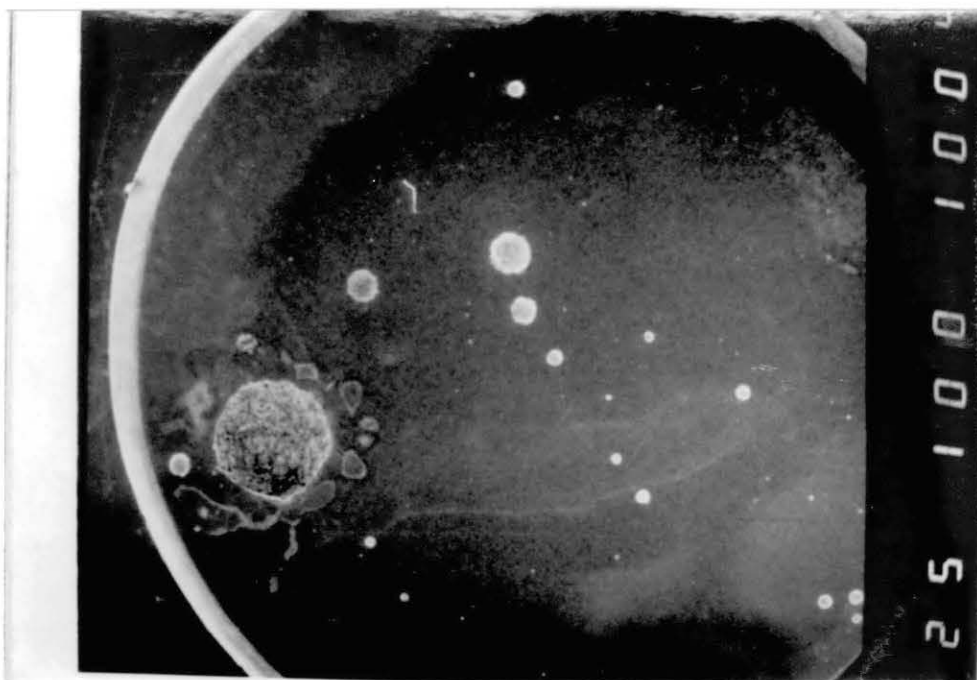


Figure 20. The Middle of the Three Pits Mentioned in Figure 19. Faceted Structure and Shiny Titanium Nitride is Visible. Seen are Precipitate Particles and Corrosion Debris on the Surfaces of the Facets (1000 x)

Figure 21. Closer View of a Medium Size Pit of Figure 18. Preferred Crystal Planes are Outlined (1000 x)

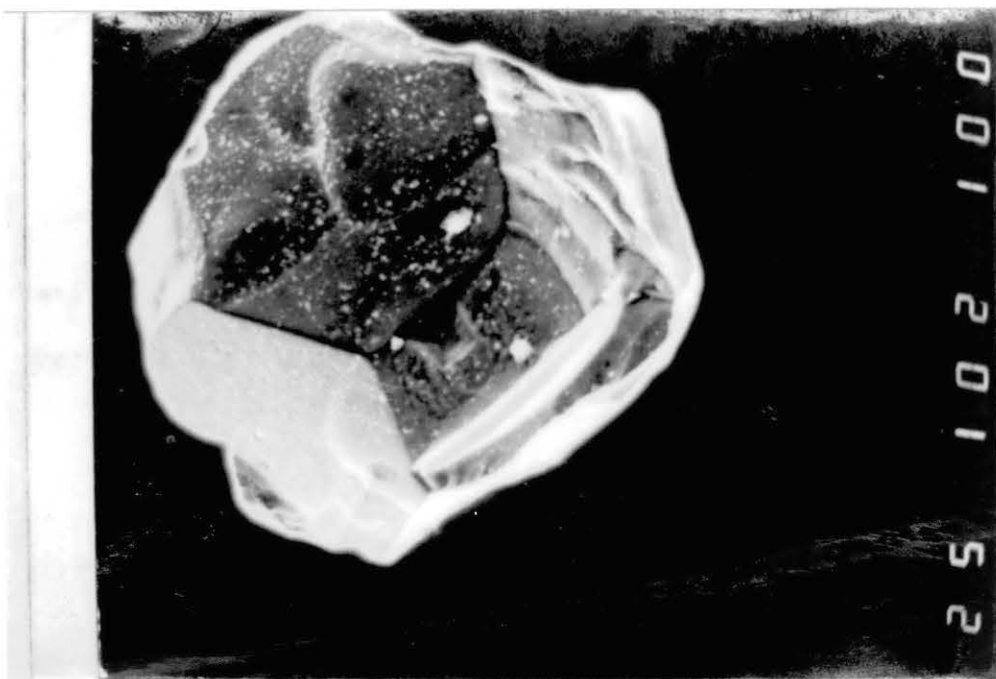


Figure 22. Structure of the Pit: Facets are Finer near the Edge and the Root While Coarser in between

Figure 23. Internal Detail of a Fully Developed Pit. Faceted, Shiny, Crystalline Structure. Features of Figure 22 Can Be Seen (200 x)

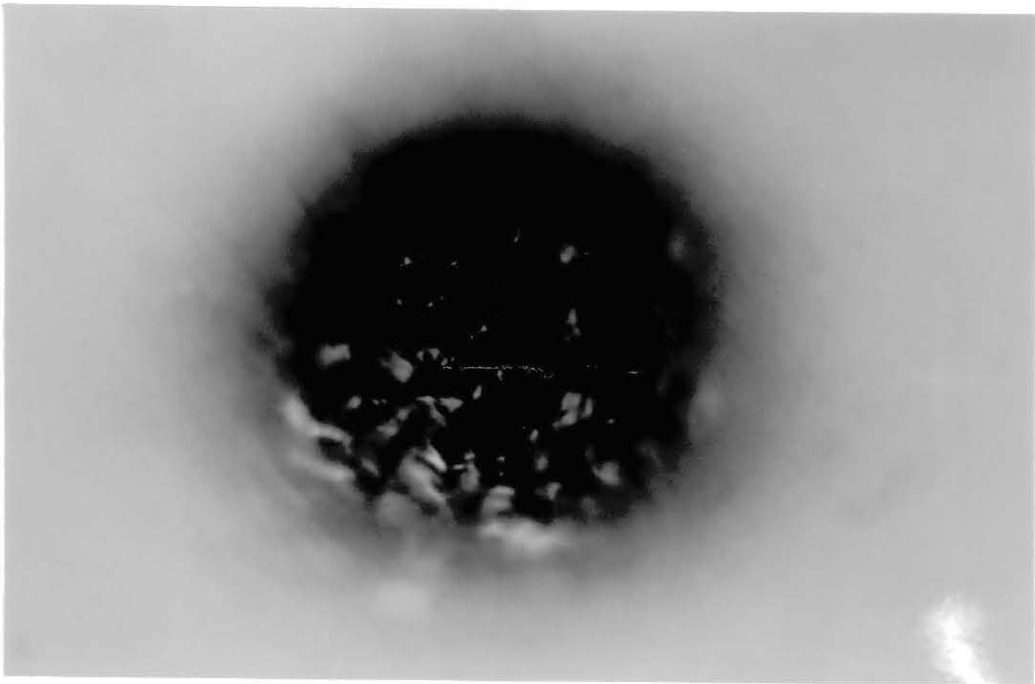
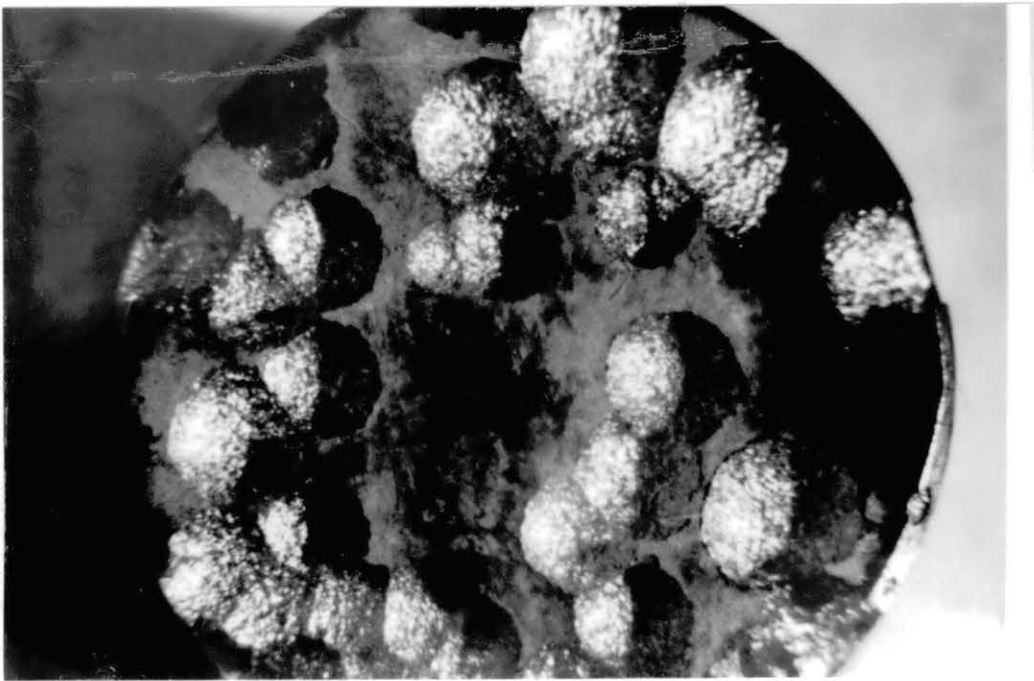


Figure 24. The Pit Shape is a Combination of Elliptical
and Horizontal Pits



Figure 25. Deep, Broad, and Undercut Pits Formed During a
24h Test in 1.85 (50%) Ferric Chloride



spot is the titanium nitride particle which is serving as a pit initiation site and hence the matrix around it is corroding. The solution used is 0.4M ferric chloride. In Figure 27 the pit size has slightly increased but the shape is more polygonal than a round one. Figure 28, 29 shows further increase but still irregularity in size. The pit shown in Figure 30 is a full grown round pit. Experimental observations indicate that a full grown pit after achieving a critical depth does not grow deeper, rather it starts widening through undercutting. Sometimes the pits also form clusters as shown in Figure 31.

Incubation time has not been increased very specifically but it was observed that after 24 hours there wasn't any appreciable increase in the number of pits. On the other hand, the span of time allowed the pits in the primitive stage to grow to a regular shape and size. The pitting tests with low concentrations of ferric chloride, for example, 0.04M (1%) and 0.2M (5%) concentration, showed that unsensitized material is nearly immune in this environment. A few very small pits were observed in 0.2M ferric chloride after 98 h showing that at low concentration larger incubation time is required.

During the study it was found that keeping all the variables (temperature, concentration, sample preparation) constant some specimens suffered pitting more severely as compared to others, for example, 4H/9 which was tested for 9 minutes in 50% (0.4M) ferric chloride got 150 well defined

Figure 26. The Black Shiny Particle at the Center is Titanium Nitride which is Serving as a Pit Initiation Site. The Solution Used is 0.4M Ferric Chloride (200 x)

Figure 27. The Pit Has Started Developing and is Polygonal (200 x)

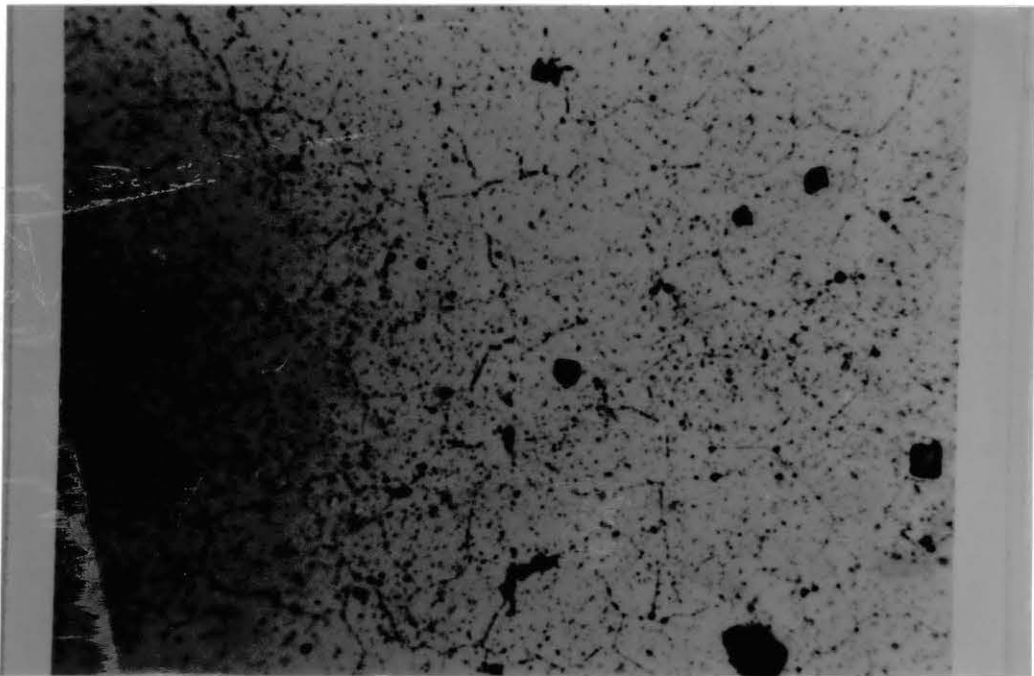
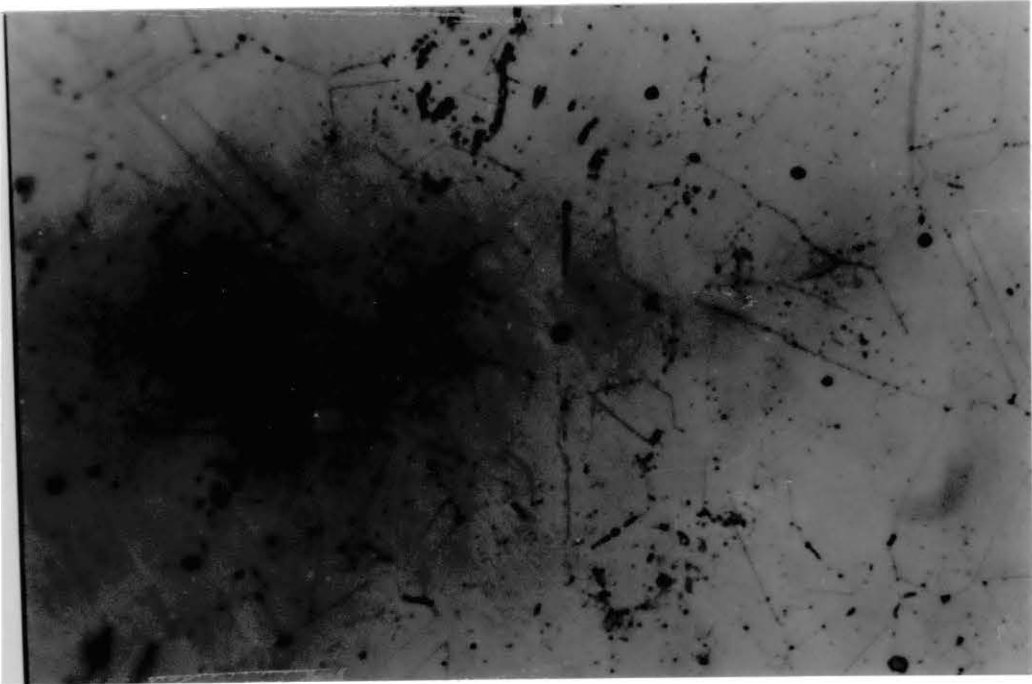


Figure 28. The Size of the Pit Has Increased as Compared to That in Figure 27 But is Irregular in Shape (200 x)

Figure 29. One-half of the Pit Has Become Round While the Other Half is Irregular in Shape (200 x)

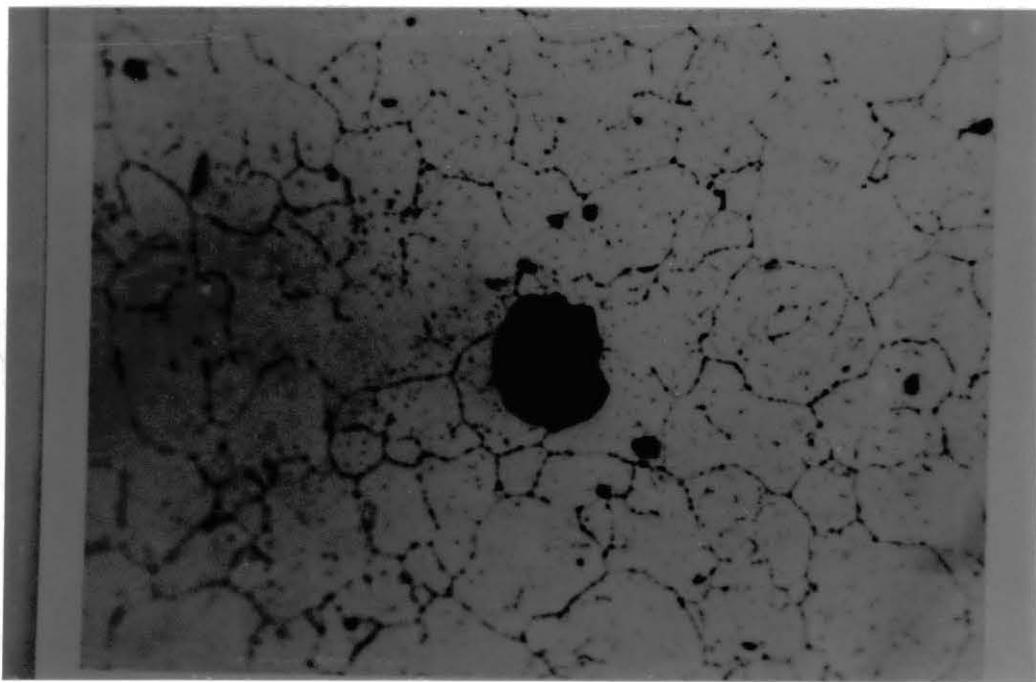
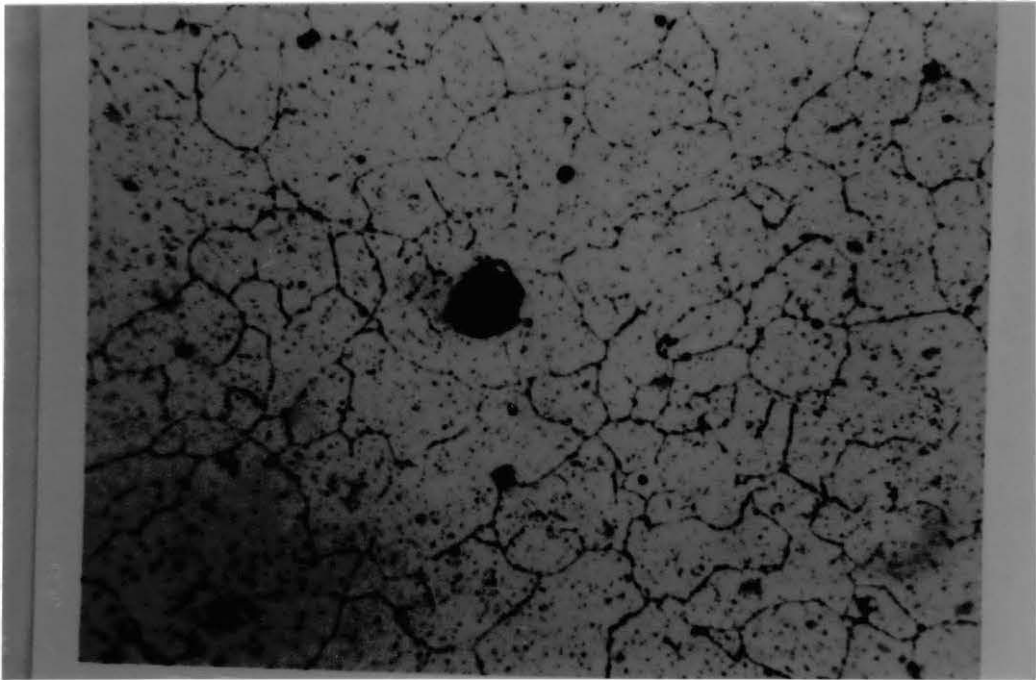


Figure 30. Fully Developed Round Pit (200 x)

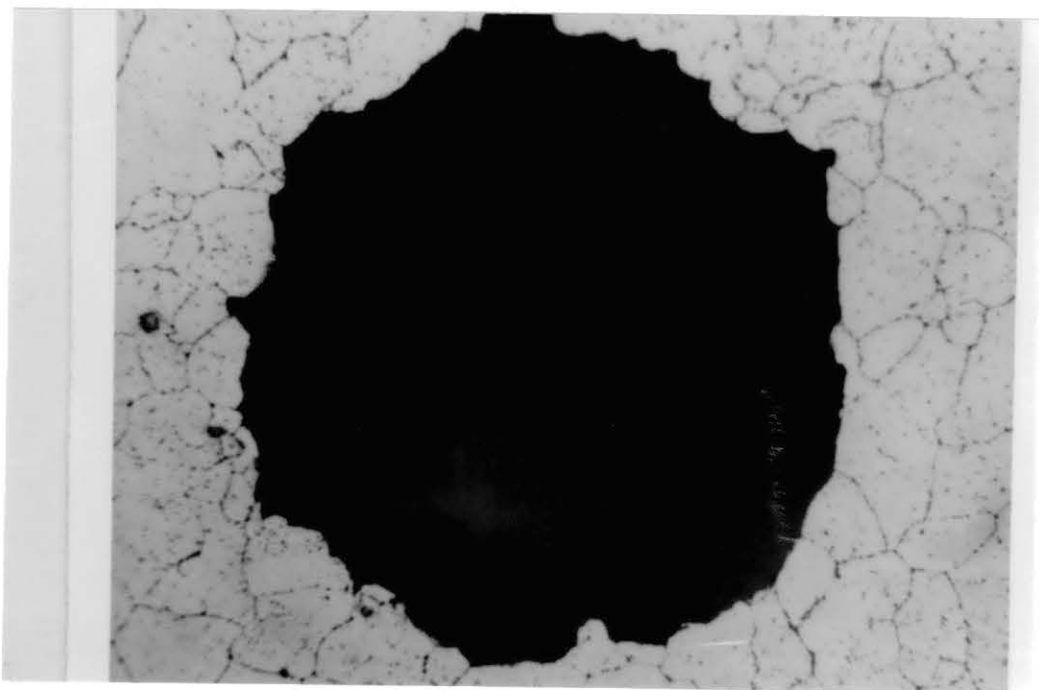
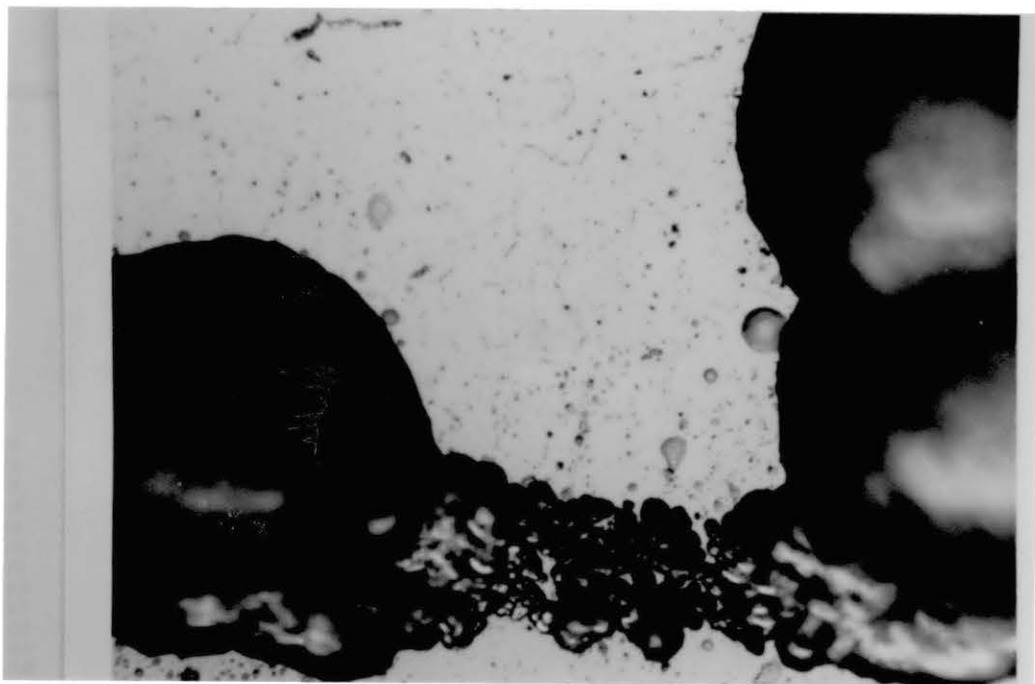


Figure 31. Coalescing Process of Pits Observed in 1.85M
Ferric Chloride in 9 min of Immersion Test
(200 x)



pits. However 4H/27 which was immersed for 27 minute in the same solution showed only 8 underformed pits. This scatter in the data triggered the study of heat treatment effects on pitting. The higher the degree of sensitization the greater was its inclination towards pitting. Visual examination of an electropolished specimen under 200x showed that an unsensitized specimen had perfect austenitic type grain boundaries with annealing twins (AT) while the sensitized specimen revealed very few annealing twins. Compare the grain boundaries of Figure 1 with Figure 2. The former is unsensitized while the latter is partially sensitized. It was also found that the unsensitized specimen had higher hardness and greater strength (Table VI). The issue of sensitization is quite delicate in the case of Alloy 800 regarding both the procedure adopted and the method of testing. It has been discussed in Chapter 2 that the degree of sensitization depends on the rate of carbide precipitation relative to the rate of chromium diffusion in the matrix [1]. Pritchard [26] chose the sensitization condition as 22 h at 550 C and tested it by a modified Strauss test. They considered this procedure better than Hooper's procedure of 7h at 600 or 700 C. Pritchard also disregarded the Streicher test because its results showed a specimen, with relatively high Ti:C ratio, as sensitized. Another study points out that Huey test dissolves TiC and hence wrongly suggests local attack possibility in an unsensitized material [1]. In the present study, the

TABLE VI
HARDNESS DATA WITH RESPECT TO SENSITIZATION

SAMPLE	SENSITIZED	HARDNESS	T.S* (ksi)
FFM1	Y**	70	78.0
FFM2	N***	93	101.0
FFM4	Y	75	80.0
FFM5	Y	73	73.3
FFM6	N	74	74.2
FFM7	Y	73	73.0

* Tensile Strength
** Yes
*** No

Streicher test has been used successfully for distinguishing between sensitized and unsensitized specimens. The experimental results suggest that it's not the Streicher test but the method of sensitization which requires better control and understanding. The Streicher test applied on the specimen with AT shows a step structure (ASTM 262-86), while the one without AT shows a ditch structure [24]. The time-temperature-sensitization diagrams of the manufacturer's handbook [25] were used to heat treat the specimens. These diagrams show that higher temperatures to bring carbides into solution can give complete sensitization. Also, the maximum corrosion region is quite spacious for higher temperatures as compared to the one in the low temperature diagram, thus giving greater flexibility. Shorter times have been preferred so as to restrict the chromium diffusion into the matrix. Optimum sensitization was achieved by soaking the specimen for 1h at 1095 C and water quenching it; re-soaking for 2h at 715 C and furnace cooling will give a completely sensitized specimen. For perfect unsensitization the specimen was soaked for 2h at 1090 C and water quenched. The Streicher test results of the two specimens show ditch and step type structures respectively. The as-received material (hot rolled bar stock 1/2" diameter) when tested for sensitization showed positive results (ditch structure). Although it is surprising, but there are chances of the material getting sensitized during hot rolling which can be performed in the

temperature range of 600 C - 720 C followed by slow cooling [25]. It is suggested that the manufacturers should apply better control over their products otherwise there can be in-operation failures, in corrosive environments. The application can be as pump shafts, valves, nozzles or boiler tubes where aggressive environments, including thermal cycles, can occur.

Heat treatment can affect pit initiation sites, morphology, and number of pits. Table VII shows that the unsensitized (US) specimen has 7 pits, the completely sensitized (IS) one has 557 pits (from $1\mu\text{m}$ - $50\mu\text{m}$), and as received (AR) has 104 pits. In Figure 32, surface of the US specimen is shown. There is some junk as well as titanium nitride particles which are acting cathodically, and hence, corroding the surrounding matrix. This can be seen in Figure 33 which is a 5000 X view of the center-right particle of Figure 32. The black spots are very tiny pits which coalesce to initiate an overall polygonal pit around the inclusion. Compare Figure 34 of the AR sample with Figure 32 of the US sample. It can be seen that the pits on the US sample are very very small. A closer view of the pit adjacent to the twin pits at the center of Figure 34, is shown in figure 35. A faceted, crystalline structure is obvious. Furthermore, there are pits within the pit. The AR sample has greater number of pits, which are well formed and round in shape, irrespective of their size. Undercutting is not significant. IS is suffered severe

TABLE VII

PITTING RESULTS OF UNSENSITIZED, COMPLETELY
SENSITIZED, AND PARTLY SENSITIZED SPECIMENS
TESTED IN 20 % FERRIC CHLORIDE

SAMPLE	SENSITIZED	# OF PITS
1 (US)	No	7
2 (IS)	Completely	557
3 (AR)	Partly	104

Figure 32. General View of the Pitted Unsensitized Specimen Tested in 20 % Ferric Chloride for 24 h. Scattered Polygonal Pits Can Be Seen where Shiny Particles are Titanium Nitride (300 x)

Figure 33. Center-right Particle of Figure 32 (5000 x) Which is Titanium Nitride. Note that the Surrounding Material is Corroding by Pit Formation

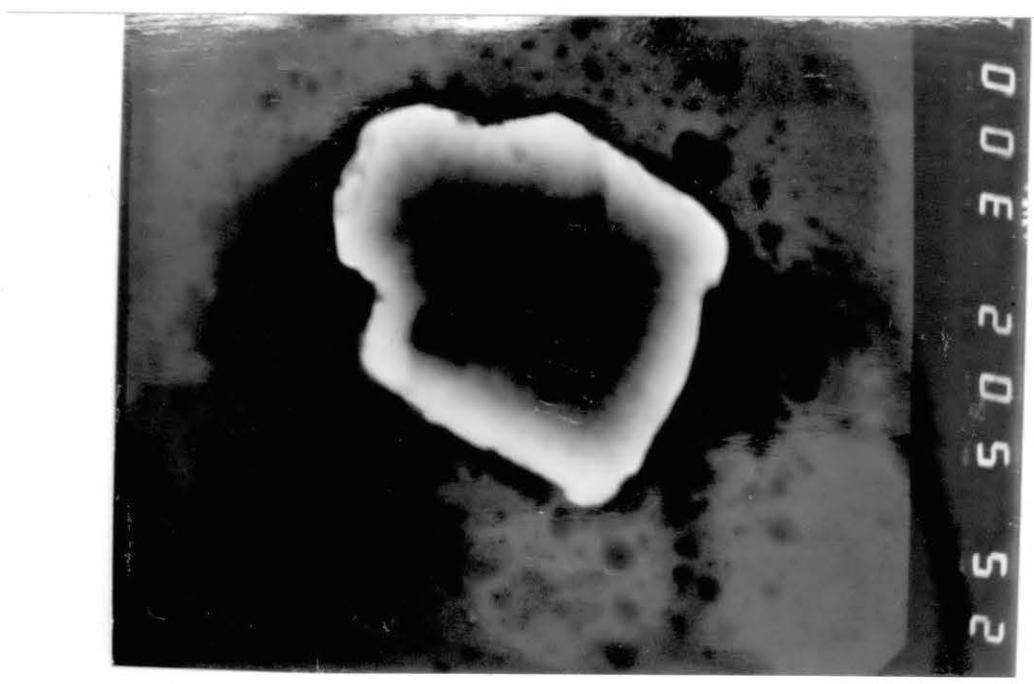
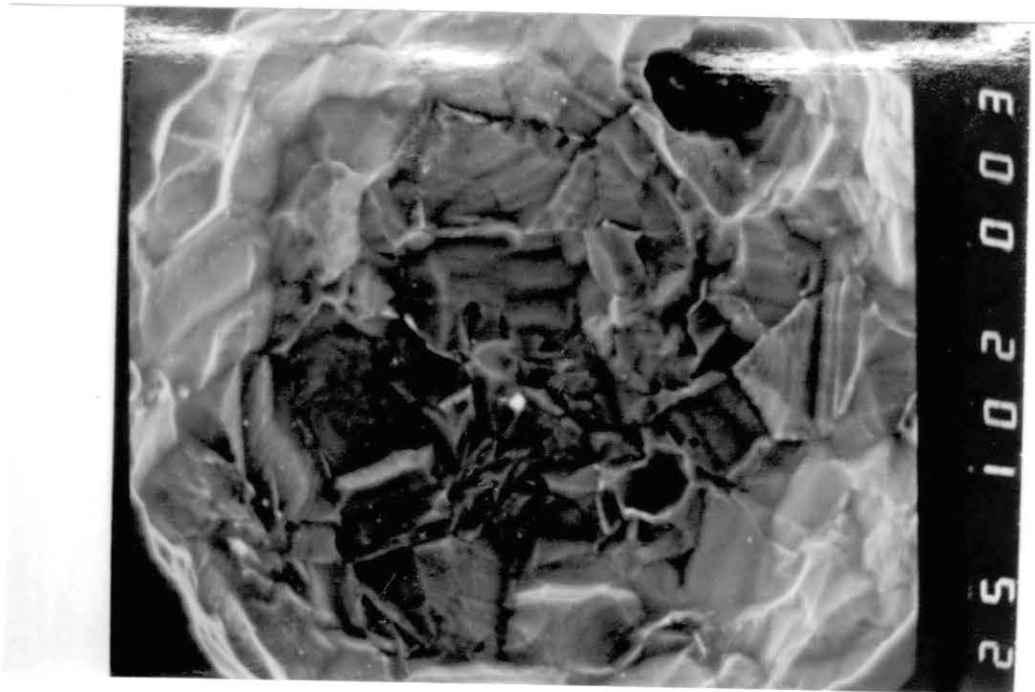
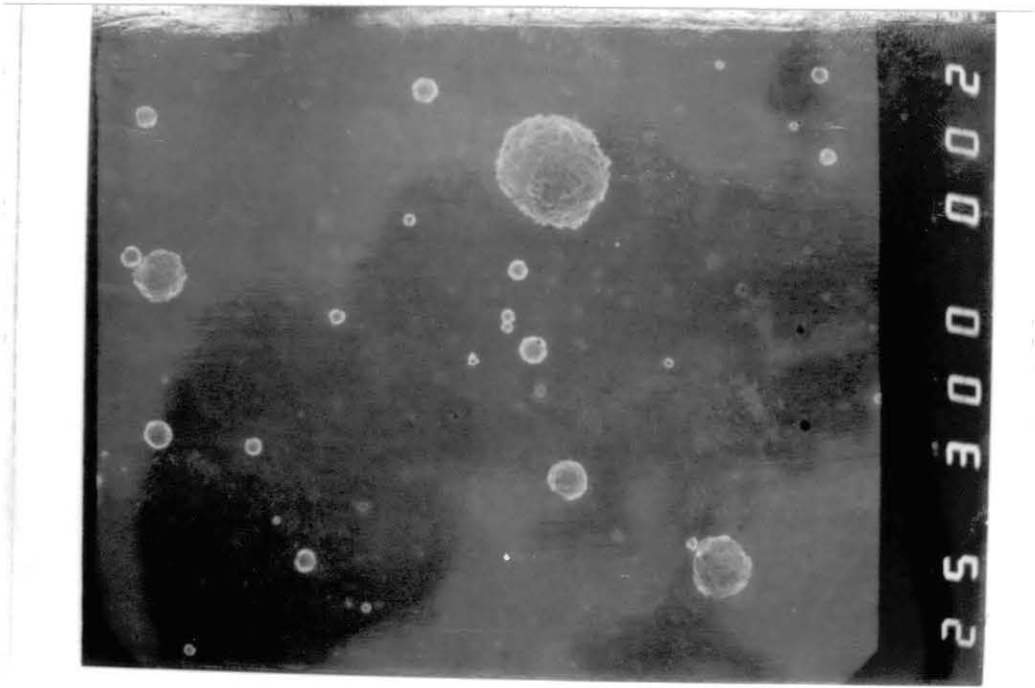


Figure 34. General View of the Partly Sensitized
(As-received) Sample Tested in 20 % Ferric
Chloride for 24 h. The Pits are Well
Formed and Round in Shape (30 x)

Figure 35. Bigger Pit, Adjacent to the Center Twin Pits of
Figure 34 (1000 x). The Structure is
Faceted and Crystalline With Pits Within the
Pit



pitting both, within the matrix and along the grain boundaries. A portion of the specimen is shown in Figure 36. Obviously the attack is intense where the grain size is comparatively smaller. The specimen has the smallest existing pits, $1\mu\text{m}$, as compared to the other two specimens. The pits following the grain boundaries are pointed and angular in shape. A closer view of the upper part of the cluster in Figure 36 is shown in Figure 37. Grain boundaries show extensive corrosion as well as the matrix. An exploded view of the center of Figure 37 can be seen in Figure 38. The intergranular attack is associated with chromium carbide formation. The upper-right matrix of Figure 37 is filled with pits (Figure 39) which are faceted. The initiation sites can be junk, titanium nitride, and titanium carbide particles. A magnificent view of these pyramidal, faceted pits is shown in Figure 40. One large pit on the IS specimen is showing undercutting, Figure 41. The edges have been attacked intergranularly. Figure 42 reveals the pit development process within the central portion of the pit. Figure 43 shows the pitting effect of 1.85M ferric chloride solution on AR sample after 45 minutes. Although it resembles general corrosion, a closer look, (200x) Figure 44, shows that it suffered intergranular pitting along with some pits within the matrix. Figure 45 shows the crystallographic, shiny, faceted structure of the attack. Figure 46 is also an AR sample but tested for 24 h.

Regarding the surface preparation, it was observed that

Figure 36. General View of a Portion of the Completely Sensitized Specimen tested in 20 % Ferric Chloride

Figure 37. Severe Pitting Along the Grain Boundries and Within the Matrix on the Completely Sensitized Specimen of Figure 36 (200 x). It was Tested in 20 % Ferric Chloride for 24 h

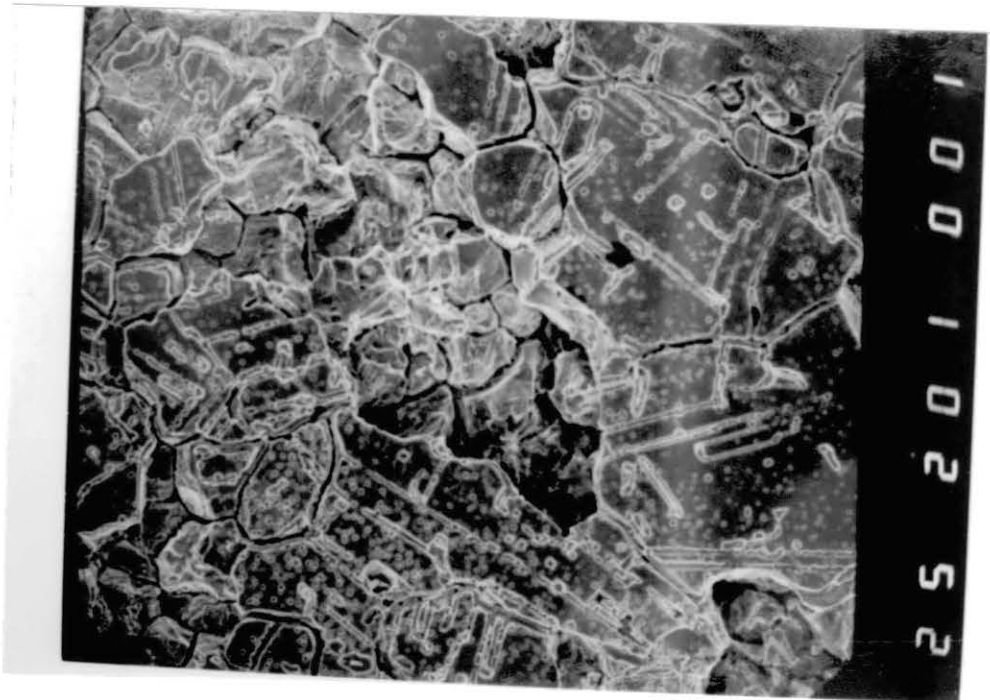
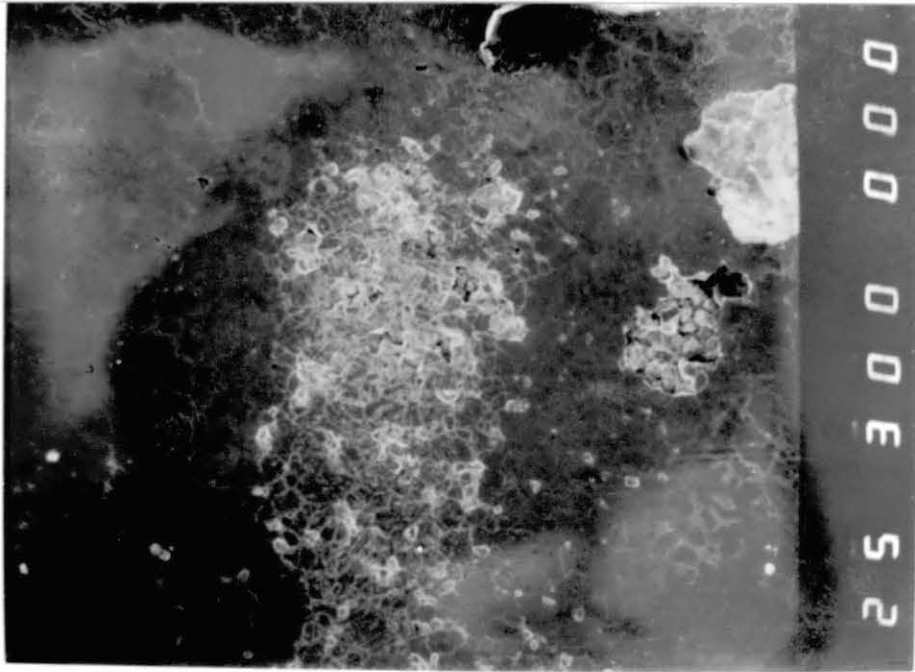


Figure 38. An Exploded View of the Center of Figure 37
(1000 x). Grain Boundaries are Severly
Attacked

Figure 39. Closer View of the Pitted Upper-Right Matrix of
Figure 37 (500 x)

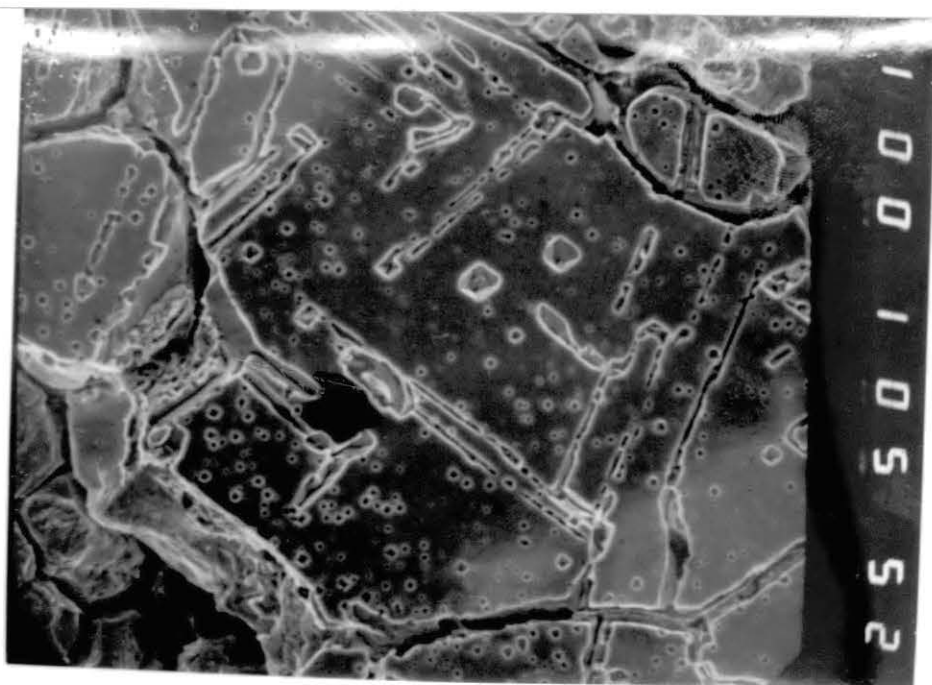
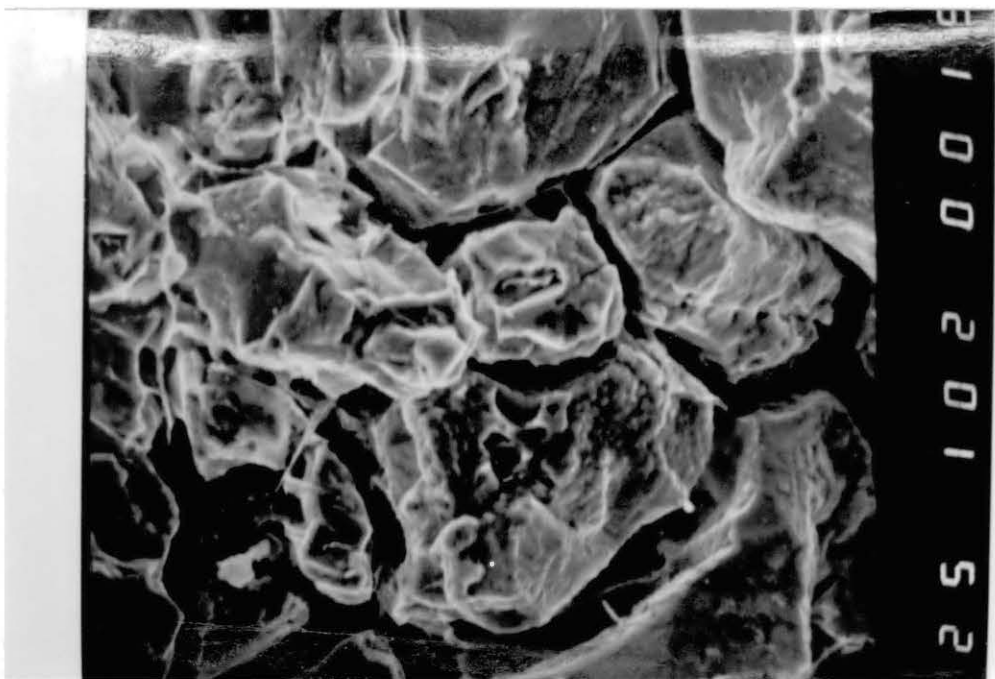


Figure 40. A High Magnification (1500 x) View of Figure 39 Showing intensive Pitting. The Pits are Pyramidical in Shape and Faceted

Figure 41. A Large Irregular Pit Formed on the Completely Sensitized Specimen Discussed in the Above Figures. Compare the Size of This Pit (30 x) With Those Shown in Figure 40 at 1500 x

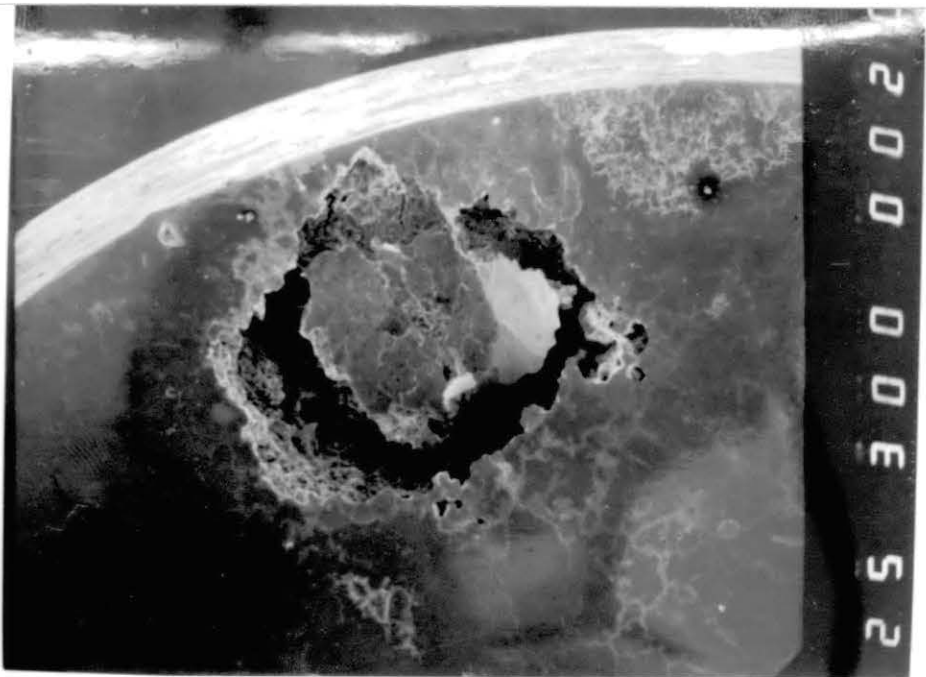
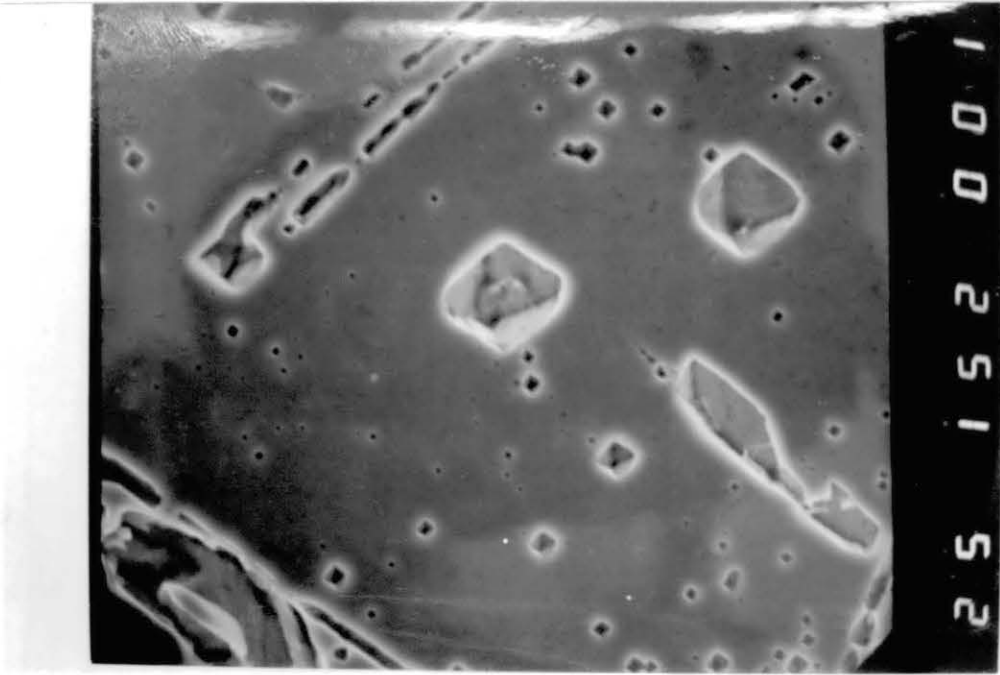


Figure 42. Detail of the Central Flat Surface of the Pit
Shown in Figure 41, Which is Under Severe
Attack (200 x)

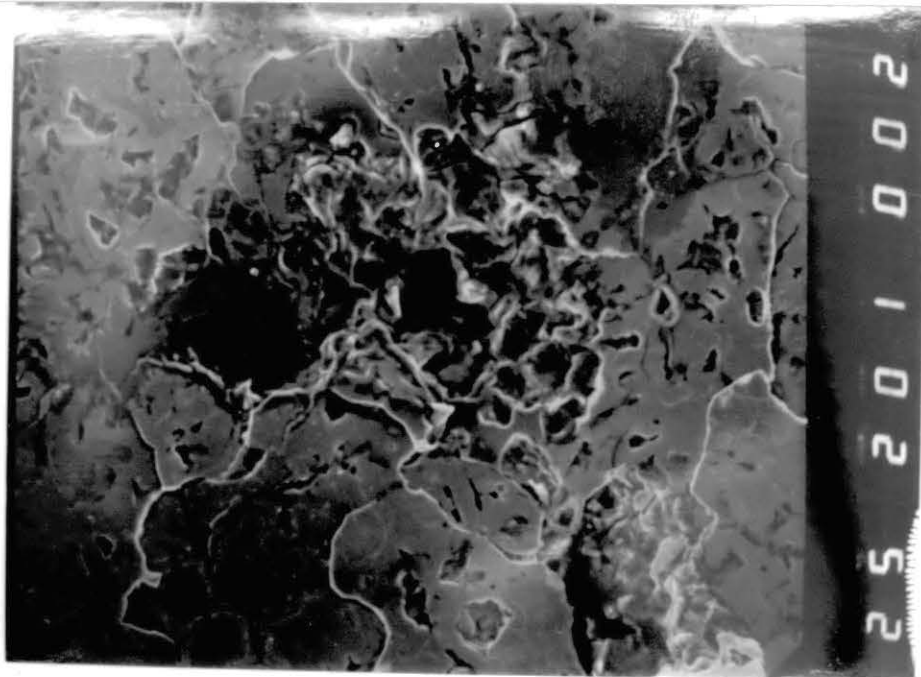


Figure 43. The Pattern of Pitting Attack when the As-received Specimen was Tested for 45 minutes in 1.85M Ferric Chloride. It Looks Like a General Attack but Actually Consists of a Number of Pits Joined Together

Figure 44. Magnified View of Figure 43. It Shows the Preferential Attack along the Grain Boundaries. This Attack Consist of Many Pits which Have Been Coalesced (200 x). The Attack is Mainly Intergranular With Pits Within the Matrix (200 x)

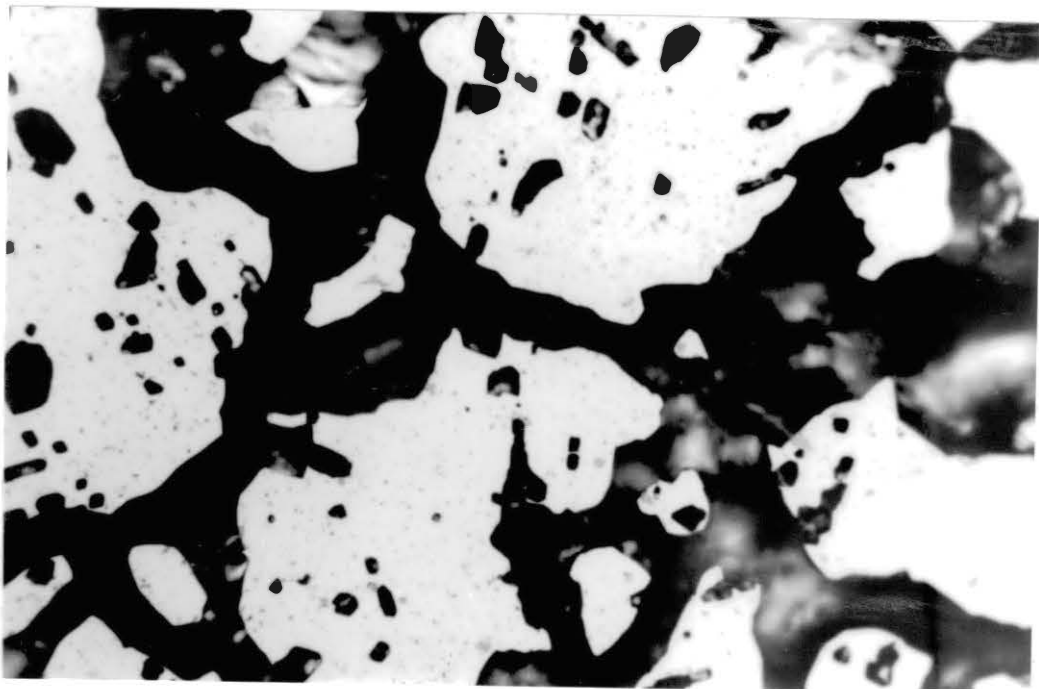
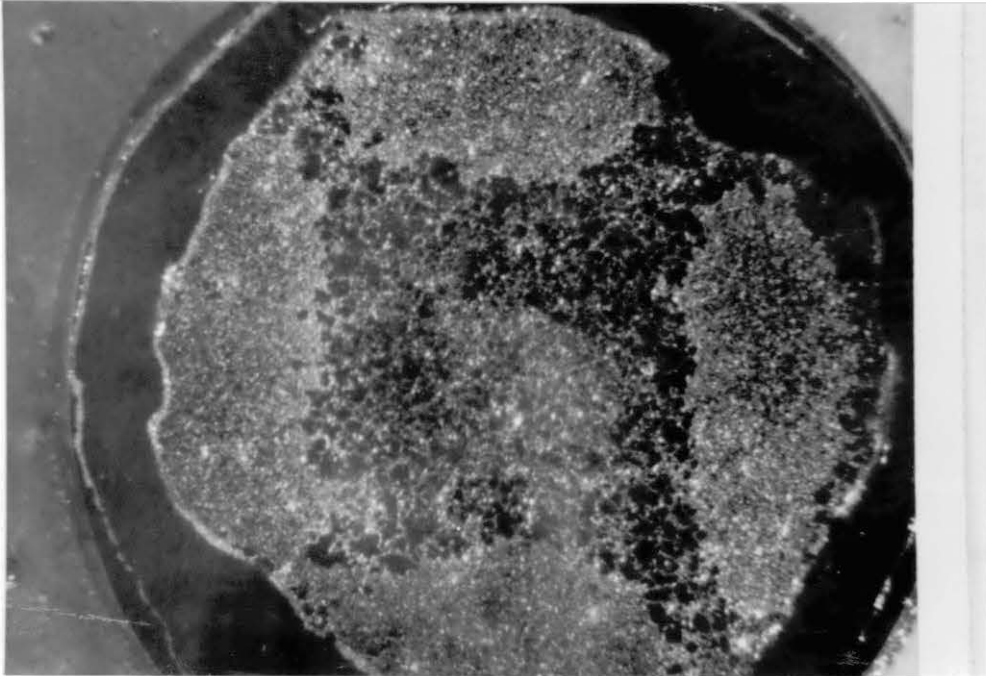
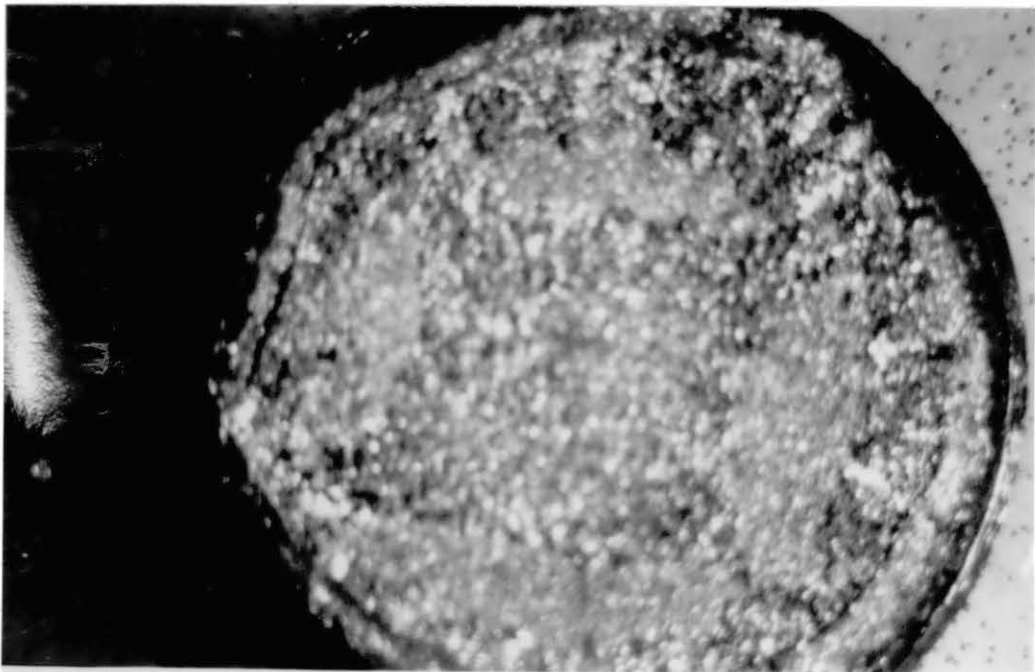
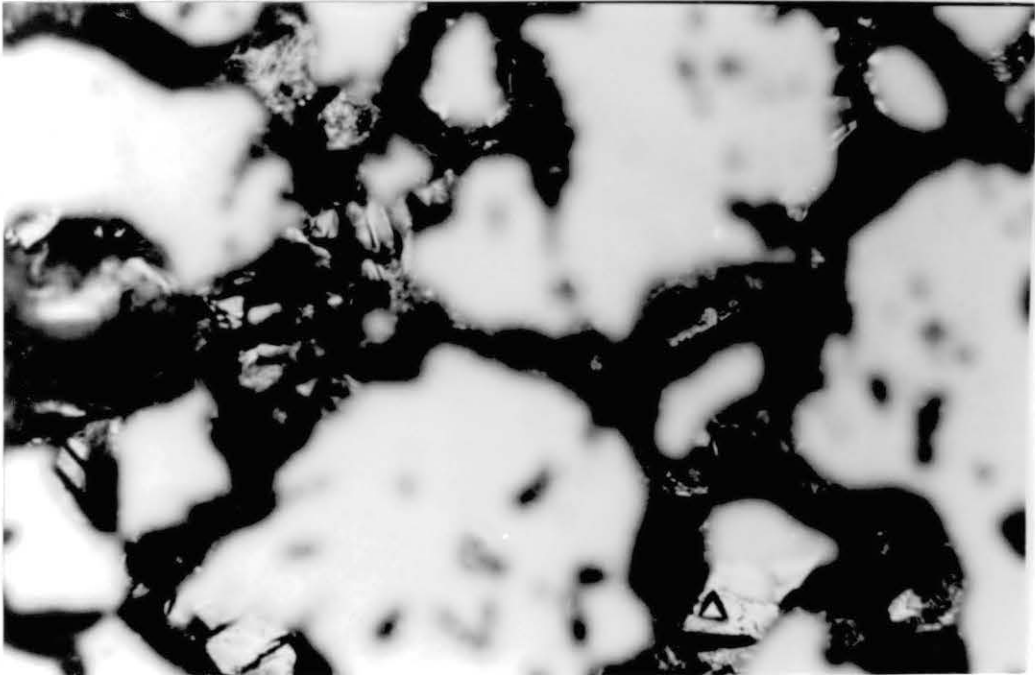


Figure 45. Detail of the Intergranular Attack Showing Crystallographic, Shiny, Faceted Structure Which is Similar to That Found at the Bottom of the Pit (200 x)

Figure 46. Photograph Taken After 24h Immersion Test in 1.85M Ferric Chloride. Although it Shows a General Corrosion but is Actually the Result of Pit Formation and Coalescence. It Has a Shiny, Crystalline Structure with Undercutting at the Edges (200 x)



the electropolished specimens get more pits than the mechanically polished one, but the pits on the latter are usually large. This can be due to fact that the pits on the mechanical polished specimen has the upper oxide film covering it while undercutting goes on. Under such conditions the solution inside the pit does not come in contact with the bulk solution and hence comparatively less diffusion takes place. Therefore, the pH inside the pit goes on decreasing, thus attacking it severely and hence widening.

Figure 47 shows a graph of concentration vs. number of pits for unsensitized specimens. It can be seen that from a 0.75M (20%) concentration onwards, the number of pits increases at a decreasing rate. The number of pits observed at this point is 5. From the pitting theory of passive film breakdown and anodic dissolution of the metal, this behavior can be justified because as the number of pits keeps on increasing, the anodic area increases while cathodic area decreases. This change retards the corrosion rate and hence the number of pits. The scatter in the data can be attributed to the degree of crevice corrosion and the quantity/quality of the pits, e.g. pits can be smaller in number but larger in size. The graph (Figure 48) of time vs. number of pits at constant concentration of 10% FeCl_3 gives a linear relationship but with a steeper slope. These specimens were sensitized. Both graphs are related to the tests performed in ferric chloride.

Figure 47. Graph of Concentration vs. Number of Pits

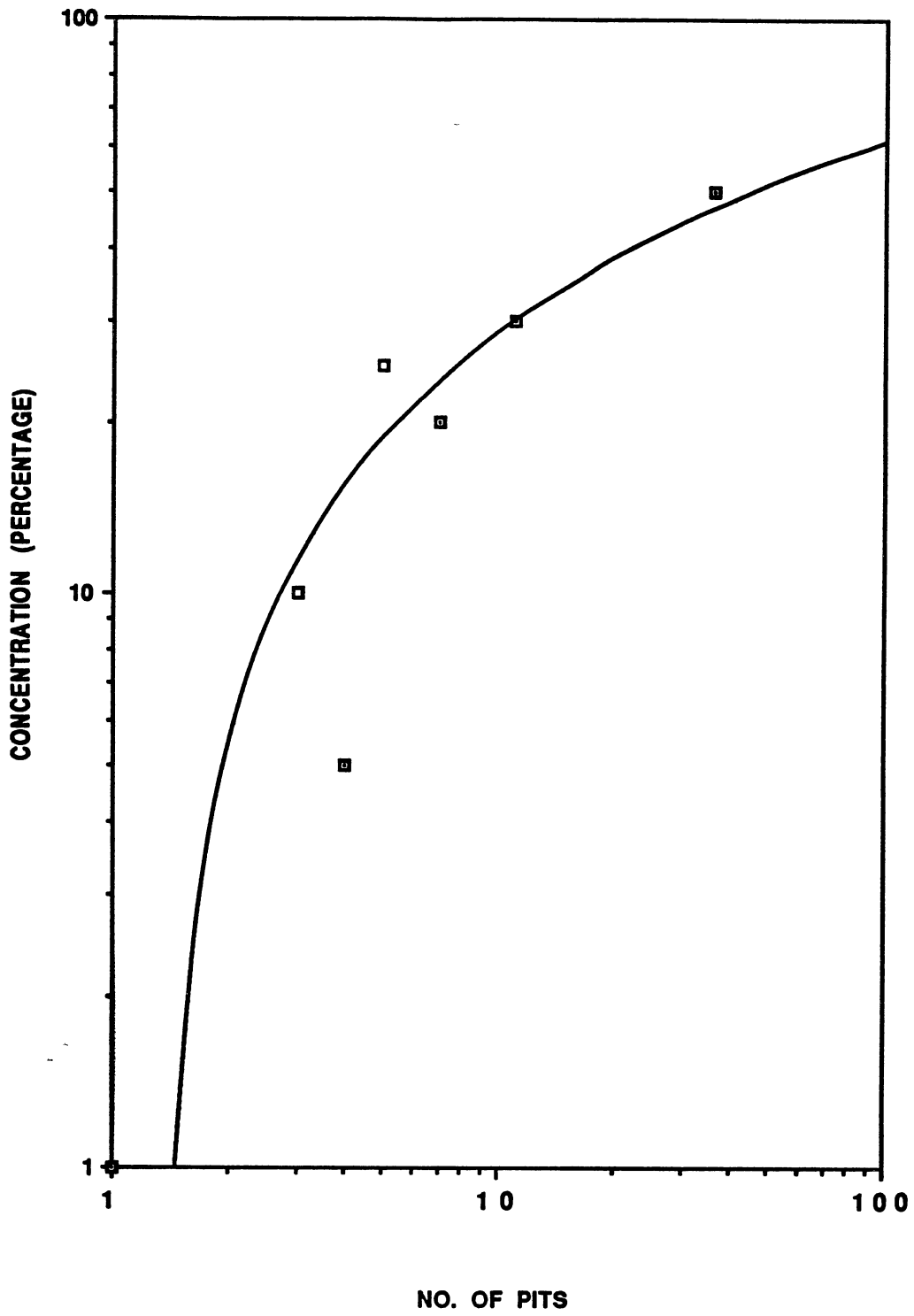
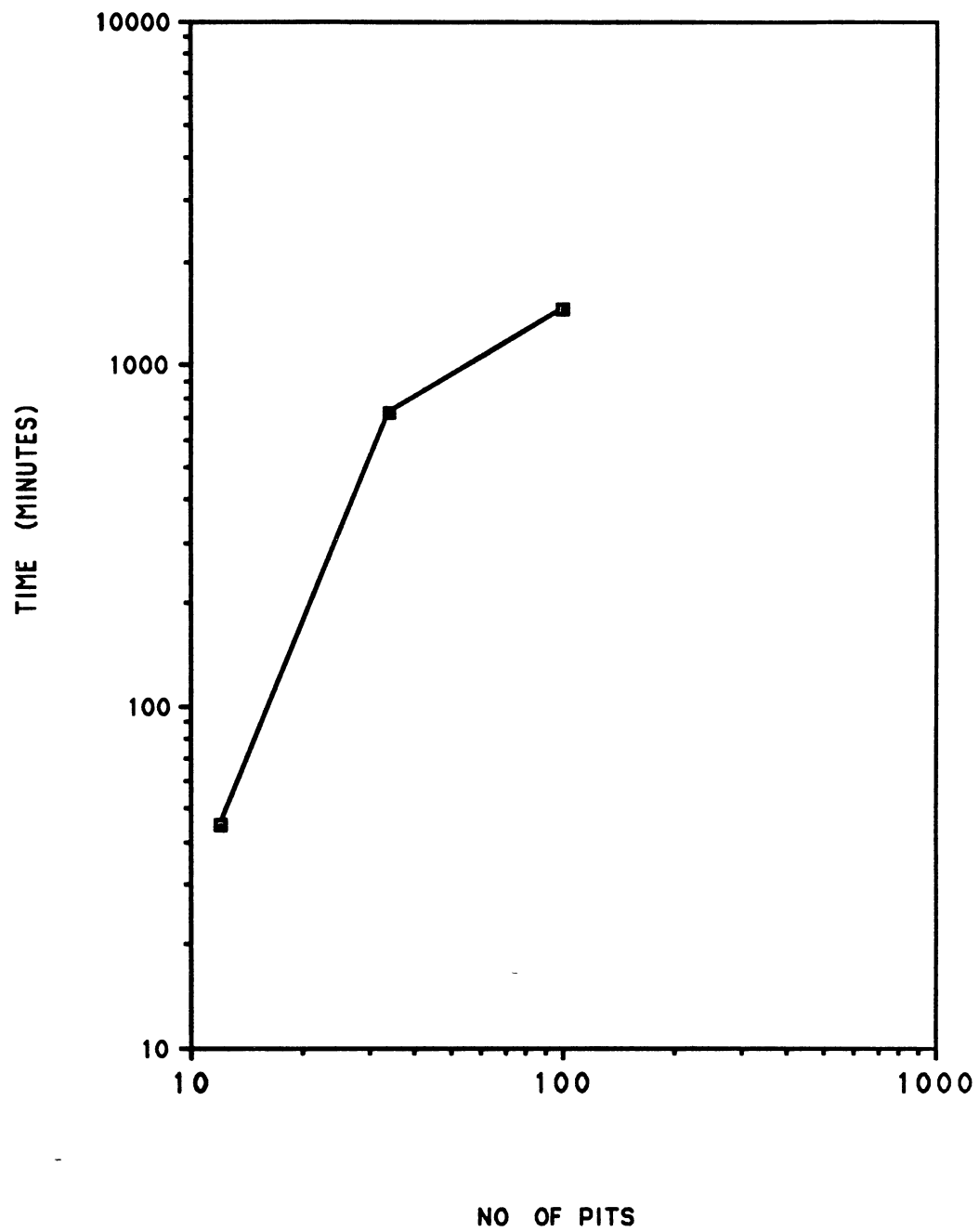


Figure 48. Graph of Time vs. Number of Pits



Immersion tests performed in 0.6M (10%) cupric chloride for 24h resulted in four very small shallow pits whose morphology cannot be studied even at 800x. The specimens tested were unsensitized. Immunity was observed with ammonium persulfate for an unsensitized specimen at 0.45M (10%) concentration. Sensitized specimens, when tested for 24 h at 0.9M (20%) concentration, showed one underformed pit; 2M (40%) magnesium chloride at 180 F didn't produce a single pit on a mechanically polished specimen in forty days.

5.3 Stress Corrosion Cracking

The pitting study preceded a few critical stress corrosion cracking tests, to endeavor to get SCC at room temperature, as a screening method. For the indentation tests, excessive cross slip was observed near the indentation. Except for the top oxide film cracking along the grain boundaries of a sensitized specimen, emanating from an undercut pit, no other intergranular attack was observed. No cracks were obtained on any specimen for times up to 10 days in ferric chloride and 30 days in 180 F magnesium chloride. To reiterate, this technique worked on stainless steel for Markey [46].

Table VIII shows the results of SSTs conducted at 20% of the 6" stroke in 10% FeCl₃. The duration of the test was selected on the basic of the pitting experiments. Initially, SF1 was given less time (1×10^5 sec) in order to

TABLE VIII

RESULTS OF THE SLOW STRAIN RATE TESTS CONDUCTED
IN 0.4M FERRIC CHLORIDE AT DIFFERENT HEAT
TREATMENTS

SAMPLE	HEAT TREATMENT	SENSITIZED	TIME (s)	COMMENTS
SF1	2h at 1050 C Furnace Cooled	Y*	1×10^5	Cup and cone fracture with appreciable plastic deformation.
SF2	2h at 1050 C	Y	5×10^5	Cup and cone fracture with appreciable plastic deformation. Crevice corrosion at the metal-solution cell interace.
SF3	As Received	Y	5×10^5	Same as above

* Yes

restrict any pit conversion from sharp to an elliptical. However, the fractured specimen didn't show any sign of pitting or SCC. Accordingly, a five fold slow strain rate was used for the next test. Again, the specimen was free of pits but did suffer crevice corrosion at the metal-solution cell interface. There was no SCC and the fractures were cup and cone. In a parallel investigation, Hussen [48] obtained SCC in Alloy 600 at room temperature after SSTs in 10% FeCl_3 .

5.4 Liquid Metal Embrittlement (Fatigue Tests)

While liquid metal embrittlement had been done previously, the different heat treatments and sensitization issue had not been addressed [35]. The liquid metal embrittlement was tested in liquid mercury using waisted specimens exposed to different heat treatments. It can be seen from Table IX that the sensitized specimens, which were furnace cooled after high temperature soaking, sustained greater number of cycles as compared to the unsensitized ones. No spalling was detected on the furnace cooled (sensitized) specimens as compared to the quickly cooled ones (unsensitized). This shows that the furnace cooled specimens get a better adhered oxide film which increases the crack initiation time hence the potential cyclic life. Figure 49 shows the three stage process of fatigue where crack initiation consists of a larger portion than crack propagation. The hardness data show that there is a

TABLE IX

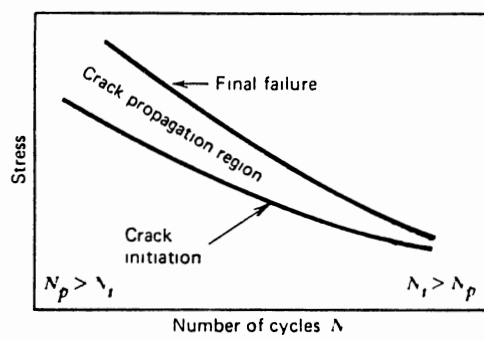
**RESULTS OF FATIGUE TESTS IN MERCURY AND FERRIC CHLORIDE
AT ROOM TEMPERATURE**

SAMP.	HEAT TREATMENT	SENS	HARD NESS	HCl FQ. CLN.	ENV.	T.S. 70%	PK.LD. kips	NO. OF CYCLES
FFM1	10h at 1090 C 12h at 680 C-FC	Y ⁽²⁾	70.0	N ⁽³⁾	15 Hg	54.6	2.63	527560
FFM2	2h at 1090 C-WQ ⁽⁴⁾	N	92.6	N	15 Hg	70.7	3.13	166040
FFM4	1h at 1090 C-WQ 2h at 710 C-FC	Y	75.2	N	15 Hg	56.0	2.76	1295890
FFM5	1h at 1090 C-WQ 2h at 715 C-FC	Y	73.3	Y	15 Hg	54.6	2.74	2930210
FFM6	2h at 1090 C-WQ	N	74.2	Y	35 Hg	55.3	2.82	1797760
FFF7	1h at 1090 C-WQ 2h at 715 C-FC	Y	73.0	Y	15 FeCl ₃ 0.4M	53.2	2.75	169590

- (1) - Furnace cooled
- (2) - Yes
- (3) - No
- (4) - Water Quenched

- KEYS**
- SAMP. - SAMPLE
 - SENS. - SENSITIZATION
 - CLN. - CLEANING
 - ENV. - ENVIRONMENT
 - PK.LD. - PEAK LOAD
 - FQ. - FREQUENCY
 - T.S. - TENSILE STRENGTH

Figure 49. Fatigue Life Depends on Relative Extent of
Initiation and Propagation Stages [38]



difference in hardness values taken on the surface of the constant diameter grip ends and the waisted portion (Table X). This difference can be due to the size effect. The hardness test on the sections of waisted portions have sometimes shown a scatter of approximately 16 HRB units. One of the reason for obtaining longer fatigue life as compared to that of Morris [35] is this issue of hardness. In the present study the peak load was calculated by using the graphical value of tensile strength which was based on the average hardness value taken at the constant diameter grip ends. This calculated peak load is quite lower than that applied by Morris which was obtained by a direct tensile strength test. The effect of peak load value on the life of the specimen has been demonstrated by Hertzberg [38] in Figure 50. Also, all the heat treated specimens of Morris got sensitized due to furnace cooling from temperatures of 1000 C and above.

The specimens FFM1, FFM2, and FFM4, were tested at 15 Hz without HCl cleaning. The peak load was calculated at 70% of the tensile strength. The SEM examination of FFM1 is shown in Figure 51. It is a general view composed of fatigue and overload zone. Details of the fracture initiation zone is seen in Figure 52 which seems to be completely transgranular. A closer look in Figure 53 shows tear ridges. Striations are quite prominent. Figure 54 is the general view of FFM2. The fatigue zone is quite smaller than that of FFM1 which is in accordance to the number of cycles sustained. Further details of the fatigue initiation zone are in Figure 55. One more view shows an open transgranular

TABLE X
VARIATIONS IN HARDNESS

SAMPLE	SENSITIZATION	HARDNESS (HRB)	
		CONSTANT DIA. GRIP ENDS	WAISTED SECTION
FFMS	Y*	73.3	73.5
FFMS	N**	74.2	103.5
FFF7	Y	73.0	99.4

* YES

** NO

Figure 50. Wohler's S-N Curves for Krupp Axle Steel [38]

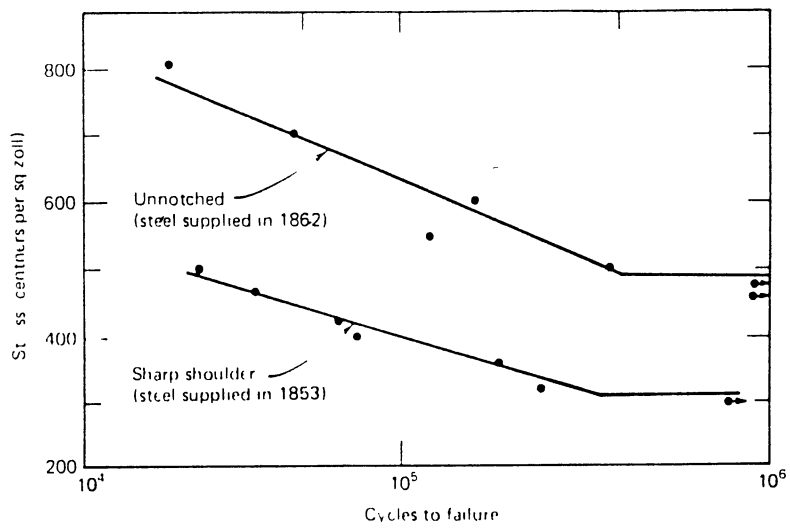


Figure 51. General View. From Right to Left Are Fatigue Zone (50 %) and Overload Zone (50 %) With Secondary Cracking (20 x)

Figure 52. The Center of the Right Hand Side is the Point of Fatigue Zone Initiation. Lines are Radiating Away From That Point. Faceted Transgranular Separation is Visible (240 x)

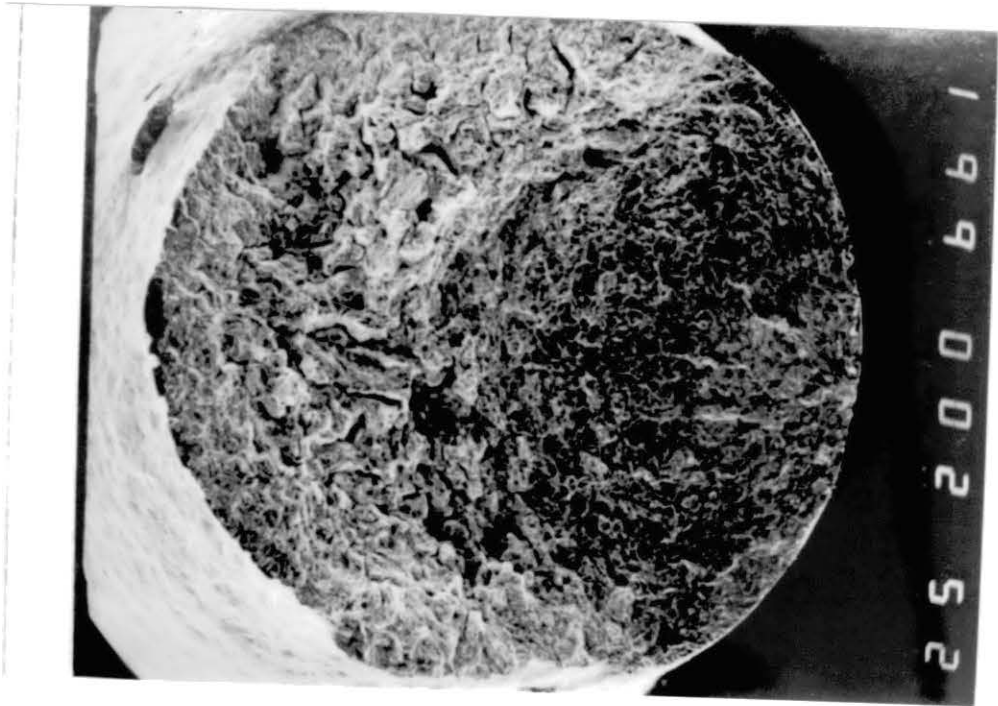
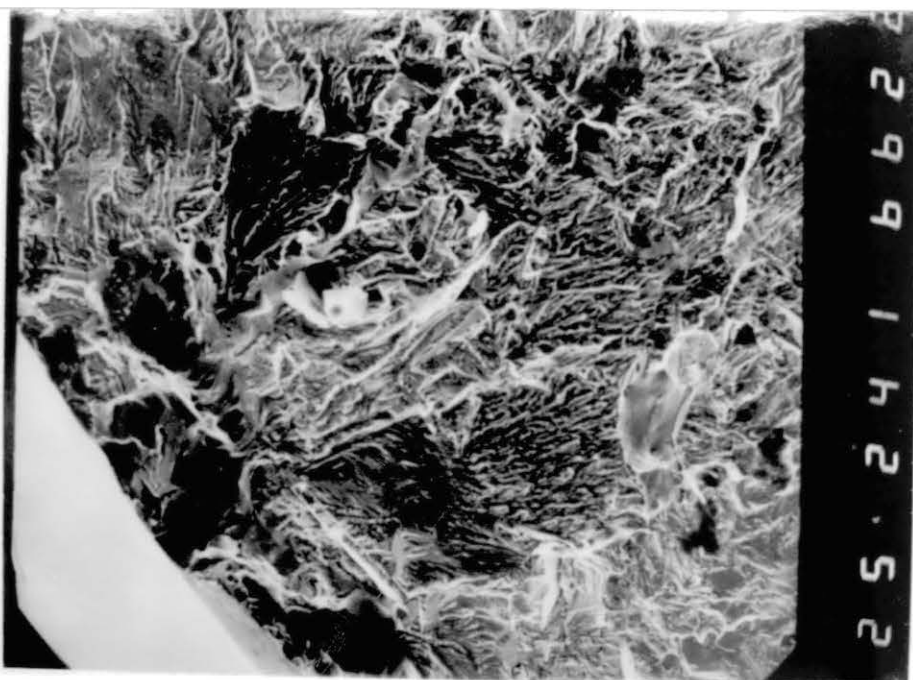
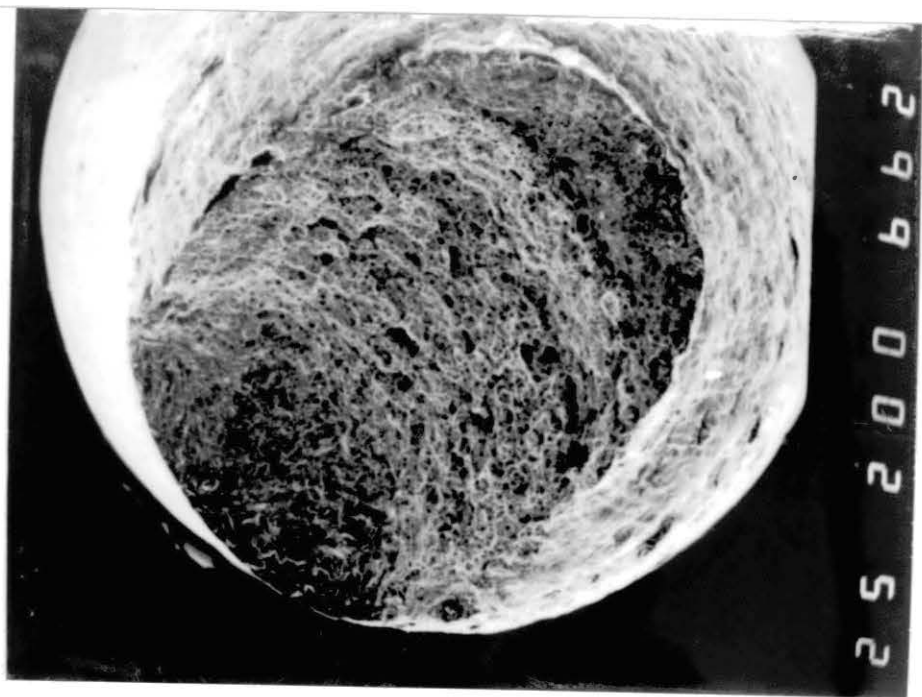


Figure 53. Detail of the Fatigue Initiation Zone Shown in Figure 52. Tear Ridges and Striations Can be Seen (1000 x)



Figure 54. General View Showing Fatigue (Bottom Right) and Overload Zones (Fatigue Zone is Approximately 25 %). Microvoids Can Be Seen in the Overload Zone (20 x)

Figure 55. Initiation of Fatigue Zone (Bottom Left). At Origin Can Be Seen Rubbing, a Very Localized IG Zone, Then a Faceted IG Zone that Quickly Becomes More Irregular, Less Planar (240 x)



crack (Figure 56). Inside detail of the crack can be seen in Figure 57. The detail of the side crack shown in Figure 58 reveals that it has not followed the grinding marks. This specimen fractured off-center. The photographs of these three specimens are quite similar to the ones obtained by Morris, Breedlove, and Valenta [35] [36] in their fatigue test conducted in air. This resemblance is due to the fact that with the oxide film wettability of the surface by mercury is not possible therefore there are very less chances of adsorption hence embrittlement. FFM1 fractured at the upper of meniscus while FFM4 fractured near the shoulder i.e. these fractures were partially in the air environment and mercury didn't play its role.

FFM5 and FFM6 were cleaned by 10% HCl to increase the wettability of mercury. Also, this helps to remove the oxide film. Figure 59 and Figure 60 are the SEM fractographs of the sensitized specimen FFM5. A combination of IG and TG attack is quite visible. Such results were also obtained by Price and Morris [37]. The reasons for an incomplete IG attack could be the lower values of peak load and insufficient oxide cleaning which resulted in lesser wetting; hence IG attack is closer to the edges than the center of the specimen. A magnified view of a portion of Figure 60 is shown in Figure 61, where the attack is IG. Connecting the Figures 60 and 61, one can see that the cracking started intergranularly. Figure 62 shows corrosion in an IG zone. The wart-like appearance is very similar to

Figure 56. Detail of the Center of Figure 55. Secondary Cracks Can Now Be Seen. They Develop as Major Cracks Grow (1000 x)

Figure 57. Lower Right Hand Side of Figure 55. Secondary Cracks and Their Internal Details can Be Easily Seen, as Can Striations That are Somewhat Disturbed by Rubbing (1000 x)

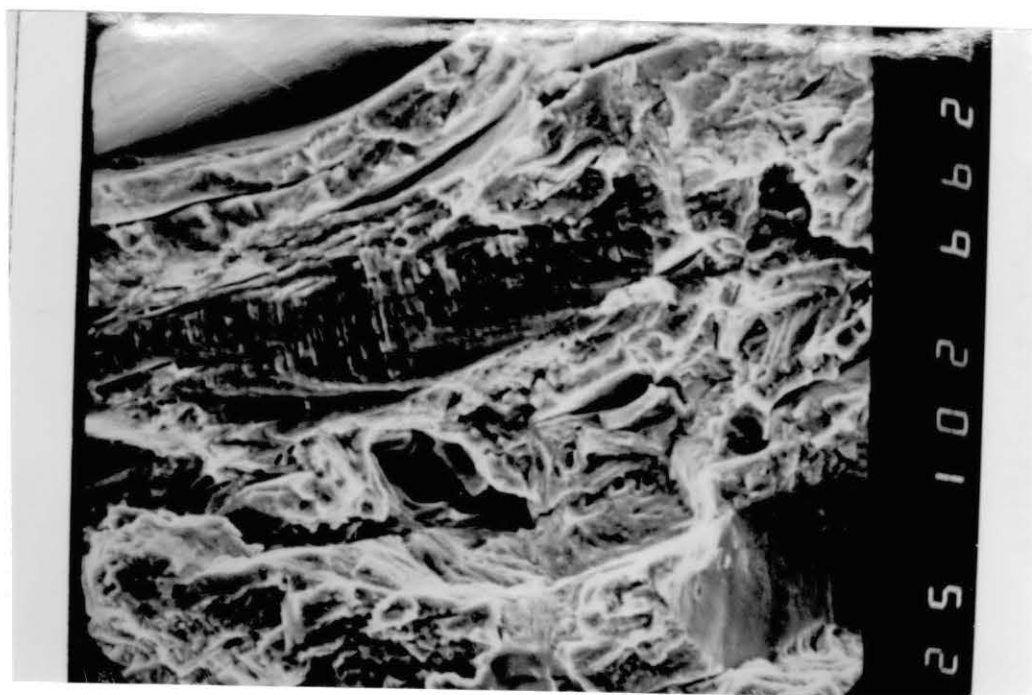
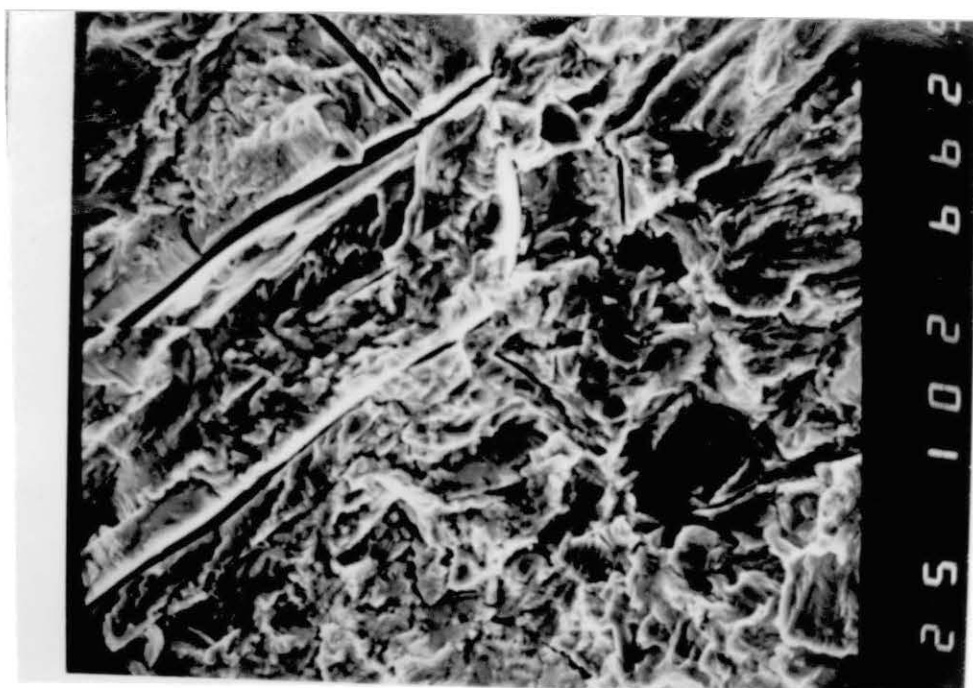


Figure 58. A Portion of a Transverse Side Crack. The Irregular Pattern Shows That it is Not Due to Any Peripheral Grinding Mark. Observe That the Crack is Open and Contain Debris (1000 x)

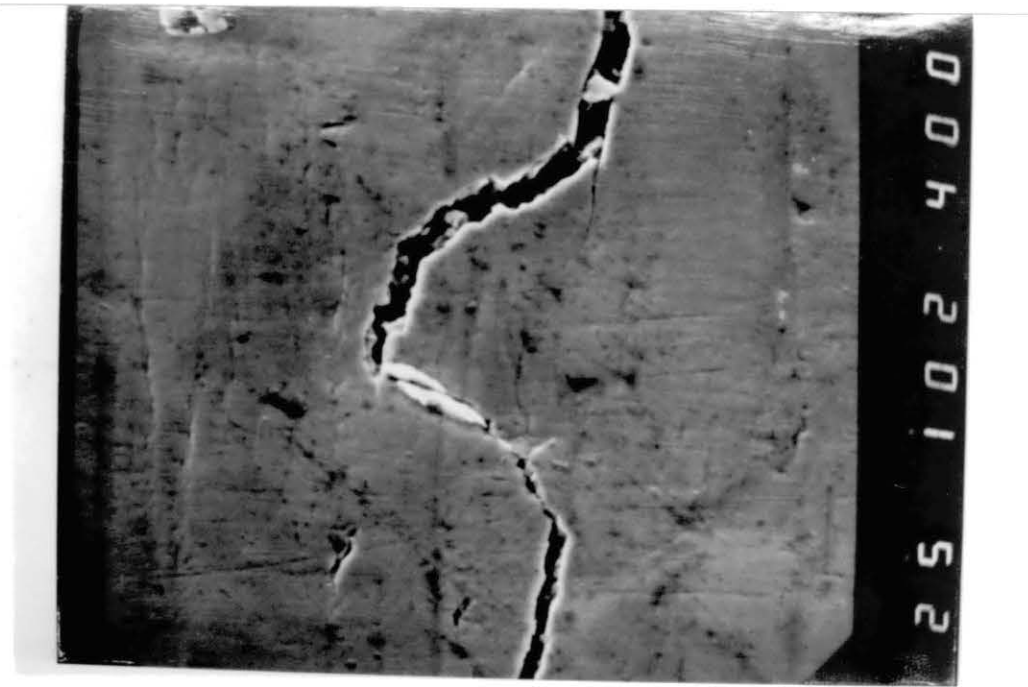


Figure 59. General View of the Fractured Surface. Center of the Right Hand Side is the Fatigue Initiation Zone (20 x)

Figure 60. Fatigue Initiation Point. Observe in This Instance Zones of IG Fracture (240 x)

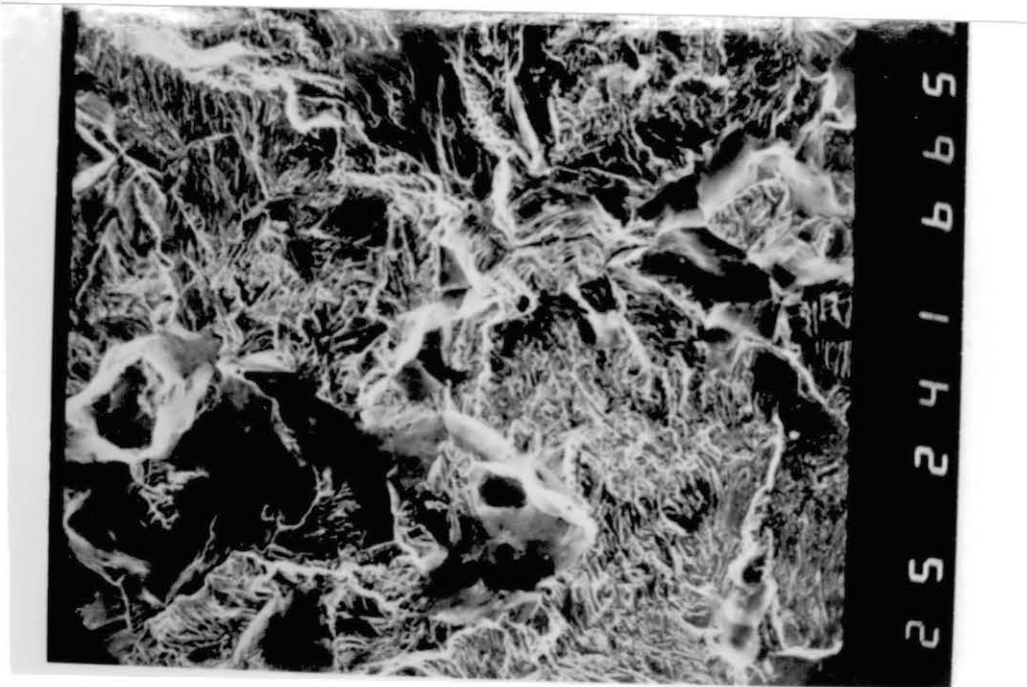
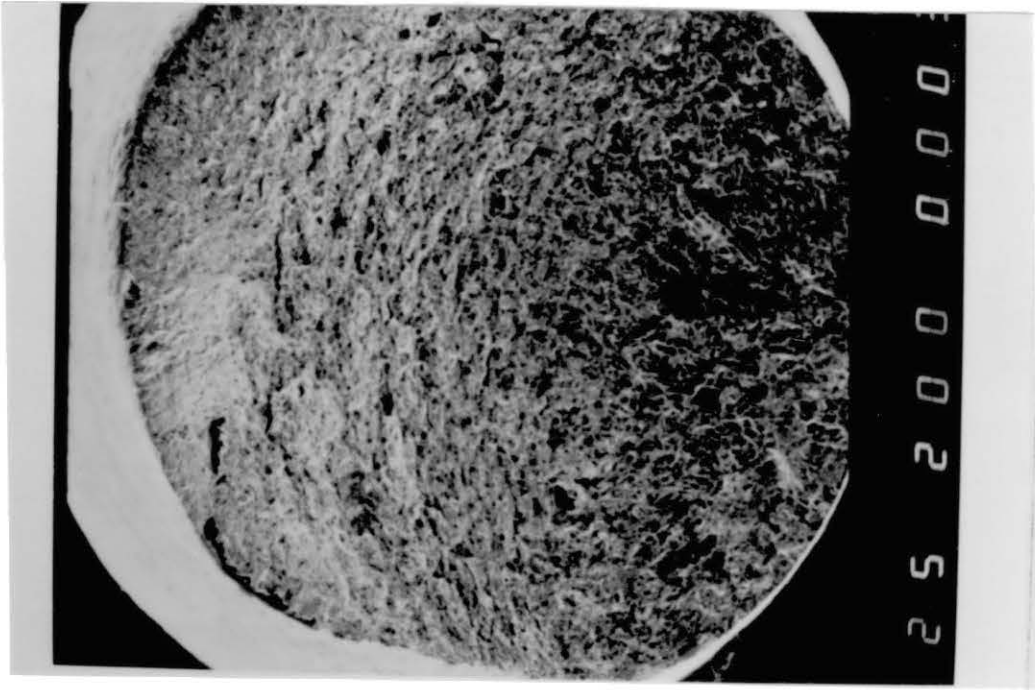
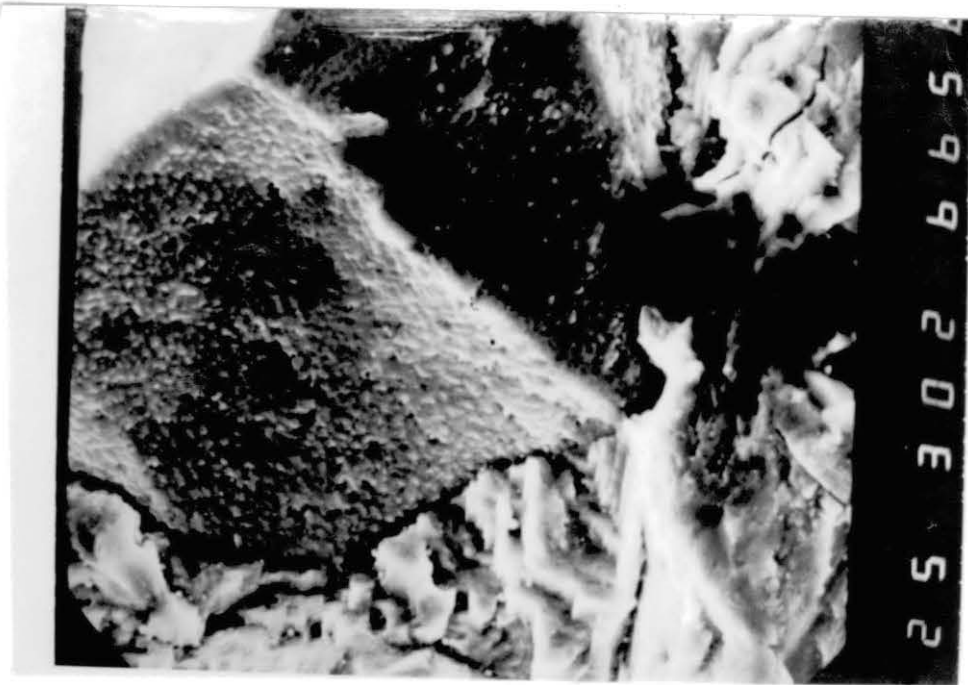
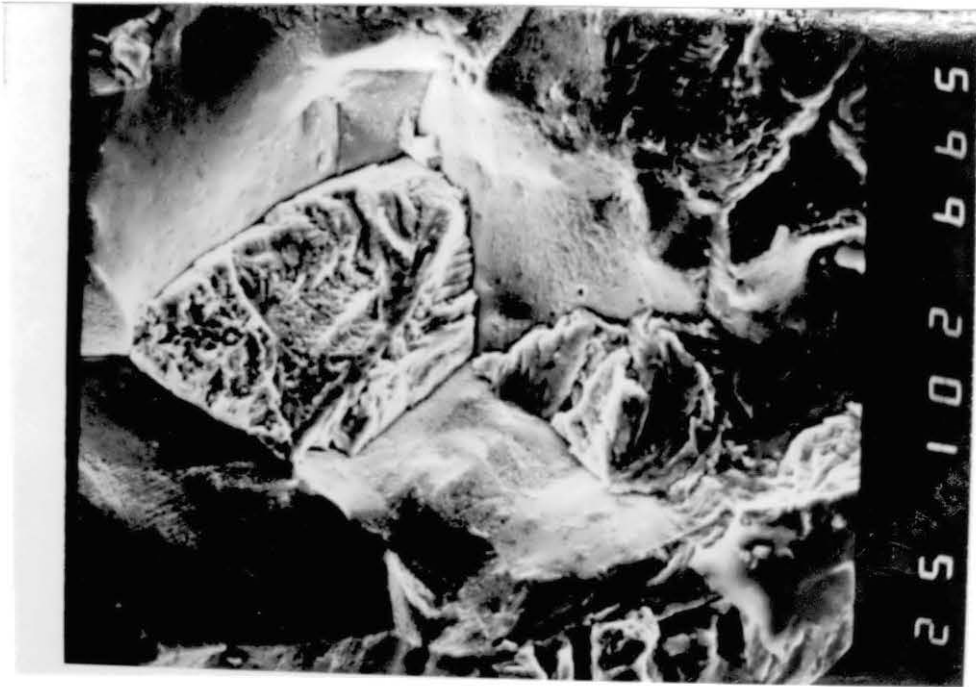


Figure 61. The Upper-right View of Figure 60. Detail of the IG Fracture Zone (1000 x)

Figure 62. An IG Zone in More Detail Showing Corrosion (3000 x)



the chromium oxide-rich outcrop observed in Elliot's [29] study of oxidation of Alloy 800. FFM6 which is unsensitized also suffered IG attack but is less severe and more scattered as compared to FFM5. This is the only test conducted at 35Hz.

5.5 Corrosion Fatigue

In the light of the foregoing, a further attempt at getting embrittlement in ferric chloride at room temperature was made, this time using the corrosion fatigue mode. Corrosion fatigue was performed at 70% of the tensile strength with 100% stroke control in 15 Hz. The sensitized specimen was cleaned by 10% HCl before testing in an environment of 0.4 M (10%) FeCl_3 . The experiment was successful for brittle fracture occurred, with three distinct fatigue zones, as shown in Figure 63. Wide side cracks (one partially visible) and some fatigue cracks can be seen. The figure also shows that the fatigue zone initiation point was an undercut side pit which is usually associated with sensitized Alloy 800 in the environment. The pit has been focused in Figure 64 where intergranular attack, cracks and faceted edges can be seen. The root of the pit is shown in Figure 65 from where the intergranular attack spreaded further. A 1000x view of the above figure is shown in Figure 66. The gaping IG cracks are apparent alongwith a rectangular titanium nitride impurity which is also becoming a pit site. Some more pits and IG attack

Figure 63. General View. 3 Distinct Fatigue Zones.
Fracture was Brittle. A Big Pit,
Which Served as a Crack Initiation Site,
is Located on the Top-left Side. The
Specimen is Sensitized Hence Undercutting
is Significant. Side Cracking
Can Also Be Seen (20 x)

Figure 64. Higher Magnification View of the Pit (240 x).
Faceted Structure, Intergranular Attack, and
Cracks are Visible

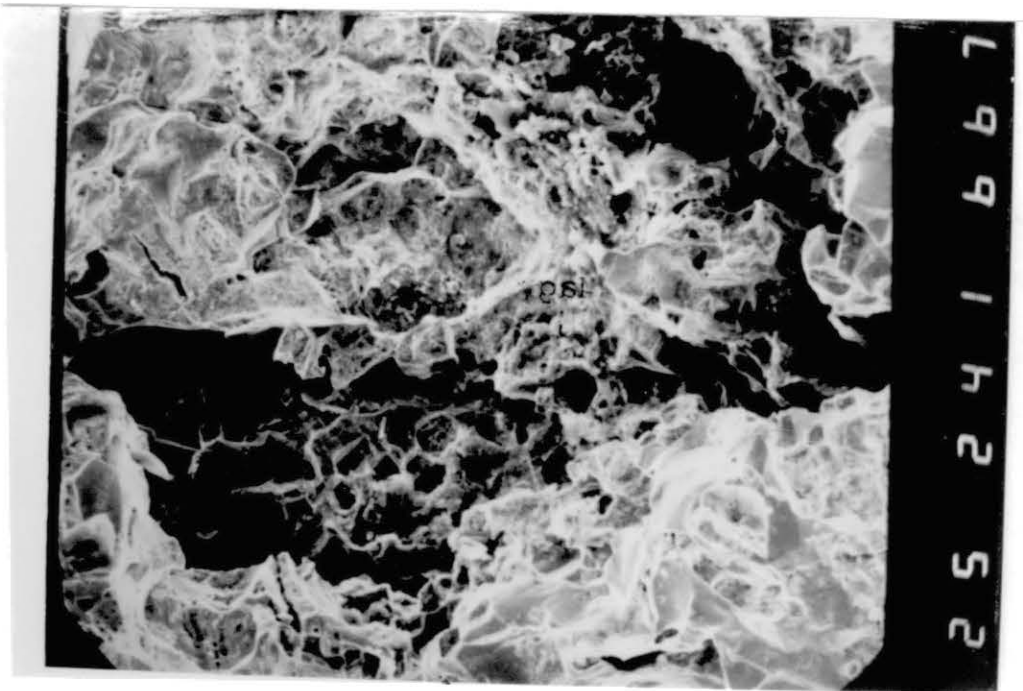
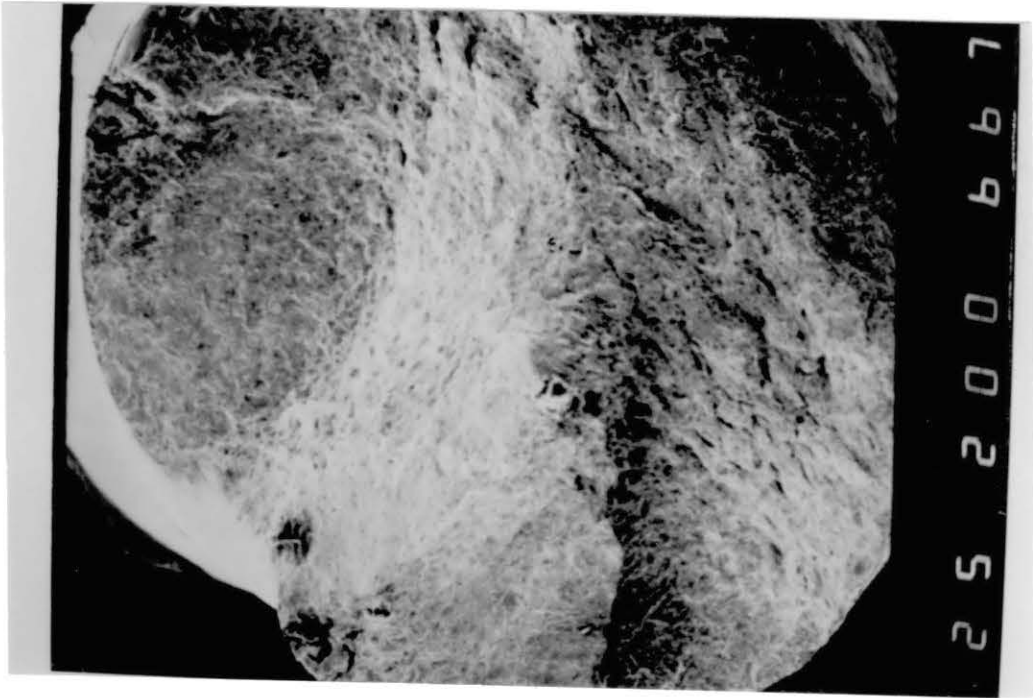
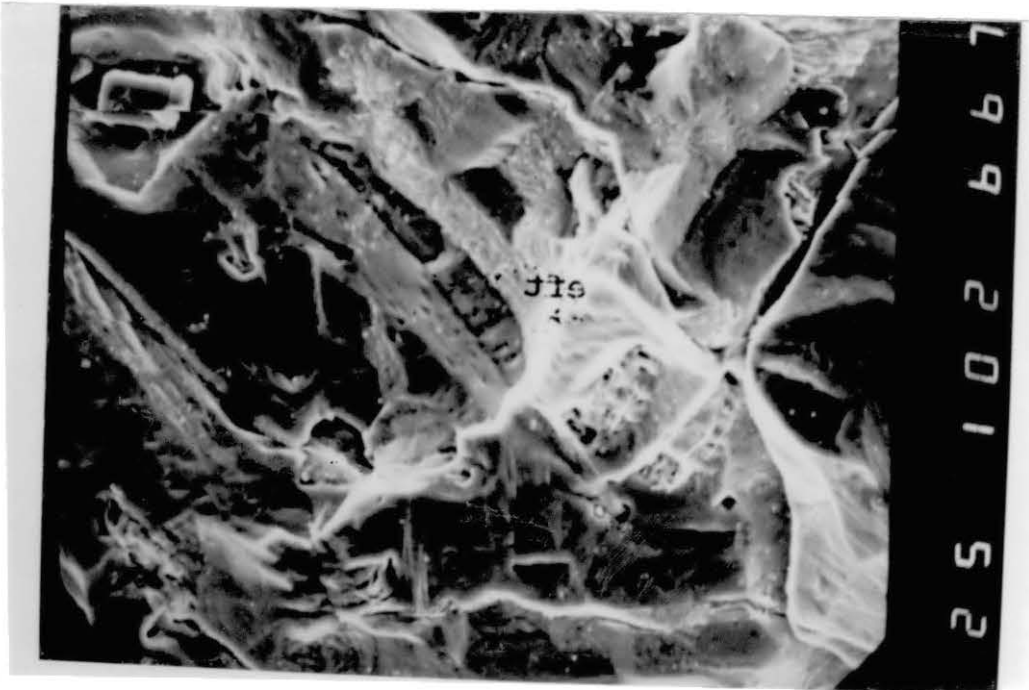
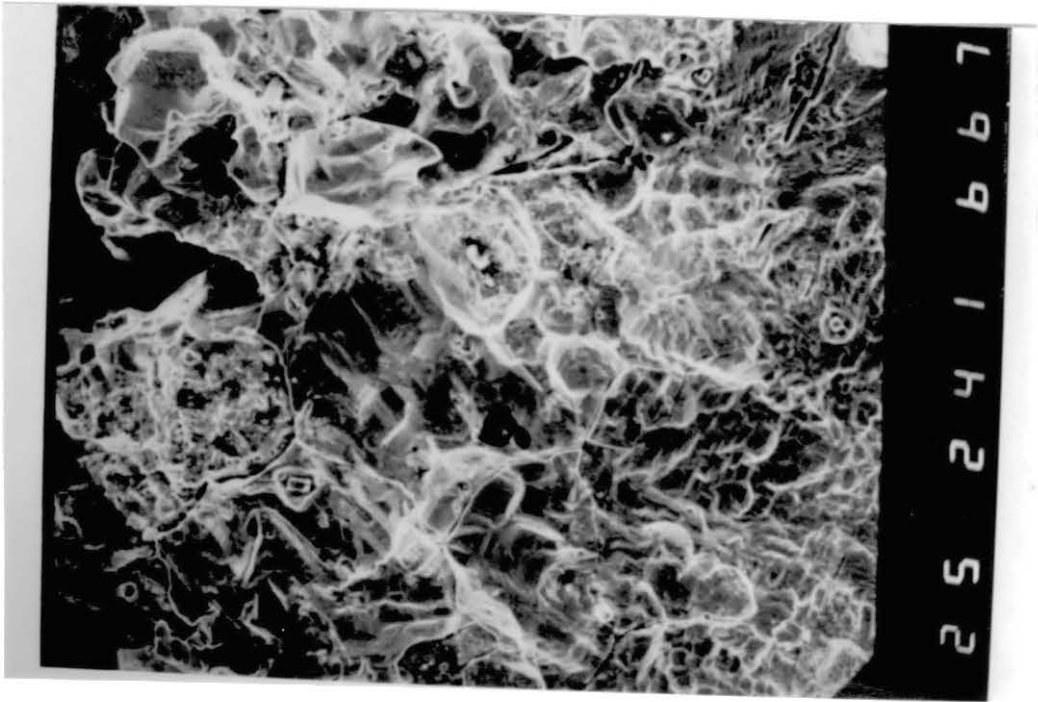


Figure 65. Extreme Right End of Figure 64 Showing the Root/Edge of the Pit. IG Cracking is Apparent

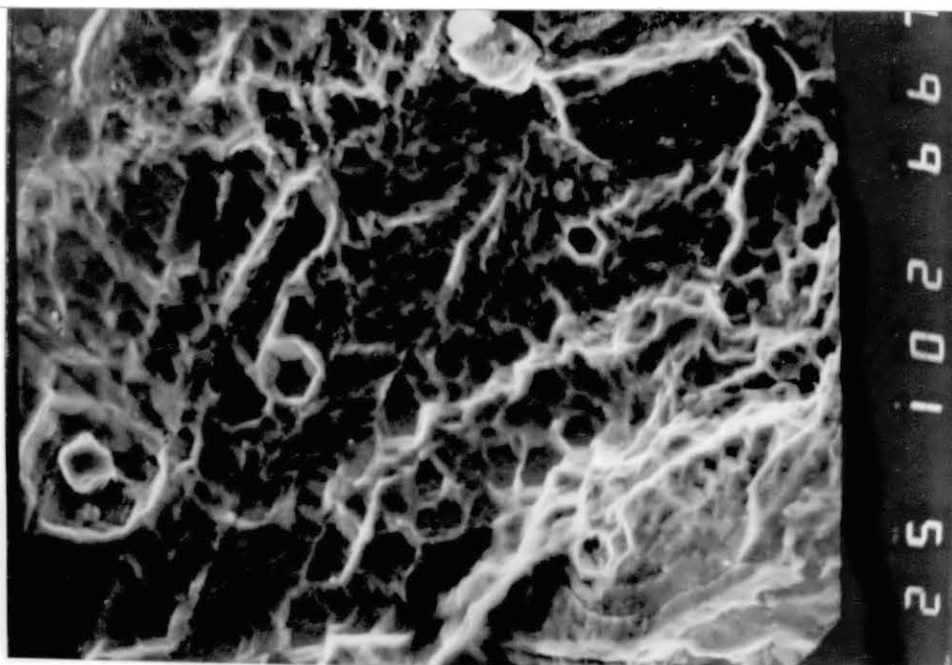
Figure 66. Lower-left View of Figure 65. IG Cracking Can be Seen. There are Some Cavities as if the Particles Have Floated Out. Observe That the Rectangular Particle of Titanium Nitride is Not Corroding Rather it is Acting as a Cathode and the Matrix Around it Corrodes. The faceted structure is Typical of a Pit and Resembles that seen in Figure 22 (1000 x)



pattern is shown in Figure 67. Apart from this side pit, which initiated the fatigue fracture, there were few more side pits heading towards side cracking. The faceted structure of Figure 58 is typical of a pit and resembles that seen in Figure 21. Note that, in both the cases, preferred crystal planes are outlined. Undercutting of the pit is quite justified by the earlier discussion on pitting results, where it was found that the pits formed on the mechanically polished specimen had a restricted opening, hence the pH inside the pit falls rapidly, thus increasing undercutting.

The factors for corrosion fatigue causing embrittlement in Alloy 800, as compared to SCC, vary according to the stages of initiation and propagation of a crack. The crack initiation period was shortened by removing the protective passive film by HCl cleaning hence, increasing the rate of surface reactions. The active surface, chloride environment, sensitized material, and loading were sufficient to initiate pits. The pits formation resulted in localized drop in pH while the cyclic loading increased the mass transport mechanism; both assisted in crack propagation [42]. These factors were not a part of the SSTs conducted. Furthermore, since the specimen fractured in less than four hours, the pit did not get enough time to fully develop and become round at the root. The pointed structure and grain boundary reactions due to sensitization, further assisted crack propagation.

Figure 67. Center of the Extreme Right-end of Figure 65. Corrosion and Intergranular Attack Can Be Seen. Again Observe the Titanium Nitride Particle and the Corroding Matrix (1000 x)



CHAPTER VI

SUMMARY

From this experimental research, the following conclusions can be drawn :

1. Alloy 800 has a great tendency towards crevice corrosion, in chloride solutions, which can be due to the higher Si content compared to Alloys 400 and 600. This can only be controlled either by improvements on the metallurgical side during manufacturing or by avoiding crevices in the design; even scratches should be avoided.
2. The hot-rolled as received bar was found to be sensitized to a higher degree which makes it vulnerable to rapid pitting as well as corrosion fatigue failure. This behavior of Alloy 800 can be disastrous if used as boiler water tubes which face thermal cycles involving slow cooling also.
3. Sensitized material behaves completely different to the data provided in the suppliers handbook which appears to be based upon unsensitized condition. Sensitized material has a very high propensity towards pitting which can also lead towards corrosion fatigue failure.

4. The Streicher test successfully distinguished between the sensitized and unsensitized specimens.
5. For the sensitized specimens, tested for 24h in 0.4M (10%) FeCl_3 at room temperature, a linear relationship was found between time and number of pits.
6. The unsensitized specimen shows a partial linear and partial exponential curve between concentration and number of pits. It can be due to the fact that after a certain number of pits, the ratio of anodic vs. cathodic area starts coming to a compromise.
7. Slight pitting was observed with CuCl_2 but ammonium per sulfate and magnesium chloride proved non-corrosive.
8. Concentrations of HCl from 5% to 10% can cause general corrosion.
9. 10% HCl is sufficient enough to dissolve the top adherent oxide film thus exposing the material to LME in mercury and corrosion fatigue and pitting in 0.4M FeCl_3 .
10. Generally titanium nitride particles are the pitting sites in Alloy 800. They do not corrode themselves instead act cathodically thus attacking the nearby matrix alloy. This behavior is similar to that of 301 stainless steel. In sensitized materials grain boundaries are attacked by the corrodant.
11. Sensitized materials suffered more intergranular than transgranular attack in liquid metal embrittlement test with mercury.

12. Pitting can become a fatigue crack initiation site especially if the material is sensitized and cleaned by HCl. The failure will be intergranular.

CHAPTER VII

RECOMMENDATIONS FOR FUTURE STUDIES

1. The issue of SCC at room temperature still needs to be resolved by further experimental work. More SCC tests should be conducted on Alloy 800 in ferric chloride after cleaning in HCl just before the SST. Initially, a completely sensitized specimen should be tested in 20 % ferric chloride at a ramp speed of $1 \times 10^5 \text{ s}^{-1}$. The idea behind selecting higher concentration is to get early and more pits. A comparatively higher ramp speed will give less time for pit development, hence the pits will be pointed which forms an effective crack. Pointed pits proved disastrous in 304 stainless steels. In case of embrittlement, SSTs can be repeated for lower concentrations e.g. 10 % ferric chloride and slower ramp speeds such as $5 \times 10^5 \text{ s}^{-1}$. Later, the as-received and unsensitized specimens should also be tested in a similar manner.
2. Heat treatment can be varied by increasing the soaking time from 2 h to 6 h at 715 C during sensitization. This specimen should then be tested for SCC and fatigue loading in order to understand the grain size effect and the influence of chromium diffusion rate to the matrix.

3. Immersion tests for pitting should be repeated with 0.4 M (10 %) Fe Cl₃ and lesser concentrations for the unsensitized, as-received, and partly sensitized specimens.

BIBLIOGRAPHY

1. Pugh, S.F., A Status Review of Alloy 800, Proceedings of a British Nuclear Energy Society Conference at the University of Reading on 25 and 26 September 1974, AERE Harwell, 1975.
2. Asphahani, A.I., "Corrosion of Nickel-Base Alloys," Metals Handbook, Vol 13, 9th ed., ASM International, Metals Park, Ohio, 641 - 657.
3. Friend, W.Z., Corrosion of Nickel and Nickel-Base Alloy, John Wiley & Sons, Inc. ,1980.
4. Cordovi, M.A., Historical Development of Alloy 800: An Overview: A Status Review of Alloy 800, AERE Harwell, 1975.
5. Fontana, M.G., Corrosion Engineering, 3rd ed., Mc Graw-Hill, Inc., 1986.
6. King, P.J. , Dautovich, D.P. " Pitting Corrosion of Nuclear Steam Generator Materials," Nuclear Technology 55, 196-206, Oct. 1981
7. Provan, J.W., Rodriguez III, E.S., "Part 1 : Development of a Markov Description of Pitting Corrosion", Corrosion, 45,3, 178-188,1989.
8. Hickling, J., Wieling, N., "Electrochemical Investigations of the Resistance of Inconel 600, Incoloy 800, and Type 347 Stainless Steel to Pitting Corrosion in Faulted PWR Secondary Water at 150 to 250 C," Corrosion, 37,3, 147-152, 1981.
9. Palumbo, G., King, P.J., Aust, K.T., "Pitting Corrosion Behaviour of Alloy 800 in Chloride-Sulphate Media," Corrosion, 43,1, 37-45, 1987.
10. Bradshaw, R.W., "Thermal Convection Loop Study of the Corrosion of Incoloy 800 in Molten NaNO_3 ," Corrosion, 43,3 ,173-178, 1987.
11. Lippold, J.C., "Cracking of Alloy 800 tubing in Superheated Steam in a Solar Receiver," Materials Performance, 24, 16-25, Oct. 85.

12. Batista, W., Louvisse, A.M.T., Mattos, O.R., Sathler, L., "The Electrochemical Behavior of Incoloy 800 and AISI 304 Steel in Solutions that are Similar to Those Within Occluded Corrosion Cells," Corrosion Science, 28,8,759-768, 1988.
13. Lee, I.S., Stansbury, E.E., Powel, S.J., "Determination of Pitting Susceptibility Using a New Sample Preparation Technique," Corrosion, 45, 2, 134-136, 1989.
14. ASTM G15-86, "Standard Definition of Terms Relating to Corrosion and Corrosion Testing," Annual Book of ASTM Standards, ASTM, Philadelphia, 134-138, 1987.
15. ASTM G48-80, "Standard Test Method for Pitting and Crevice Corrosion Resistance of Stainless Steels and Related Alloys by the Use of Ferric Chloride Solution," Annual Book of ASTM Standards, ASTM, Philadelphia, 284-287, 1987.
16. ASTM G46-76 (Reapproved 1986), "Standard practice for Examination and Evaluation of Pitting Corrosion," Annual Book of ASTM Standards, Philadelphia, 268-275, 1987.
17. ASTM G1 - 81, "Standard Practice for Preparing, Cleaning, and Evaluating Corrosion Test Specimens," Annual Book of ASTM Standards, ASTM, Philadelphia, 89-93, 1987.
18. Srivastava, S.C., Ives, M.B., "The Role of Titanium in Pitting Corrosion of Commercial Stainless Steels," Corrosion, 45,6, 488-493, 1989.
19. Tomashov, N.D., Chernova, G.P., Marcova, O.N., "Effect of Supplementary Alloying Elements on Pitting Corrosion Susceptibility of 18 Cr - 14 Ni Stainless Steel," Corrosion, 20, 166t - 173t, May 1964.
20. Newman, R.C., Franz, E.M., "Growth and Repassivation of Single Corrosion Pits in Stainless Steel," Corrosion, 40,7, 325-329, 1984.
21. Kaesche, H., Metallic Corrosion, 2nd. ed. National Association of Corroison Engineers, Texas, 1986.
22. Evans, U.R., The Corrosion and Oxidation of Metals, Butler and Tanner Ltd., London, Great Britain, 1960.

23. ASTM STP 665, "Stress Corrosion Cracking - The Slow Strain-Rate Technique", edited by Ugiansky/Payer, American Society for Testing and Materials, Philadelphia, 1979.
24. ASTM A262-86, "Standard Practices for Detecting Susceptibility to Intergranular Attack in Austenitic Stainless Steels, " Annual Book of ASTM Standards, ASTM, Philadelphia, 1 - 18, 1988.
25. Handbook of Huntington Alloys, The International Nickel Company, Inc., Huntington, West Virginia, 1986.
26. Pritchard, A.M., "Some Laboratory - Scale Corrosion Tests on Alloy 800 Boiler Tubing Under Simulated High-Performance Boiler Conditions, " A Status Review of Alloy 800, AERE Harwell, 1975.
27. Pohlman, Steven L., "General Corrosion," Metals Handbook, vol. 13, 9th ed., ASM International, Metals Park, Ohio 44073, 99-101.
28. Kobrin, G., "Materials Selection," Metals Handbook, vol. 13, 9th ed., ASM International, Metals Park, Ohio 44073, 328-329.
29. Elliot P., Marsh, G., " The Oxidation of Incoloy 800 in Moist Air Containing HCl (g) at 800 C, " Corrosion Science, 24, 5, 397-409, 1984.
30. Wilde, B.E. , "The Influence of Silicon on the Pitting Corrosion Resistance of an 18 Cr - 8Ni Stainless Steel," Corrosion, 42,3, 147-151, 1986.
31. Roberge, R., "Effect of the Nickel Content in the Pitting of Stainless Steels in Low Chloride and Thiosulphate Solutions," Corrosion, 44,5, 274-279, 1988.
32. Ijzermans, A.B., "Pitting Corrosion and Intergranular Attack of Austenitic Cr - Ni Stainless Steels in NaSCN," Corrosion Science, 10, 607-615, 1970.
33. Pathania, R.S., Cleland, R.D., "The Effect of Thermal Treatments on Stress Corrosion Cracking of Alloy 800 in a Caustic Environment", Corrosion, 41,10, 575- 581, 1985.
34. Bradford, S.A., "Fundamentals of Corrosion in Gases," Metals Handbook, vol. 13, 9th. ed., ASM International, Metals Park, Ohio 44073, 70-74.

35. Morris, J.A., "Hydrogen and Mercury Embrittlement of Selected Nickel-based Alloys," Thesis, Oklahoma State University, Stillwater, Texas, 1984.
36. Breedlove, J.D. Valenta, A., "The Embrittlement of Incoloy 800 by Hydrogen and Mercury," Unpublished Research, Oklahoma State University, 1985.
37. Price, C.E., Morris, J.A., "The Comparative Embrittlement of Example Nickel Alloys by Hydrogen and Mercury," J. Materials for Energy Systems, 7,3,246-255, Dec. 1985.
38. Hertzberg, R.W., Deformation and Fracture Mechanics of Engineering Materials, 3rd. ed., John Wiley & Sons, Inc., 1989.
39. Atkinson, J.T.N., Van Droffelaar, H., Corrosion and its Control, NACE, Houston, Texas, 1982.
40. Nishimura, R., "Pitting Corrosion of Nickel in Borate and Phosphate Solutions," Corrosion, 43, 8, 486-492, 1987.
41. Nishimura, R., Kudo, K., "Pitting Corrosion of AISI 304 and 316 Austenitic Stainless Steels Covered with Anodic Oxide Films," Corrosion, 44,1,29 - 35, 1988.
42. Craig, B., "Environmentally Induced Cracking," Metals Handbook Vol. 13, 9th ed., ASM International, Metals Park, Ohio, 145-189.
43. Everheart, L.G., "Stress Corrosion Cracking in Alloy 400 at Room Temperature," Thesis, Oklahoma State University, Stillwater, 1989.
44. Phatania, R.S., McVey, E.G., "The Effect of Cooling Water Leakage on Corrosion of Steam Generator Materials," Corrosion/79, NACE, March 1979, Paper No. 97.
45. Lizlovs, E.A., Bond, A.P., "Anodic Polarization of Some Ferritic Stainless Steels in Chloride Media," J. of Electrochemical Society, 116,5,574-579, 1969.
46. Markey, C., Unpublished research, Oklahoma State University, 1990.
47. Lynch, S.P., "Liquid-Metal Embrittlement in an AL 6 % Zn 3 % Mg Alloy," ACTA Metallurgica, 29,2,325-340, 1981.

48. Hussen, I., Unpublished research, Oklahoma State University, 1991.

VITA

Zaheer Babar Khan

Candidate for the Degree of

Master of Science

Thesis : AN INVESTIGATION OF CORROSION BEHAVIOR OF ALLOY
800

Major Field : Mechanical Engineering

Biographical:

Personal Data: Born in Karachi, Pakistan, May 14,
1960, the son of Mr. and Mrs. Ansar Ahmad Khan.
Married to Amera Khan on December 16, 1989.

Education : Graduated from St. Lawrence Boys School,
Karachi, Pakistan, in May, 1976; graduated from
D.J.S. Govt. Science College, Karachi, Pakistan,
in June 1978; received Bachelor of Engineering
Degree (Mech. Engr.) from N.E.D. University of
Engineering and Technology, Karachi, Pakistan, in
September, 1987; completed the requirements for
Master of Science Degree in Mechanical Engineering
at Oklahoma State University in May 1991.

Professional Experience : Mechanical Engineer, SASM
Engineering, Pakistan, November 1987 to December
1988; Mechanical Engineer, Sakrand Sugar Mills
Ltd., Pakistan, January 1989 to July 1989.

Professional Organizations: P.E. of Pakistan
Engineering Council, American Society of
Mechanical Engineers.